A COMPARISON OF THE ARCUATE FOLD AND

THRUST BELTS OF THE WESTERN ALPS AND

CARPATHIAN MOUNTAINS TO THE OUACHITA

ARCUATE FOLD AND THRUST BELT,

SOUTHEASTERN OKLAHOMA



By

BRADLEY D. HOLLAND

Bachelor of Science Geology

Midwestern State University

Wichita Falls, Texas

2004



Submitted to the Faculty of the
Graduate College of the
Oklahoma State University
in partial fulfillment of
the requirements for
the Degree of
MASTER OF SCIENCE
May, 2009

A COMPARISON OF THE ARCUATE FOLD AND

THRUST BELTS OF THE WESTERN ALPS AND

CARPATHIAN MOUNTAINS TO THE OUACHITA

ARCUATE FOLD AND THRUST BELT,

SOUTHEASTERN OKLAHOMA

Thesis Approved:

Dr. Ibrahim Çemen
_____
Thesis Adviser

Dr. Jim Puckette
_____

Dr. Darwin Boardman
_____


_____

Dr. A. Gordon Emslie
_____
Dean of the Graduate College

TABLE OF CONTENTS

Supplementary:

    Table: List of Hand Samples

    Plates: 1-15 (Larger Versions of Inserted Figures)

LIST OF FIGURES

CHAPTER 1

INTRODUCTION

1. **Statement of Purpose**:

Many of the fold-thrust belts of the world contain a portion that is arcuate in its map view appearance. These include: the Western Alpine Mountains, the Apennines, the Appalachian Mountains, the Banda arc, the Carpathian Mountains, and the Jura arc. The Ouachita fold-thrust belt is no exception (Fig. 1 (A)), with an arcuate bend making up the breadth of the Ouachita Mountains of southeastern Oklahoma and central Arkansas (Fig.1(B)).
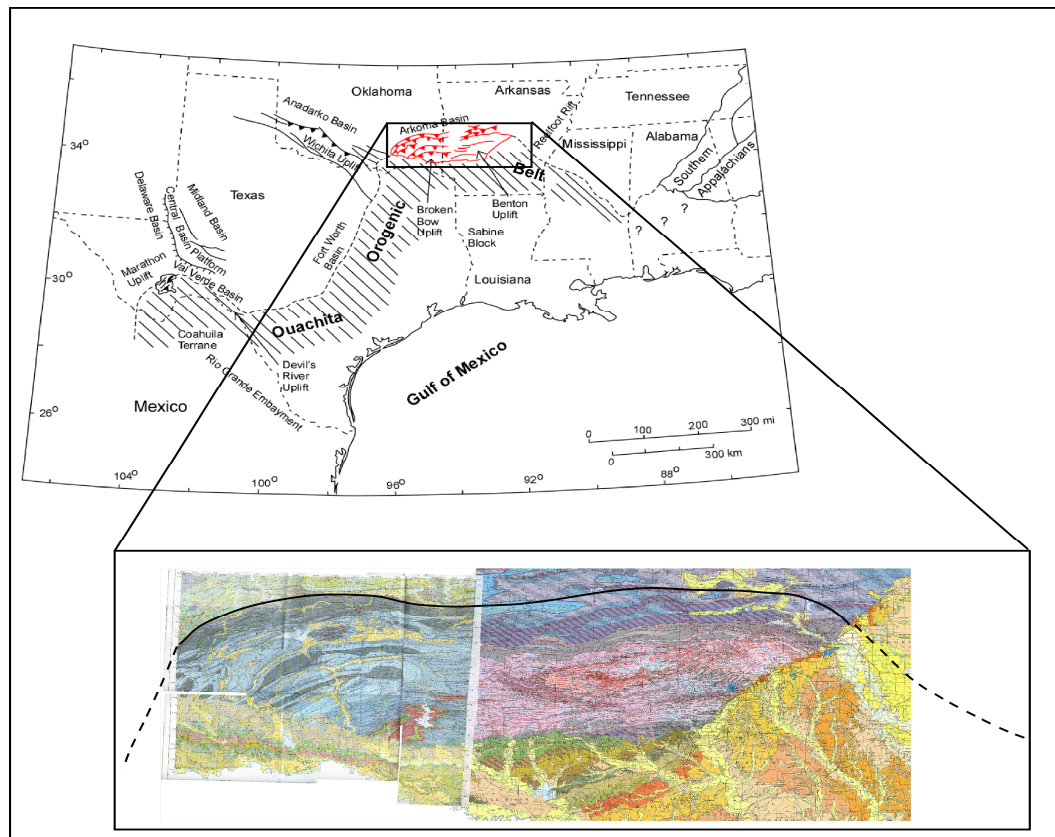


Figure 1: A location map depicting the location of the arcuate bend of the Ouachita Mountains. A.) A map of the entire Ouachita Orogenic Belt (Modified from Keller et al., 1999). B.) A geologic map of the Ouachita Mountains with the arc outlined (Geologic map a combination of the Marcher et al., 1994 Oklahoma Geologic map and the Haley et al., 1993, Arkansas Geologic map).

The main objective of this study is to compare the arcuate bend exposed within the Ouachita Mountains to three Alpine arcuate bends (the Jura arc, the southern Western Alps, and the Western Alps) and the entire Carpathian Mountain Chain (Fig. 2), chosen simply for their arcuate shape in map view.  This study will include comparisons based on: 1) orogenic evolution of the arcuate bend, 2) arcuate bend type, 3) fault geometries (cross sectional and map view), 4) sedimentological studies (pre- and post orogeny), and 5) gravity profiles (where applicable). These five criteria were chosen because they are the most intensely studied aspects of the above mentioned arcuate bends.



Figure 2: A relief map of the four European arcuate bends used in this study. Each arcuate bend is outlined and numbered. 1) Jura Arc 2) Southern Portion of the Western Alps 3) Western Alps 4) Carpathians (Map modified from: www.freeworldmaps.net/.../europe/physical.jpg)

The orogenic evolution of the arcuate bends, is the most encompassing criterion. It can shed light on some of the most basic and vital aspects of an arcuate bend, such as: 1) the passive margin geometry, 2) the timing of events, 3) the rate and direction of the movement of the plates, and 4) the orientation of the convergent boundary. The arcuate bend type is an important criterion because it shows how the arcuate bend was formed. Fault geometries within a structural cross section allow comparisons to be made, and provide insight on what type of subduction zone might have been present at the convergent boundary, whereas, map view fault geometries give insight on how the indentor deformed the passive margin during convergence. The pre- and post-orogenic sedimentation, as well as the gravity profiles are the product of the type of subduction zone.

There is almost no published data on the Ouachita arcuate fold-thrust belt and its comparison with other arcuate fold-thrust belts. In order to provide data on the Ouachita arcuate fold-thrust belt, several studies have been conducted during this investigation. These studies include: 1) hand sample evaluations, 2) outcrop correlations of the Lower Pennsylvanian rocks exposed on the hanging wall of the leading edge thrust, the Choctaw Fault Zone, and 3) construction of balanced structural cross sections.  The location selected to conduct these studies was an area along the frontal belt of the Ouachita Mountains that contained the tightest curve of the arcuate bend. The study area includes portions of both Pittsburg and Atoka Counties, with the main area of focus within four $7^1/_2$ minute quadrangles: Pittsburg, Kiowa, Limestone Gap, and Colgate SE (Fig. 3). Supplemental data was collected to the northeast along the frontal belt up to the town of Wilburton, OK.
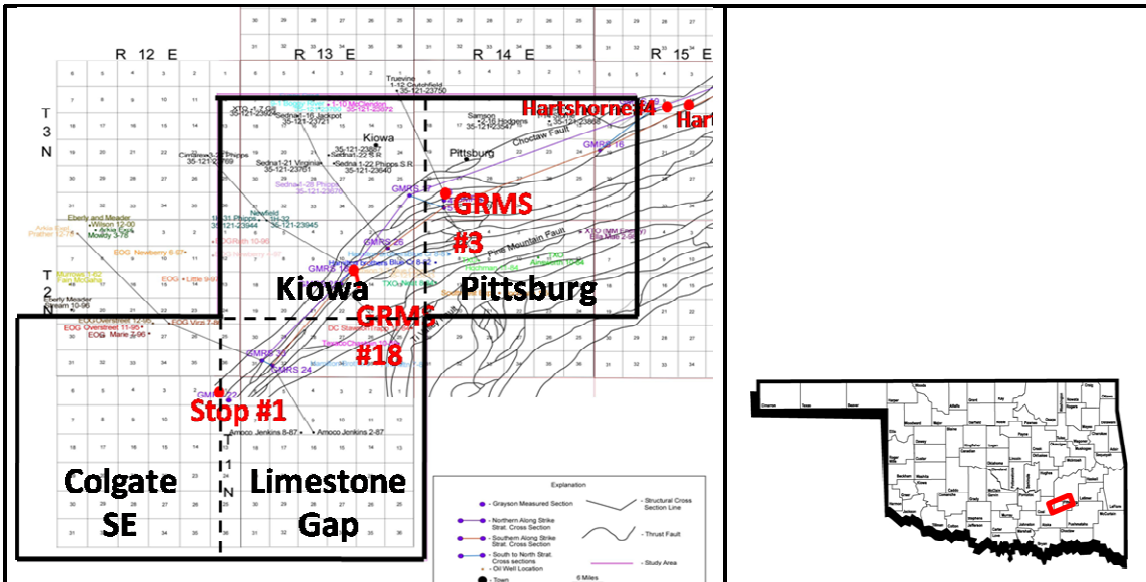
Figure 3: Location map of the four principle $7^1/_2$ minute quadrangles: Pittsburg, Kiowa, Limestone gap, and Colgate SE

There are no published detailed geologic maps for the four $7^1/_2$ minute quadrangles listed above. However, there is a 1:63,360 scale geologic map by Knechtel (1937), that covers the Arkoma basin north of the Choctaw Fault and a 1:250,000 geologic map of the McAlester and Texarkana Quadrangles (Map HA-9) by Marcher and Bergman (1971). These geologic maps were used to compile a geologic map of the area, to evaluate the map view fault geometries, and to crudely measure displacement. Fifty-two limestone hand samples were collected from three Wapanucka Limestone outcrops along the Ouachita frontal belt (Grayson #3, Grayson #18, and Stop #1), along with ten sandstone samples collected from Grayson #3. Ten supplemental hands samples were gathered from six outcrops outside the study area (Wilburton #1 and #2, Hartshorne #1-#4). These hand samples were collected with the purpose of generating thin sections and conodonts to examine. The thin sections were prepared both along strike and dip to facilitate the recognition of shearing, and to aid in the petrographic study of the Wapanucka Limestone. The conodonts were collected to assist in detailed outcrop and

bathymetric correlations, which allowed for the recognition of the lateral, along strike, movement and rudimentary displacement measurements.  The balanced structural cross sections were used to compare the Ouachita arcuate fold-thrust belt cross section fault geometries to those observed in the Western Alps and the Carpathians.

CHAPTER 2

ARCUATE BEND TYPES

2.1 **Arcuate Bends**:

2.1.1 Types:

      Arcuate bends have long been recognized as along-strike variations in the bearing of the structural grain of an orogenic belt. Marshak (1988) defined two end member types of arcuate bends: 1) non-rotational arcs; and 2) oroclines. Hindle et al. (1999) added a third end member called a "Piedmont Glacier". Marshak's (1988) non-rotational arc and Hindle's (1999) primary arc are synonymous, and they are defined as arcs where the strike orientation does not change during its development. Oroclinal arcs are arcuate bends that exhibit some manner of rotation, and a piedmont glacier is a special type of orocline that exhibits radial thrusting. These arc types are only seen in thin skinned fold-thrust belts, and each one can be further subdivided by determining if they formed during or after the development of the orogen (Fig. 4).

      Non-rotational arcs (Fig. 4) generally occur along irregular plate margins that act as a mold for the arc, or when an indentor or micro-continent is swept in between two converging plates. Marshak (1988) recognized three types of non-rotational arcs: 1) arcuate bends that conform to a concave portion of an irregular margin, but show no further movement, 2) arcuate bends where the displacement trajectories are equal along every part of the bend, 3) arcuate bends that exhibit changes in trajectory in a way that allows the strike along the bend to remain unchanged.
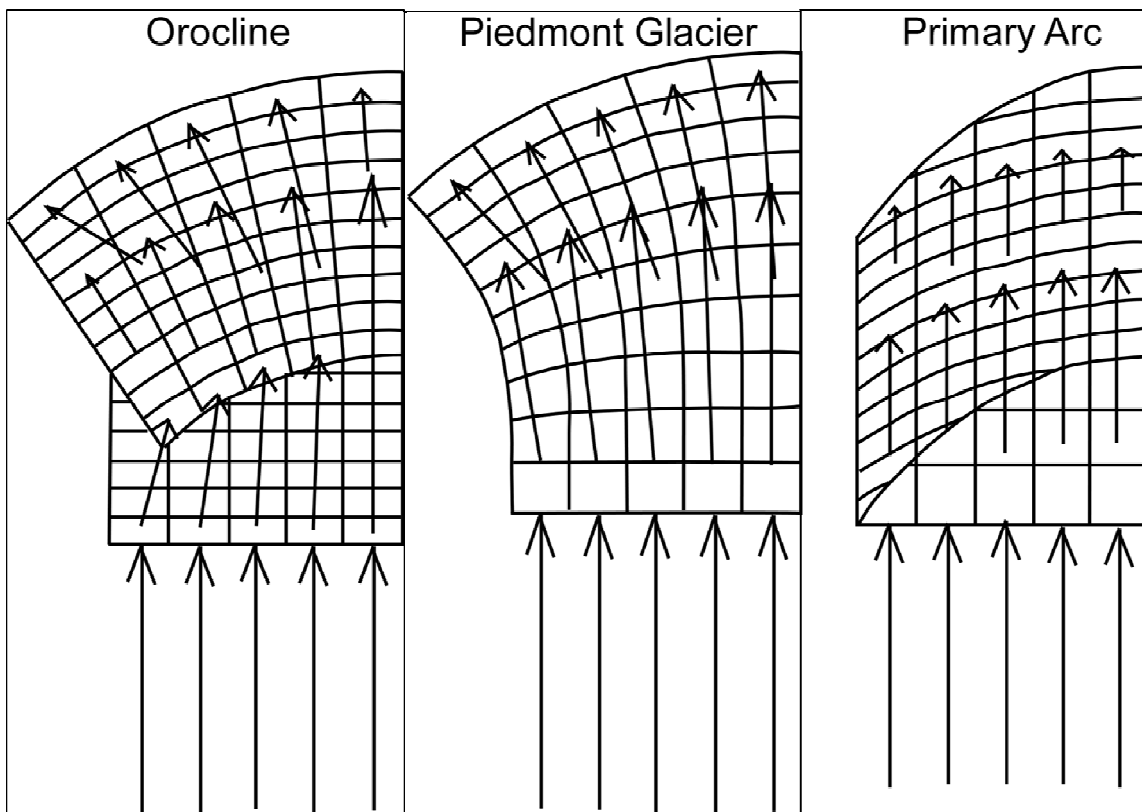
Figure 4: Arc classification chart. This chart shows the differences in the three end members according Hindle and Burkhard, 1999. (Modified from Hindle and Burkhard, 1999)

Oroclines are arcuate bends that show some degree of rotation during their formation (Fig. 4). They generally require a secondary deformation event. These events can include a combination of a second round of compressional forces, tensional forces, wrench faulting, or an impediment in the foreland or basement. They can form in several kinematics: 1) the end points are not stationary and as the displacement is increased so is the circumference of the marker line, 2) the end points are locked in place and as the marker line moves forward the trajectory paths are forced inward, but the tangential strain remains unchanged, and 3) the end points move in as the marker line moves toward the foreland. Example three is described as a "pure bend" by Hindle et al. (1999). There are also oroclines that require an obstacle in the foreland. These oroclines form as a straight

orogen collides with an obstacle and the trajectories remain orthogonal to the orogen as it bends around the buttress, or the end points move around the obstacle; while, the center of the bend remains stationary.

Piedmont glaciers described by Hindle et al. (1999) are special type oroclines. These are the most common of all arcuate bends. They form when the thrusts in the arc radiate out as the bend moves toward the foreland basin (Fig. 4). It is not uncommon to have an extensional stress regime in the rear of a piedmont glacier arc and a compressional regime at the front (Hindle et al., 1999). This type requires a complete separation from the emplaced nappe and an undeformed foreland (Hindle et al., 1999). These arc classification schemes all suffer from one distinct problem; they rely solely on displacement vectors rather than strains, rotations, and shape as the distinguishing factor (Hindle et al., 1999). The displacement vector is difficult to obtain accurately in simple field studies; therefore, assigning an arc type to a certain arcuate fold-thrust belt is always speculative.

2.1.2 – Arc Nomenclature

In order to effectively discuss the kinematics of these three end member types of arcs several terms have to be defined (Fig. 5). They are: 1) end points, 2) reference line, 3) marker line, 4) amplitude, 5) trajectory, and 6) tangential strain. All of these terms can be defined by studying the arcs in map view. The end points are the points along the arc where the orientation of the structure no longer changes along strike. The reference line is the line that connects the two end points. The marker line is a line that represents the furthest extent of the arc. Amplitude is the distance between the reference line and the

marker line. Trajectory describes the path that points along the marker line take as the arc develops. Tangential strain is a two dimensional component of extension or compression that occurs parallel to the tangent of the marker line.
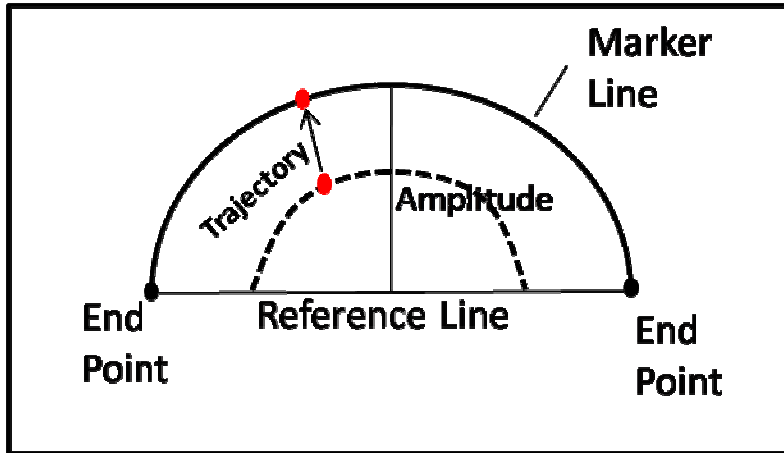


Figure 5: Nomenclature of an arc.
(Modified from Marshak, 1988)

.

CHAPTER 3

METHODOLOGY

3.1 **Geologic Map**

The Oklahoma Geologic Survey (OGS) has not published geologic maps for any

of the $7^1/_2$ -minute quadrangles within the study area. During this investigation, a

geologic map was compiled by

splicing a 1:63,360 scale geologic

map of the McAlester District,

Oklahoma, published in 1937, by

M. M. Knechtel with a 1:250,000

scale geologic map of the

McAlester and Texarkana

Quadrangles (HA-9) by M. V.

Marcher and D. L. Bergman, 1994

(Fig. 6 and plate 15).

Figure 6: The two geologic
maps that had to be spliced to
generate a workable geologic
map for the study area.
 A.) McAlester District,
Oklahoma
B.) McAlester-Texarkana
Quadrangle (HA-9)
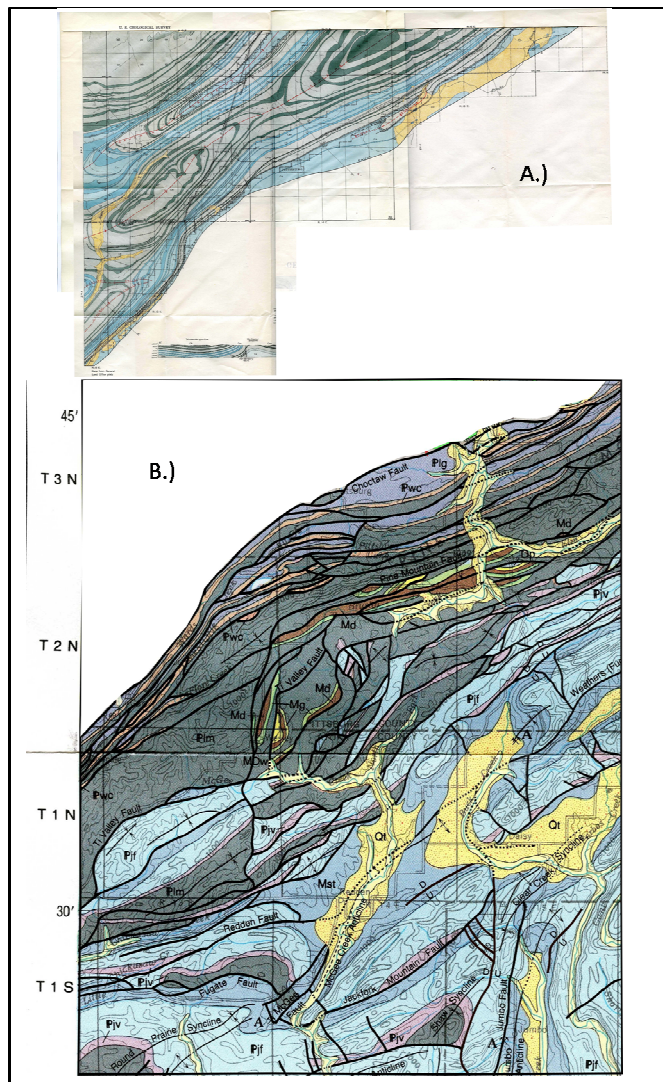
3.2 **Balanced Structural Cross Sections**

Balanced structural cross sections are the most widely used and accepted tools in studying fold-thrust belts. A structural cross section must be restorable to an undeformed state and should be admissible to be a balanced structural cross section (Boyer and Elliot, 1982). The two ways in which to draw a balanced cross section are the Busk Method and the Kink Fold Method (Suppe, 1985). The Busk Method maintains constant bed thickness throughout a fold by breaking the fold down into small pie shaped pieces and using concentric folding (Fig. 7). The center of each bend acts as the pivot point for a compass

## Busk Method

*Normal to bedding*

*Inflection Line*

*Center of Curvature*
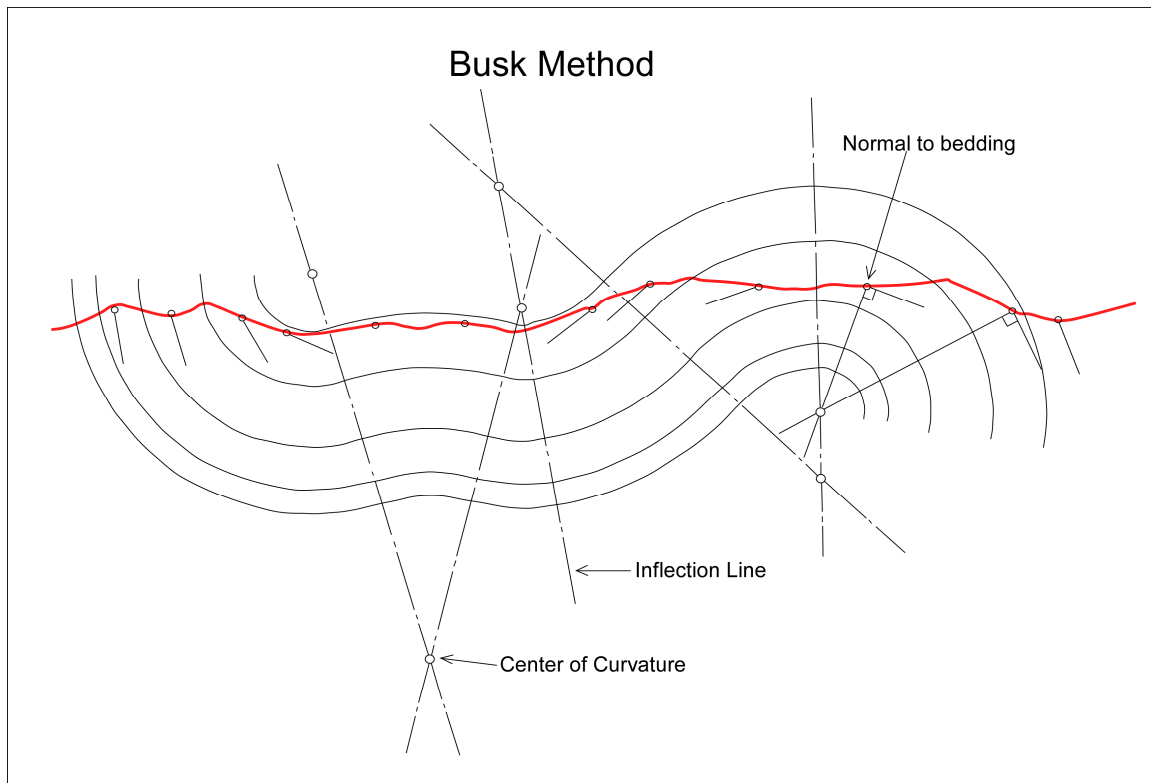
Figure 7: The Busk Method. (Modified from Suppe, 1985)

to construct the concentric folds that maintain bed thickness (Suppe, 1985). The Kink

Fold Method was developed by Suppe (1983). Instead of using the concentric circles to

describe a fold the Kink Method uses angular kinks and straight limbs to describe the

structure. This method allows for easy measurement of displacement along a fold, while

maintaining bed integrity. Therefore, the cross section is more easily restored than using

the Busk Method. Moreover, the Kink Method uses trigonometric relationships that can

be used to extrapolate the fold into areas where there is little no data (Suppe, 1983).

The limited amount of data obtained from the geologic map and the few oil and

gas exploration wells within the study area would not allow for the construction of the

proposed balanced structural cross sections (Fig. 8). However, a simplified structural

cross section

was

Figure 8: Cross section location map. The red line indicates the location of the simplified structural cross sections. The black lines are the locations of the proposed balanced structural cross section.
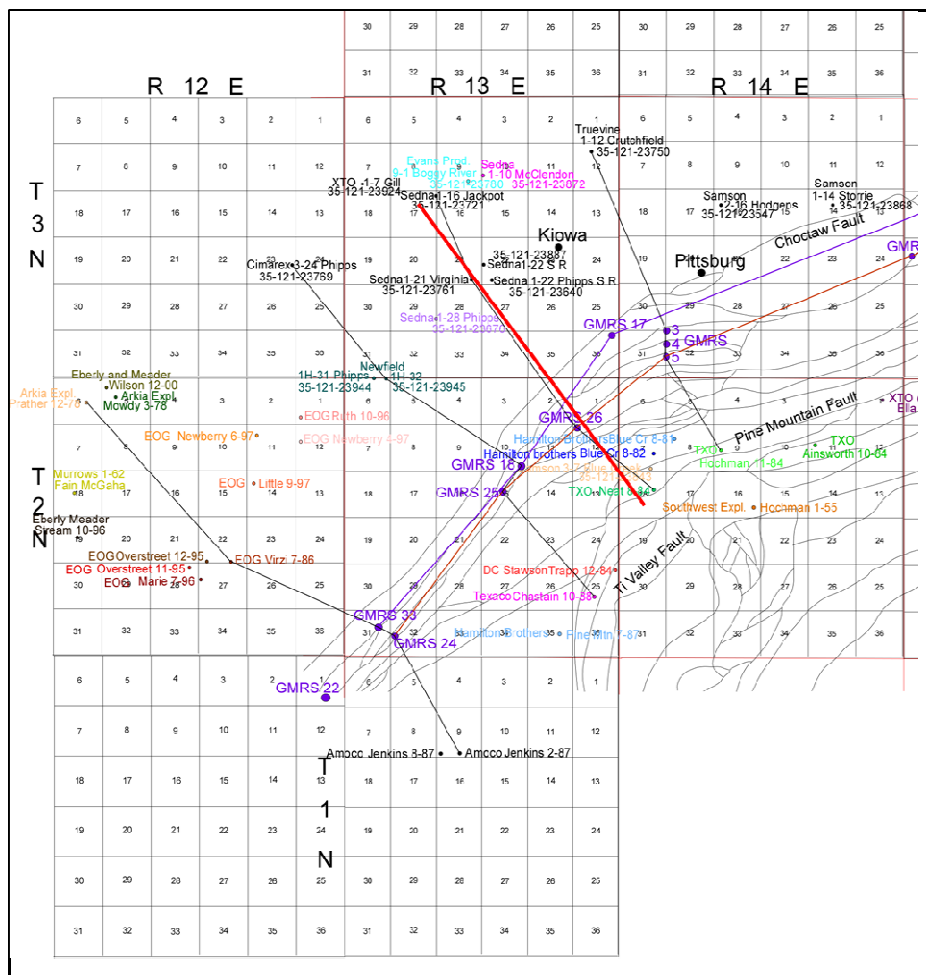
constructed where enough data could be collected (Fig. 8). Both Busk and Kink Fold

methods were attempted during the construction of this structural cross section (Fig. 9).
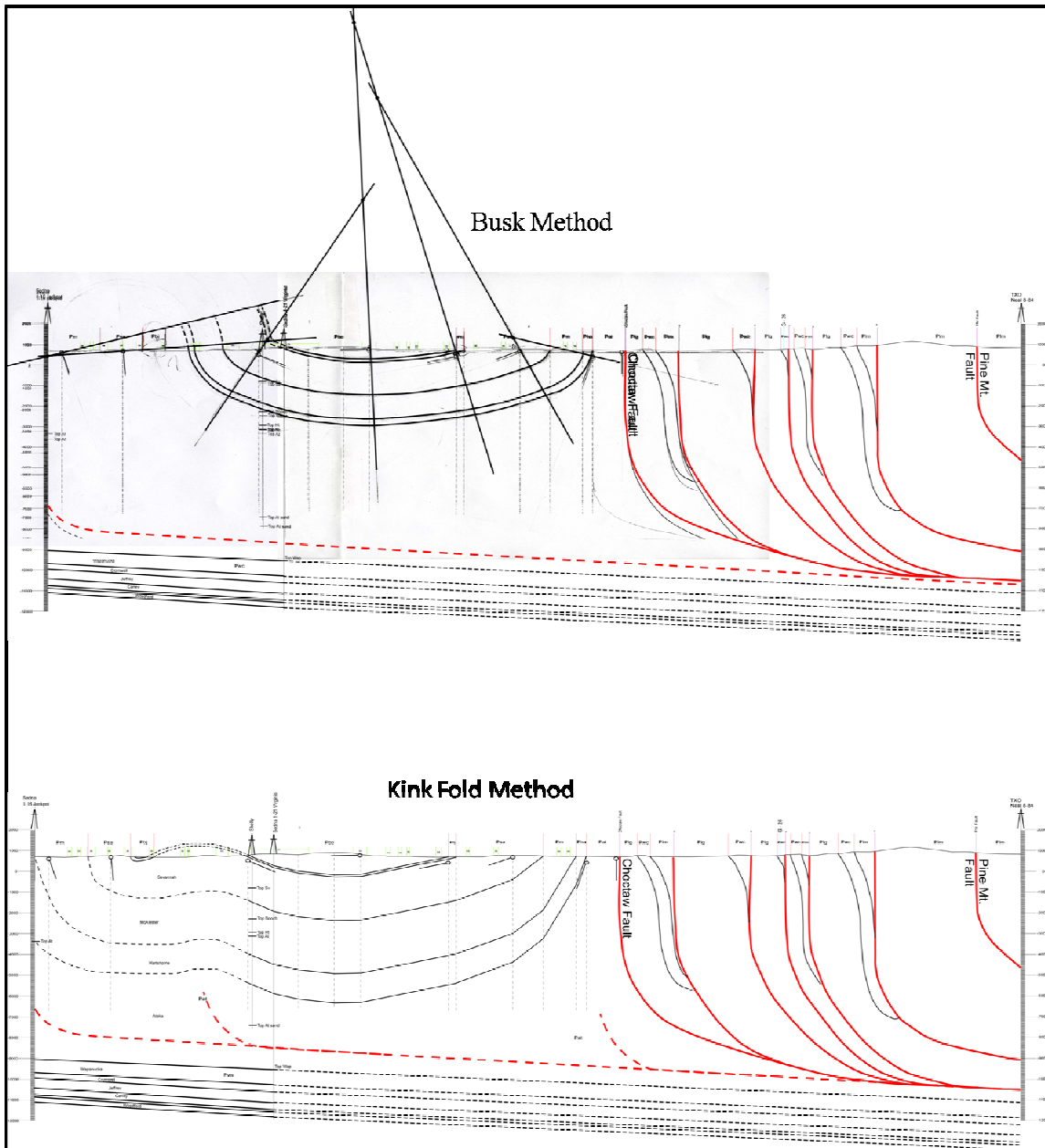


Figure 9: Two attempts at generating an acceptable simplified structural cross section using both the Busk Method and the Kink Fold method. The cross section line is indicated by the red line in Figure 8.

3.3 **Measured Sections**

The Upper Morrowan Wapanucka Limestone is well exposed in the Ouachita

arcuate fold-thrust belt (Fig. 13). It is used for all of the detailed research presented in this

investigation. Grayson (1980), described 33 measured sections of the Wapanucka
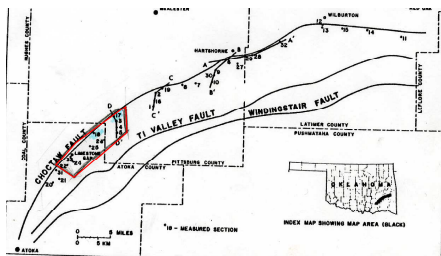
Limestone along the frontal belt of the Ouachita

Mountains (Fig. 10). Grayson's (1980) detailed

descriptions of these outcrops allowed me to develop



Figure 10: Location map of Grayson's measured sections.
Study area is outlined in red. (Modified from Grayson, 1980)

profiles of each outcrop within the study area, and select which beds to be sampled. Not

all of Grayson's (1980) locations were accessible, but enough of them were to get good

coverage along the frontal belt (Fig. 11, plate 1). Once the collection sites were selected,

samples were collected from each section. After finding the basal contact of the

Wapanucka, the sections were measured using a Jacob's staff and a Brunton® transit.

Strike and dip at each section was measured to fill in some of the missing data on the

geologic map. Supplementary hand samples were gathered in the field at random exposed

outcrops of the Wapanucka Limestone to allow for greater coverage (Fig. 11, plate 1).


3.4 **Conodont Collection and Identification**

A total of 72 samples were collected from the locations indicated in Figure 11

(plate 1) for the purpose of petrographic analysis. A mere 56hand samples were

processed to collect conodonts. Limestone samples were broken down using formic acid.

14

The procedure is outlined in Appendix A. The limestone will usually dissolve within a twenty-four hour period, leaving only residual constituents, the conodonts. The conodonts collection process is given in Appendix A. After conodonts are collected, they can be identified using the published literature on the local assemblages.

The shale samples collected were processed using 35% $H_2O_2$. The procedure for this method is given in Appendix A. After each sample is broken down, the retrieval process is the same as described above. The Wapanucka Limestone samples were difficult to break down using either method. The best results were obtained by alternately repeating both methods several times.
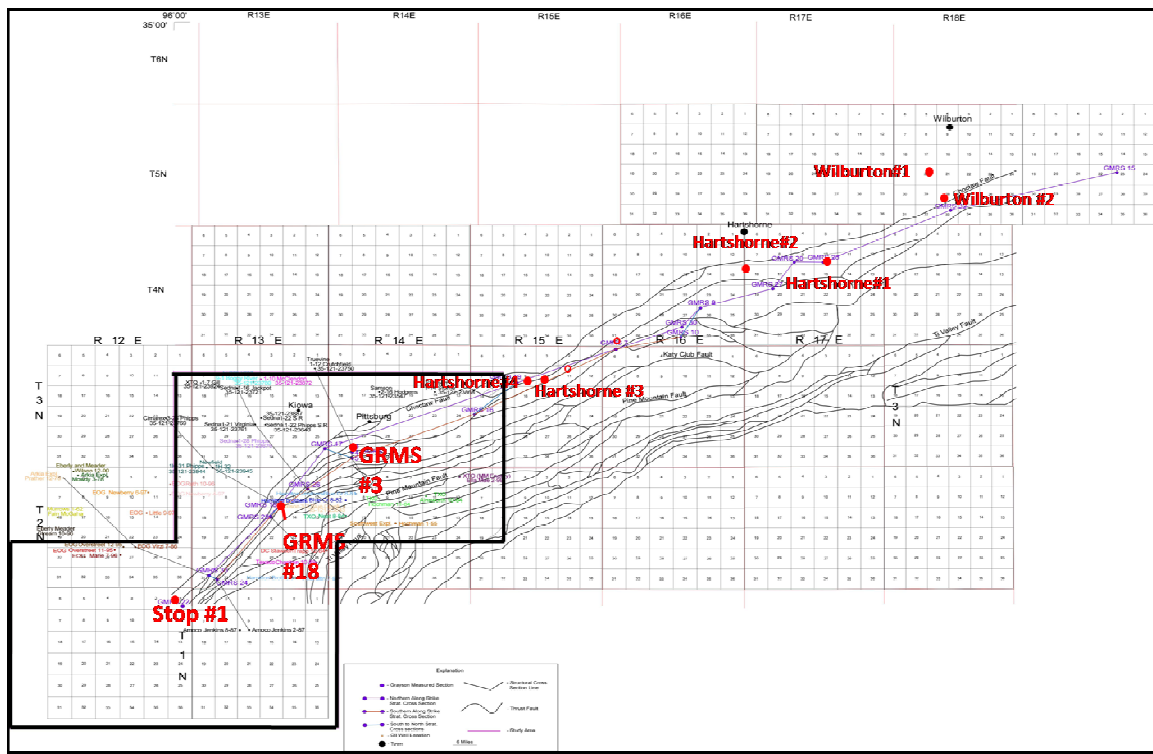


Figure 11: Sample collection location map. Purple "GMRS #__" are the locations of Grayson (1980) measured sections. The red dots indicate collection sites. The outlined circles indicate intended collection sites (unable to collect because of landowner). The black box outlines the thesis area and extensive collection took place at the three locations indicated. Supplementary Collection Sites: The Hartshorne samples were restricted to the Upper Sandstone/Limestone Member of the Wapanucka Ls. The Wilburton samples were taken from the Atoka Formation.

3.5 **Thin Section Preparation**

Two thin sections were prepared from each sample, one in the strike direction and one in the dip direction. Thin sections were prepared using the procedure established by Houseknecht (1992). A 1" by 2" cube (plug) was cut from each sample along strike and another of the same dimensions was cut perpendicular to strike. They were then dried in an oven to drive off the water in the pore spaces. The plug was then mounted to a non-frosted slide (working slide) with a clear epoxy ( Loctite 0151-Hysol) and allowed to sit to ensure bonding. After bonding satisfactorily, the top of the plug is coated with a generous amount of a dyed epoxy (Buehler Epo-Color, Red) and placed under a vacuum (Buehler Vacuum). The vacuum facilitates movement of the epoxy into the pore space of the sample. The dye is to help in the observation of the porosity once the thin section is completed (Houseknecht, 1992). Once the epoxy dries, the dyed side of the plug is polished to a glossy sheen, using the Hillquist Thin-Section grinder (15 micron grinding wheel). The glossy polished side of the plug is then mounted to the frosted side of the finishing slide with the clear mounting epoxy. After the mounting epoxy is allowed to dry, the working slide is cut off and the plug is carefully ground down to 30µm or until the quartz grains are first order gray under cross polarized light. The working slide was cut off using an Ingram Thin Section Cut-off Saw model 137. The rough grinding was accomplished with the Ingram Thin Section Grinder model 400U, whereas the finishing polish was completed using the Hillquist Thin Section Grinder beginning with the 45 micron wheel and finishing with the 15 micron wheel.

3.6 **Thin Section Analysis**

A Nikon polarizing microscope (Type 104) was used in the thin section analysis.

The Nikon microscope has a graduated ocular that is sub-divided into one hundred units.

The size of each subdivision is 0.01mm at 10X magnification. The intersection of a grain

with one of these subdivisions is called a point, and for each thin section 600 point counts

were recorded. These point counts allow the amount and size of the constituents within

each thin section to be quantified. At this point the limestone samples can be named,

because all of the pertinent information is available. The sandstone samples require

further evaluation. Once the thin section constituents of the sandstone samples have been

quantified, the quartz, feldspar, and lithic grains are normalized and plotted a ternary
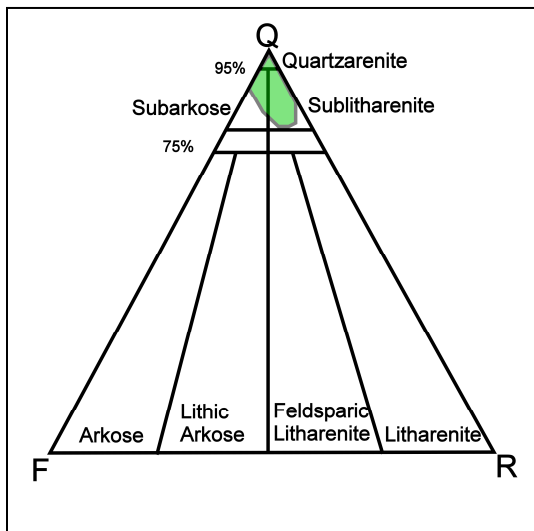
diagram (Fig. 12). The location of the plot will allow you to identify the siliciclastic sample correctly.



Figure 12: An example of a ternary diagram. Q = quartz, F=feldspar, R(L)= lithic fragments
The green shaded area is how the Spiro sandstone plotted according to Houseknecht, 1987.
(Modified from Houseknecht, 1987)

The grains within each sample were carefully evaluated while the point counts are

being conducted. Deformation of the grains can indicate shearing. The relative position of

the Wapanucka outcrops to the fault plane makes this type of microscopic evaluation

necessary.  The quartz grains of the siliciclactic samples were also examined for the

presence of clay coatings. If the type of clay coating can be established, the environment

in which the sediments were deposited may be discerned.

## 3.7 **X-ray Diffraction**

Several samples of siliciclastic rocks were analyzed using X-ray diffraction to
help identify the constituents not apparent in thin sections, including detrital matrix and
authigenic clays. The procedure used for the X-ray diffraction analysis is as follows: 1) a
small amount of each sample is pulverized into a fine powder and placed into the opening
of a specially designed slide, 2) the excess powder and anomalous pieces are removed at
this point, 3) the slide is loaded into the sample holder of the X-ray diffractometer, 4) the
diffractometer is programmed to sweep from $5^o$ to $40^o$ 2$\square$, to capture the unique
signatures of the most common constituents of sandstone, 5)  the computer program
selects the most probable mineral matches for the recorded peaks, and  6) the appropriate
matches are selected from the computer generated list.

## 3.8 **Gravity Profiles**

Data was provided by the USGS for southeastern Oklahoma. It was collected with
10km spacing but has been reduced down to 1km spacing by the USGS. The data was
processed for this study by using Oasis-Montaj software along with GYM-SYS. The
GYM-SYS software works on the data after it has been imported into Oasis-Montaj and
allows the gravity data to be plotted in a more usable cross sectional format (Fig. 78 (B)).
Then the lower crustal model (Fig. 78 (Bb)) is manipulated by changing densities and

depths of each unit until your gravity profile (Black Dots in figure 78 (Ba)) matches the imported data (very ambiguous). The error is recorded by the difference between the red and blue lines running through the middle of the profile (~ -54 mgals). The resultant gravity profile (Fig. 79) is used as a comparison tool in the "Discussion" chapter.

CHAPTER 4

GEOLOGY OF THE OUACHITA ARCUATE FOLD-THRUST BELT

4.1 **Geologic Map**

Combining the two maps was successful (Fig. 13, Plate 2). The only slight

discrepancy with combining the two maps was the location of the Choctaw Fault. The

major problem encountered was not in the

mixing of these two maps, but rather the data

contained within each map. The compiled

geologic map lacked the detail needed for a

comprehensive examination because the

necessary strike and dip data were lacking

from both halves.  The combined map,

however, does define large broad synclines

and a tight narrow anticline in the Arkoma

Basin, northwest of the Choctaw Fault.
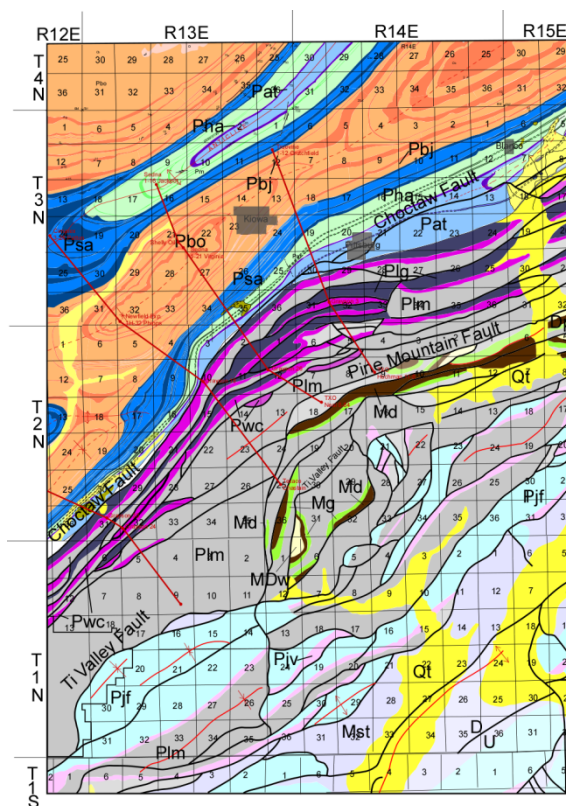


Figure 13: The compiled geologic map. The red lines are the locations of the proposed balanced structural cross sections.

4.1.1 **Geology**

The compiled map contains major

structural features and rock units of the Ouachita arcuate fold-thrust belt. The structural

features exhibited in the Arkoma Basin consist of two broad synclines and a narrow

anticline. The southern syncline is the Kiowa Syncline; while, the northern syncline is the

Krebs Syncline. The narrow anticlinal fold is the Savanna Anticline. The limbs of the

anticline have dips in excess of 80$^{o}$, which could be indicative of faulting; further studies need to be conducted in order to be conclusive.

Three major thrust faults are present in the compiled map, the Choctaw, the Pine Mountain, and the Ti Valley. Numerous splay thrusts are located between the Pine Mountain and the Choctaw Faults. These splays are indicative of greater displacement in the area and could possibly provide evidence on how the arcuate belt formed (discussed later Section 8.2).

4.1.2 **Stratigraphy**

The stratigraphy of the mapped area is given in Figure 14 and plate 2. The majority of the rock units within the combined geologic map are Pennsylvanian in age except a few Mississippian aged rock units between the Pine Mountain Fault and the Ti Valley Fault. The Pennsylvanian aged rocks are subdivided between the Morrowan and the Desmoinesian. The Morrowan aged rock units are the Pennsylvanian rock units located within the Ouachita Mountains; while, the Desmoinesian aged rock units are the Pennsylvanian rock units in the Arkoma Basin. The Atokan rock time unit is completely ignored in the Marcher et al. (1994) map. The Upper Morrowan Wapanucka Limestone (Pwc) is the bright magenta rock unit on the combined geologic map, and it expresses the intensive splaying south of the Choctaw Fault.

**PENNSYLVANIAN**

**DESMOINESIAN**

(Arkoma Basin)

| | |
|---|---|
| Pbo | – Boggy Formation |
| Pbj | – Bluejacket Sandstone |
| Psa | – Savanna Formation |
| Pm | – McAlester Formation |
| Pha | – Hartshorne Sandstone |
| Pat | – Atoka Formation |

**MORROWAN**

(Exposures North of Ti Valley Fault)

| | |
|---|---|
| Plm | – Lynn Mountain Formation |
| Pwc | – Wapanucka Limestone and Chickachoc Chert |
| Plg | – Limestone Gap |

(Exposures South of Ti Valley Fault)

**MORROWAN**

| | |
|---|---|
| Pjv | – Johns Valley Shale |
| Pjf | – Jackfork Group |

**MISSISSIPPIAN**

**CHESTERIAN**

| | |
|---|---|
| Mg | – Goddard Shale |

**CHESTERIAN**

| | |
|---|---|
| Mst | – Stanley Group |

**CHESTERIAN, MERAMECIAN, OSAGEAN, AND KINDERHOOKIAN**

| | |
|---|---|
| Md | – Delaware Creek Shale |

**MISSISSIPPIAN AND DEVONIAN**

**KINDERHOOKIAN AND UPPER DEVONIAN**

| | |
|---|---|
| MDw | – Woodford Shale |

**DEVONIAN**

**LOWER DEVONIAN**

| | |
|---|---|
| Dp | – Pine Top Chert |

Figure 14: Simplified stratigraphic column for the mapped area. (Modified from Marcher et al. (1994))

## 4.2 **Balanced Structural Cross Sections**

The amount of data obtained from the geologic map and the few oil and gas exploration wells within thesis area (Fig.15) made developing admissible balanced structural cross sections for my study area unrealistic. I was, however, able to generate a simplified structural cross section (Fig. 16 and plate 3). This simplified structural cross section relies heavily on conjecture where data are scarce.

The well control showed that the main detachment surface is shallower at a depth of ~10, 500 feet and is contained within the Atoka Formation. A leading imbricate fan is present in front of the Pine Mountain Fault, with the Choctaw Fault as the leading edge fault. A complete stratigraphic section is present in the Arkoma Basin below the Atoka Formation. The geologic data acquired from the map implies that there is at least one thrust fault present in the Arkoma Basin, but its orientation could not be discerned.
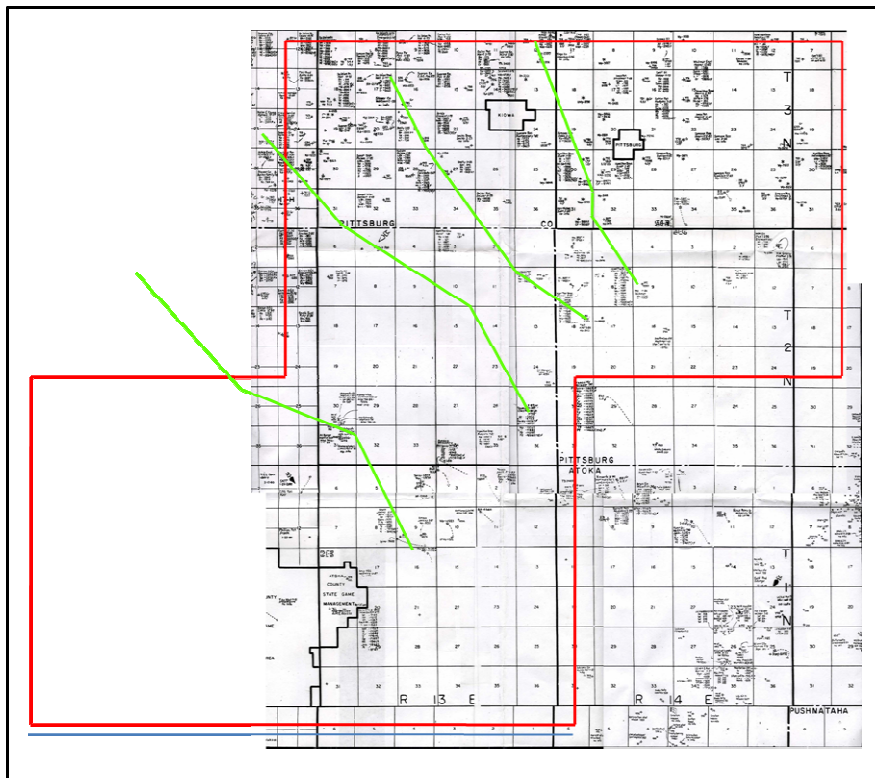


Figure 15: The oil well base map of the study area. Not all of the base maps were available. The study area is outlines in red and the location of the proposed cross sections are outlined in green. Note: the scarcity of oil well locations in the thesis area, thus insufficient well control for the cross section.

Figure 16: Simplified structural cross section, developed along the red line in Figure 8.
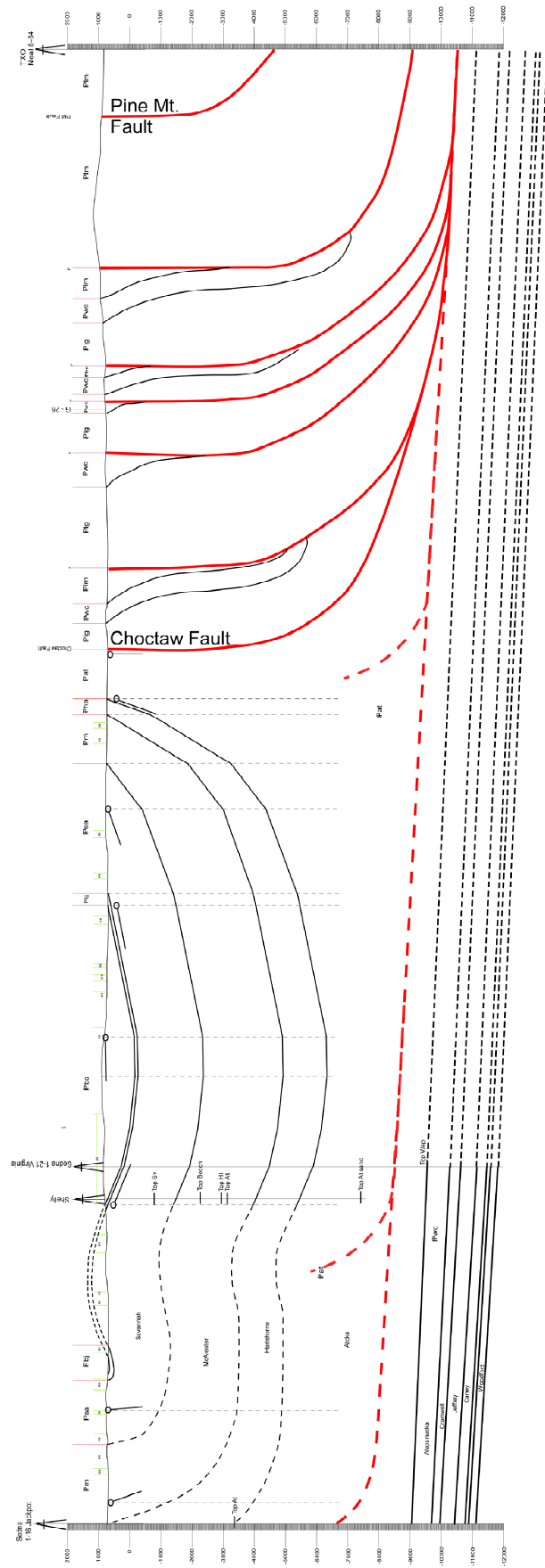
4.3 **Measured Sections**

       The measured sections described by Grayson (1980), allowed for the collection of

hand samples, conodonts, and for the rough correlation throughout and beyond the thesis

area. Two stratigraphic cross sections were constructed along strike and six stratigraphic

cross sections were developed in the dip direction (Fig. 17and plate 4). The cross sections

are presented in Figure 18 and plates 5, 6, and 7. The along-strike stratigraphic cross

sections were constructed to act as a control, whereas, the dip direction cross sections, in

combination with the control, were developed to see if there was any recognizable lateral
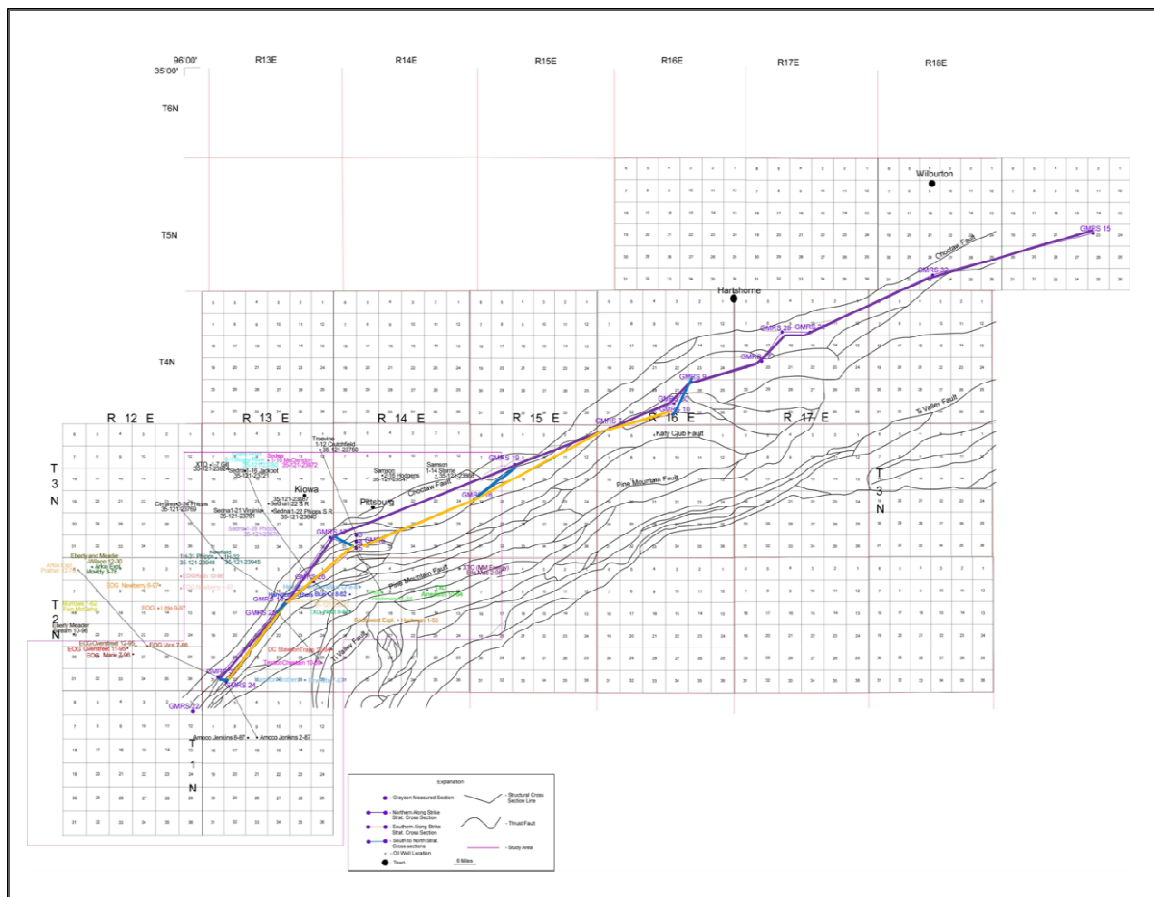


Figure 17: Location map of the stratigraphic cross sections.
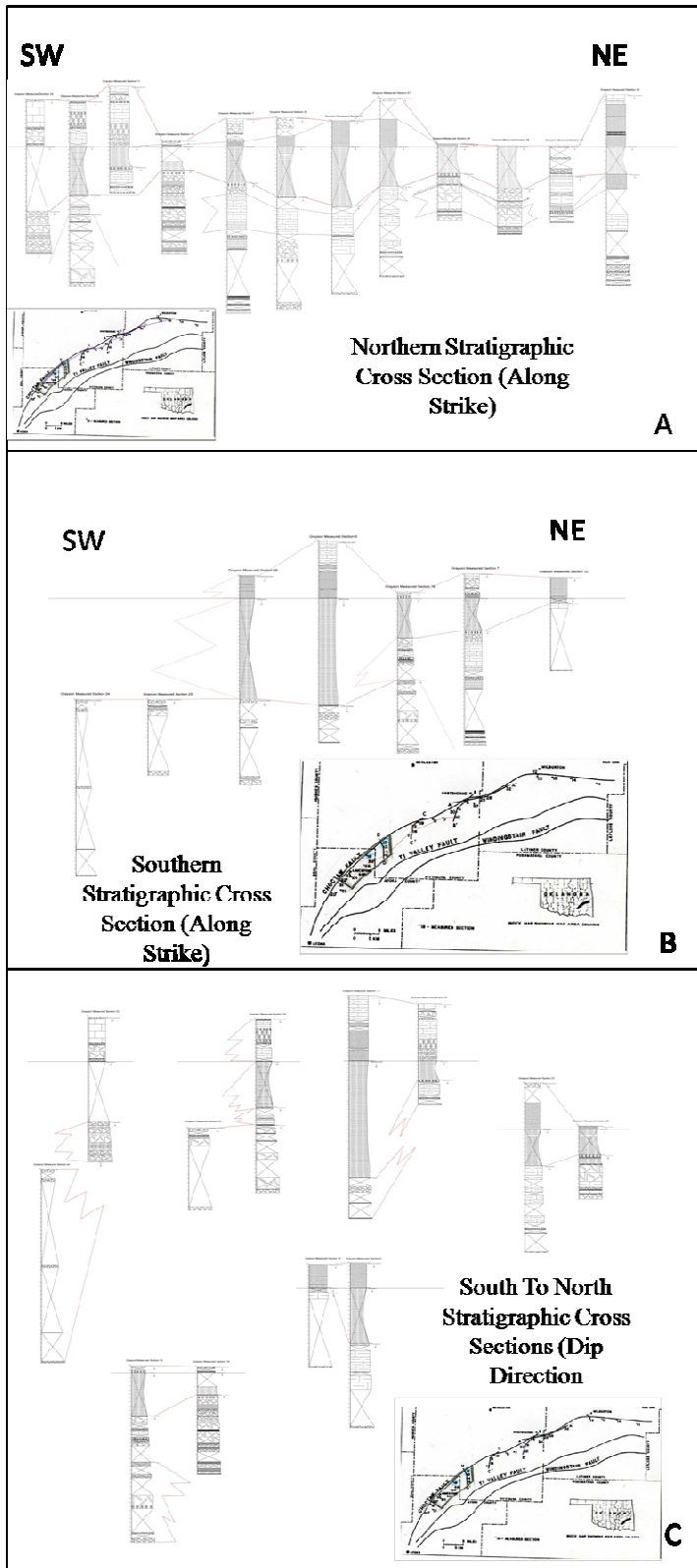
Figure 18: Stratigraphic cross sections developed using the measured sections of Grayson (1980). A) northern along strike cross section (purple line on location map, plate 5), B) southern along strike stratigraphic cross section (gold line on location map, plate 6), C) south to north stratigraphic cross sections (Blue lines on location map, plate 7)

movement within the Ouachita arcuate fold-thrust belt. A more direct measurement of lateral movement is not available within the thesis area, because the fault planes of the thrusts are not exposed. Lateral movement in the frontal belt would effectively rule out the primary arc as the type of arc. The use of a limestone bed for the correlation of the cross sections proved to be the demise of the experiment. The stratigraphic cross sections did show an important fact that Grayson (1980) noticed, which was that the basin in which the limestone formed seemed to deepen toward the west. The stratigraphic cross sections demonstrate that the amount of sandstone decreases to the west, whereas, the amount of spiculite increases.

### 4.4 **Conodont Analysis**

The Upper Morrowan Wapanucka Limestone proved to be too quartz rich to break down effectively. The alternating treatment method described in section 3.4, only produced a few grams of residue from each sample. A total of four conodonts were retrieved from the 56 samples processed, and they were all form the same sample (GMRS 18, CLS 5, Sample # 15'). Therefore, they could not be used to test the presence of lateral movement in the Ouachita arcuate fold-thrust belt. Conodonts were intended to be used to correlate the outcrops at such a detailed level that any lateral movement could be detected. A detailed conodonts collection and analysis should be conducted in future studies to test this hypothesis.

### 4.5 **Thin Section Analysis**

### 4.5.1 Wapanucka Limestone

Thin sections were analyzed to identify microscopic evidence of shearing (grain distortion, granulation, or micro-faulting) within the Wapanucka Limestone. Thin sections prepared in the dip direction were to act as a control, because the Wapanucka Limestone was emplaced in its present location through thrust faulting. Therefore, if there is any evidence of shearing through the distortion of the grains, it should be evident in these thin sections. Thin sections prepared in the strike direction were intended to indentify lateral movement, because consistent lateral movement within the frontal fold-thrust belt of the Ouachitas, along with other lines of evidence, would suggest that the Ouachita arcuate fold-thrust belt was an orocline.

Evidence of shearing in either direction was not observed in the thin sections (Fig. 19). This does not preclude the shearing in the area. The lack of observation could be due to several of reasons, including the proximity of the Wapanucka to the shear zone, the quality of the thin sections, and/or the manner in which the samples were collected. The major reason for the lack of shearing maybe that the Wapanucka Limestone sampled is too distal from the fault planes.

Another reason shearing may have not been observed could be the quality of the thin sections. Several of the thin sections were at a thickness greater than 30µm as evident in Figure 20 (A). The beveled grinder wheel caused an irreversible bevel to the slide, thus half of the slide would be ground down to the point of being unusable, while, the other half would still be several grain layers thick. Plucking of grains was another consistent problem caused by the aforementioned beveling. This not only caused an incorrect point count because of exaggerated pore spaces, it also allowed air to seep
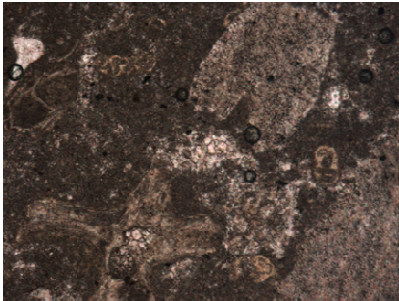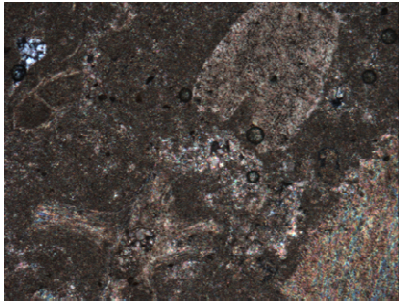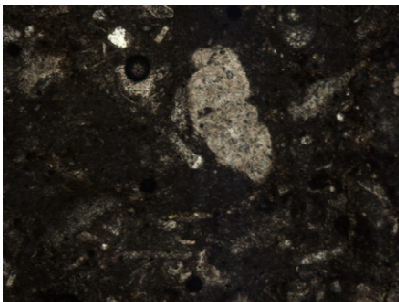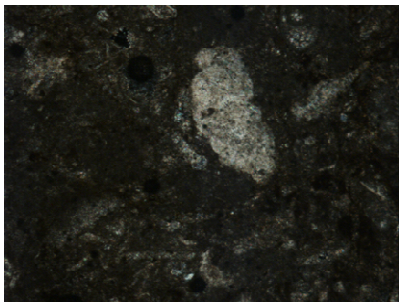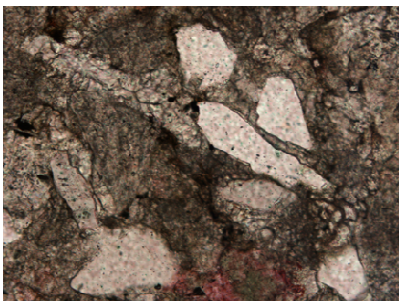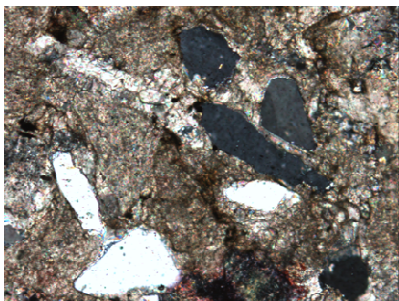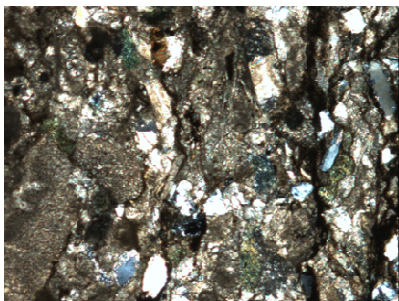
| 0.1 mm | PPL 10X | CPL 10X |
|---|---|---|
| Stop #1 Sample 10.1 <br><br> Strike |  |  |
| Stop #1 Sample 10.1 <br><br> Dip |  |  |
| GMRS #3 CH #4 <br><br> Strike |  |  |
| GMRS #3 CH #4 <br><br> Dip |  |  |

Figure 19: Photomicrographs of representative thin sections prepared in both the strike and dip direction.
Note: There is no evidence of shearing
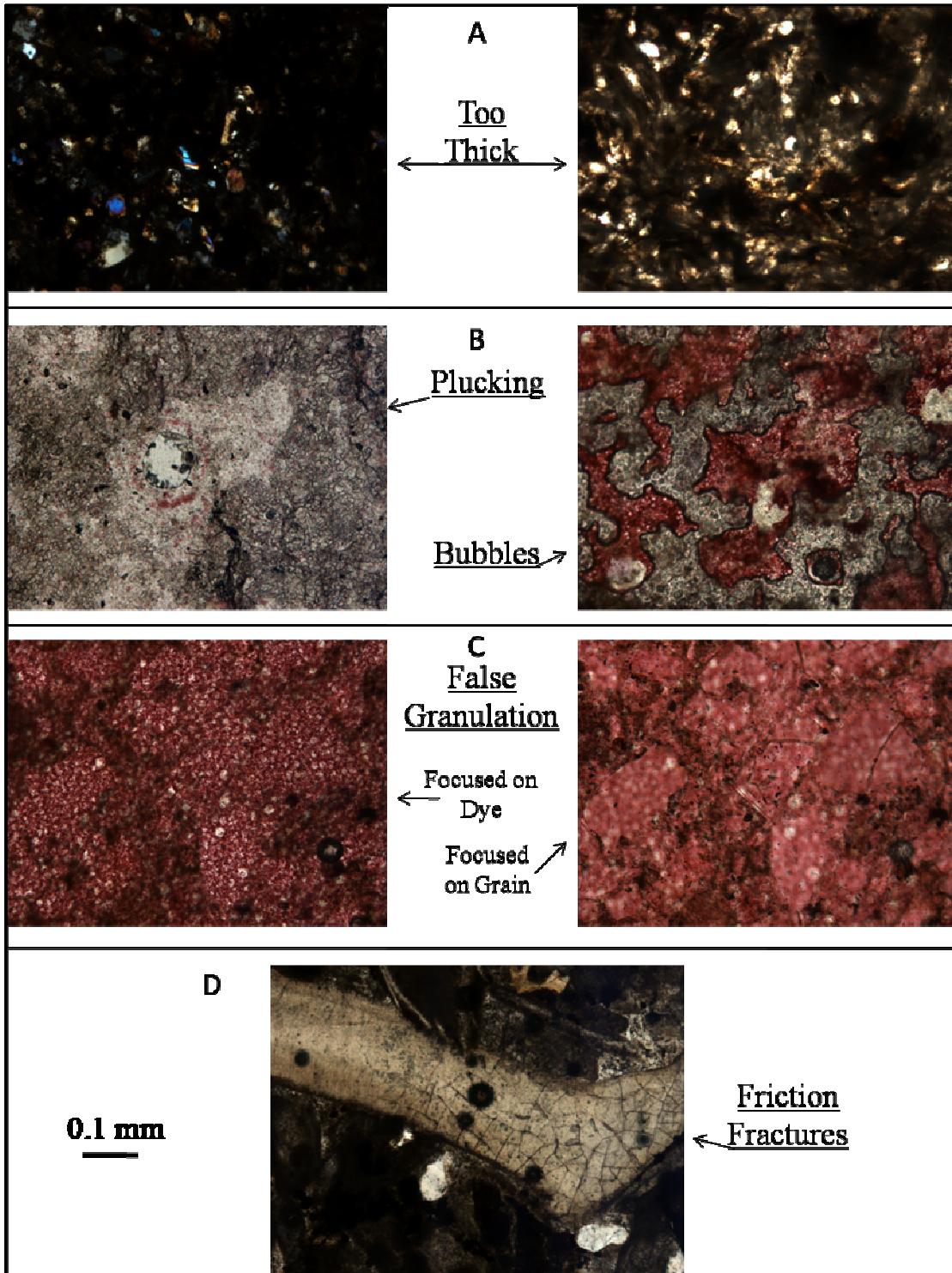
Figure 20: The multitude of problems with handmade thin sections. A) Too thick and multiple layers thick, B) Grain plucking and bubbles caused by plucking, C) False granulation caused by the red dye epoxy, D) Friction induced fractures

between the plug and the slide causing bubbles, or detachment of the thin section entirely (Fig. 20 (B)). The red epoxy used also gave rise to its own problems because it dyed the grains in such a way that they appeared to show evidence of granulation (Fig.20 (C)). Friction generated during the grinding process also led to induced fracturing of grains (Fig. 20 (D)).

The samples were collected in areas where strike and dip measurements were easily obtained (Fig. 21). This generally restricted the collection sites to exposed weathered bedding planes, thus, evidence of shearing may be over-printed by the effects of telegenesis, because sparry calcite is actively replacing all of the constituents of the Wapanucka Limestone (Fig.22). This problem may be resolved, in later studies, by taking a sample from deeper less exposed portions of the outcrop.



Figure 21: Photograph of a well exposed Wapanucka Limestone outcrop. Sampled interval and sample locations are indicated by the arrows.

Figure 22: Photomicrograph showing the gradual replacement of the quartz grains by sparry calcite. The rainbow colored rim around the quartz grains is the sparry calcite.

0.1 mm
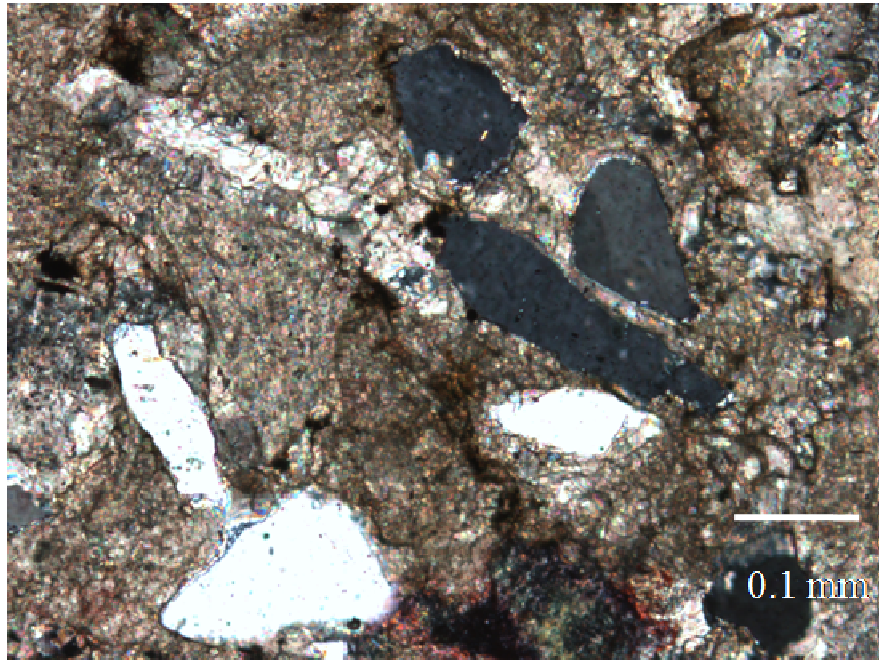
### 4.5.2 **Siliciclastic Samples**

A number of siliciclastic samples where gathered for petrographic analysis of the Upper Morrowan Wapanucka Limestone, the Atokan Formation, and the Lower Desmoinesian Hartshorne Formation. These include 10 from GMRS #3 (Wapanucka), 4 from the Hartshorne sites (Wapanucka), 2 from the Wilburton sites (Atokan), and 3 (Atokan) and 3(Hartshorne) from NW of GRMS #18. There precise location of all of the samples collected is given in Table 1. Many of these samples lacked the competence to be made into thin sections (GMRS #3 samples: BS1sample 2 and $M^1/_3$ sample 2 and all of the siliciclastic samples from the Hartshorne and Wilburton sites). These less competent samples were pulverized and processed for X-ray diffraction analysis, while, competent samples were used for thin section analysis.

There are several reasons why these siliciclastic samples were analyzed. The first

reason was to accurately plot each sample on a ternary diagram in order to identify the source of the sediment. Another reason was to look for clay coatings around the quartz grains. The petrographic analyses of the competent samples show that the samples contain greater than 80% quartz with minute percentages of both feldspar and lithic fragments (Fig. 23). The limited number of samples plotted is not indicative of any source area.

The quartz grains of the basal Atoka unit, the Spiro, within the Wilburton gas field are generally coated by chamosite, which is a shallow marine iron-rich chlorite clay. The depositional range of chamosite is in water less than 150m deep, whereas, its counterpart glauconite is indicative of a deeper depositional environment of ~300m. The
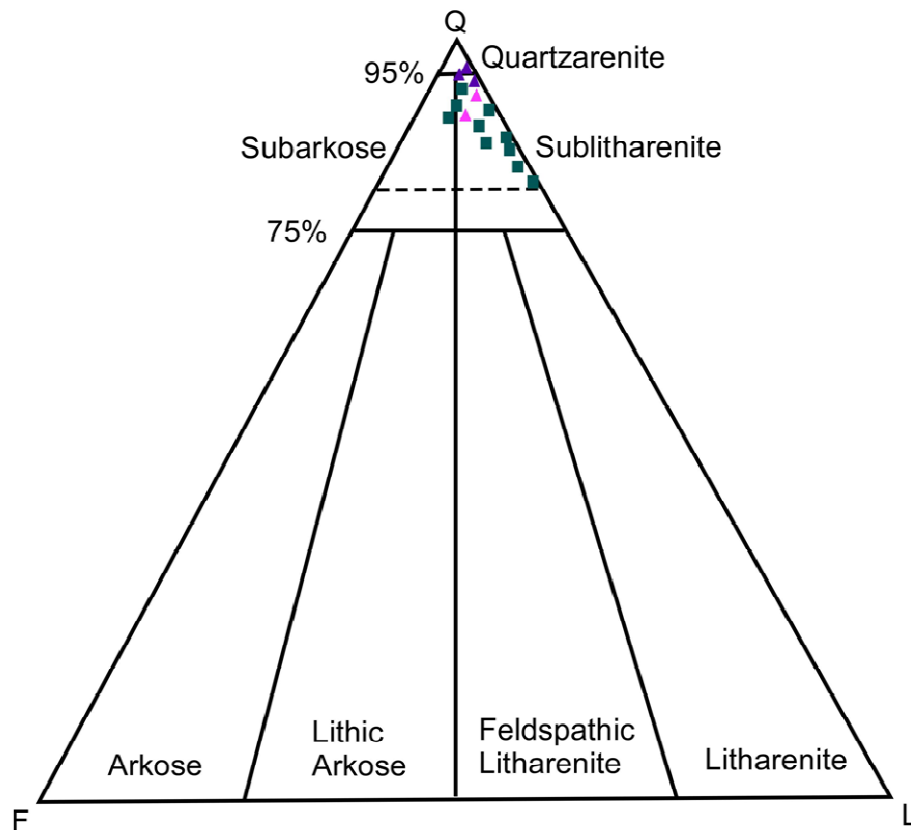


Figure 23: Ternary diagram showing the percentages of quartz, feldspar, and lithic fragmentsin the fourteen siliciclastic samples. (Purple triangles= Atoka, Pink triangles= Hartshorne, Green squares= Wapanucka, dashed line = 80%)

competent siliciclastic samples show no evidence of the presence of chamosite or glauconite (Fig. 24), but the replacement of the quartz grains with sparry calcite (Fig. 22) may overprint the evidence of clay coatings. The less competent siliciclastic samples show no evidence of the presence of chamosite, except Wilburton # 2 collected south of Wilburton, OK (Fig. 25). This sample was collected from an aggregate quarry ~ 2.25 miles south of Wilburton, OK, on State Route 2 (C, NE$^1$/$_4$, sec 29, T5N, R19E).Glauconite, however, is relatively abundant in the Wapanucka Limestone samples (Fig. 26); which indicates the limestones sampled for this study were deposited in deeper water than  the siliciclastic samples.
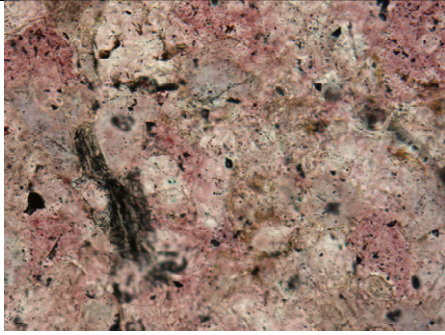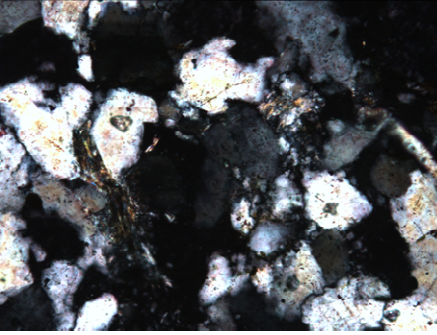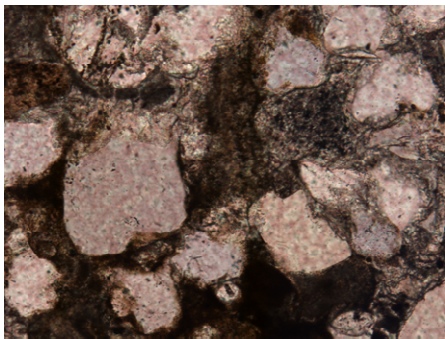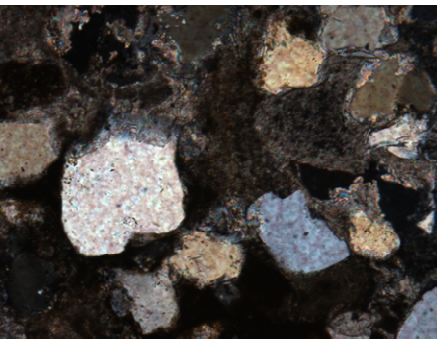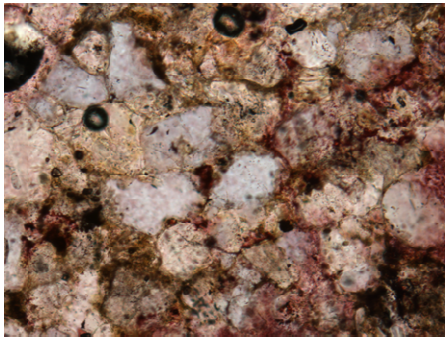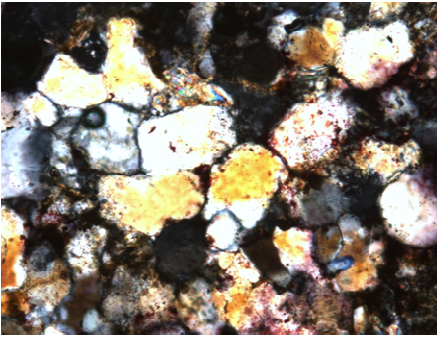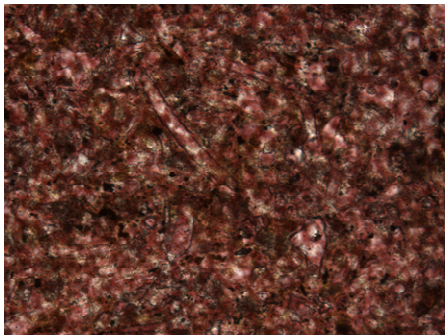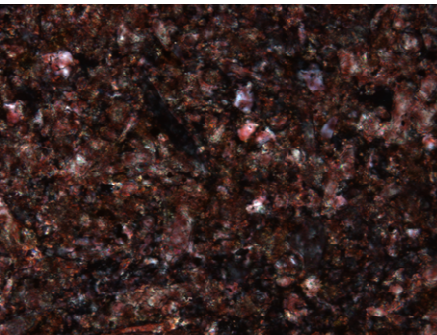
| 0.1 mm | PPL 10X | CPL 10X |
|---|---|---|
| Atoka-CS-2 Sample #1 |  |  |
| Wapanucka GMRS #3 FW-1 |  |  |
| Hartshorne Ridge 1 Sample a |  |  |
| Wapanucka GMRS #3 TS-2 |  |  |

Figure 24: Photomicrographs of select siliciclastic samples.
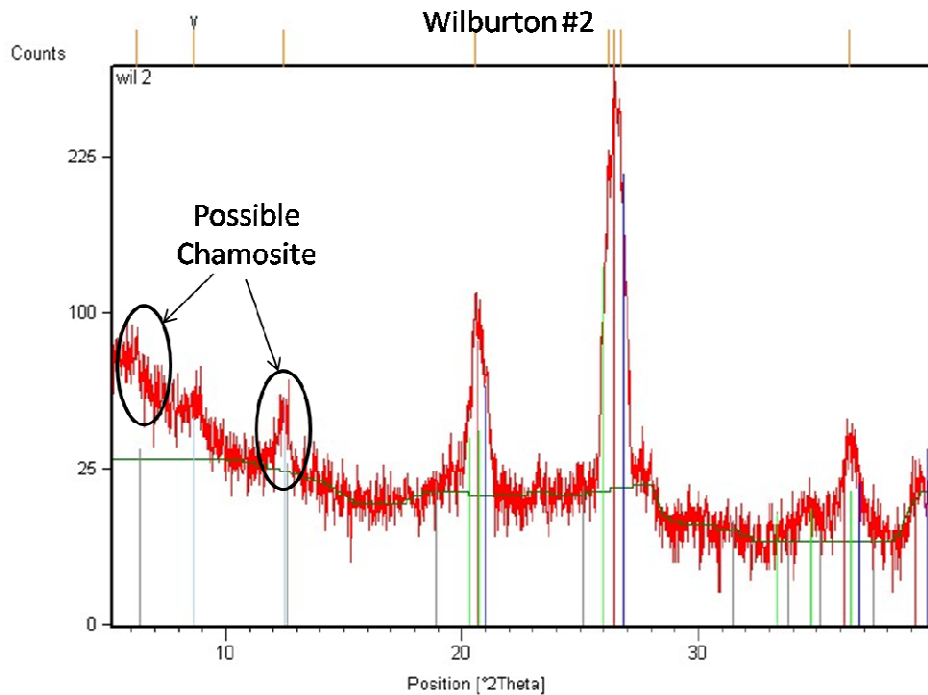
Figure 25: The results for the X-ray diffraction analysis of Wilburton #2, taken ~ 2.25 miles south of Wilburton, OK, on State Route 2. This is the only sample that shows any indication of Chamosite
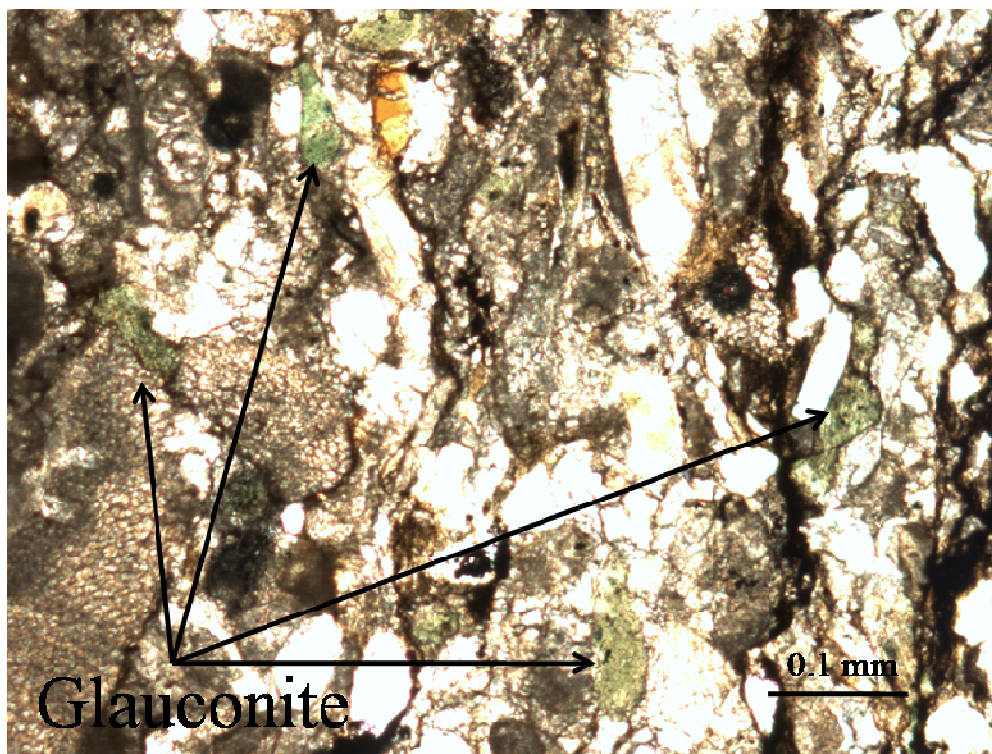


Figure 26: The glauconite grains are the light green grains speckled throughout this thin section. (GMRS # 3 sample CH#4)

CHAPTER 5

NATURE OF THE OUACHITA ARCUATE FOLD-THRUST BELT

The data generated and collected during this investigation is insufficient to make conclusive remarks on the Ouachita arcuate fold-thrust belt. However, the following conclusions can be suggested on the arc-type, structural features, and provenance of the sedimentary rocks in the area.

5.1 **Arc Type**

Arc type studies require vast amounts of data including, for example, the examination of displacement vector maps, paleomagnetic studies, and paleo-stress studies. The ability to acquire such data was simply beyond the scope of this study.

However, there was one characteristic of the different arc types that could be tested with simple field examinations, and, that is the along strike lateral movement involved in an orocline. If lateral movement exists, then, it should be evident along the fault planes within the frontal belt. Since the fault planes are covered within the Ouachita Mountains, this study was designed to indirectly investigate the along strike lateral movement, both macroscopically and microscopically, through the examination of the Wapanucka Limestone because of its competent nature.

The macroscopic correlation of Wapanucka Limestone was the first step in this study (Fig. 18, plates 5, 6, and 7 ). Attempts were made to correlate the formation both in the strike direction and in the dip direction. This study was designed to allow for the recognition of large scale (greater than a kilometer) lateral movement. The organic nature

of the limestone made the macroscopic correlation of the Wapanucka Limestone inconclusive; thus, a more detailed approach was designed.

The use of conodonts has been proven to be effective in correlating limestone units. Therefore, numerous samples of the Wapanucka formation were collected from several outcrops along the frontal belt for the purpose of collecting conodonts. The inability to collect the conodonts is documented in the prior section (4.4). The attempted conodont correlation of the Wapanucka did not produce any usable results.

The macroscopic correlation, however, did show that the Wapanucka Formation in the study area was deposited much more basinward than the Wapanucka to the northeast near the towns of Hartshorne and Wilburton, OK. This conclusion was based on both the increase of the Chickachoc Chert unit and the decrease of sand in the Upper sandstone/Limestone unit to the southwest. The Chickachoc Chert unit is made up of mainly Spiculite, which is a sponge spicule chert deposited either on the continental slope or the abyssal plain. This basinward shift in the Wapanucka shows that there is increased displacement in the study area as compared to the Hartshorne/Wilburton area. Therefore a lateral displacement may be suggested between the Hartshorne/Wilburton area and the thesis area.

Lateral movement along strike should leave evidence of shearing, which is commonly in the form of slickensides along fault planes, but, without an exposed fault plane in the study area this evidence is not readily available. Thus, a study was designed to look for microscopic evidence of shearing (distorted grains, granulation, and/or micro-faults) in the only competent formation in the study area, the Upper Morrowan Wapanucka Limestone. Thin sections were attempted of all 74 hand samples collected

from the Wapanucka Formation.  No evidence of shearing was visible in the thin sections, in either the strike or dip direction (Fig. 19). The lack of evidence of shearing in the strike direction would lead to an assumption that the Ouachita arcuate bend is a non-rotational/primary arc, however, the lack of shearing in the dip direction shows that the shearing involved in the emplacement of the limestone lacked the energy to imprint itself on the constituents of the Wapanucka Limestone.

5.2 **Balanced Structural Cross Sections**

Balanced structural cross sections consistently spaced along the Ouachita frontal fold-thrust belt account for the rapid changes in thrust geometry; thus, one structural cross section was constructed for this study using the available data (Fig. 16). This cross section shows that a southeast dipping imbricate fan is the dominant fault geometry for the frontal fold-thrust belt in the study area in the hanging wall of the leading-edge thrust, the Choctaw Fault.  This geometry is compliant with other fault geometries seen in published balanced structural cross sections northeast of the study area (Fig. 34). The differences between this structural cross section and the published cross sections include: 1) the detachment surface is shallower, because it has jumped up to the Atoka Formation rather than the Devonian Woodford or the Morrowan Springer and 2) the presence of a duplex structure or a triangle zone cannot be confirmed.

5.3 **Provenance**

The fourteen competent siliciclastic samples gathered for this study were point counted and the results were plotted on QFL ternary diagrams (Fig. 23). The results were

compared to the findings of Mack et al. (1981), Carlson (1989), and Graham et al. (1976), to determine the provenance of the siliciclastic sediment in the study area (their ternary diagrams are presented in Appendix B). The limited number of siliciclastic samples collected for this study left the comparisons inconclusive (Fig. 27). The source area cannot be determined without further studies.
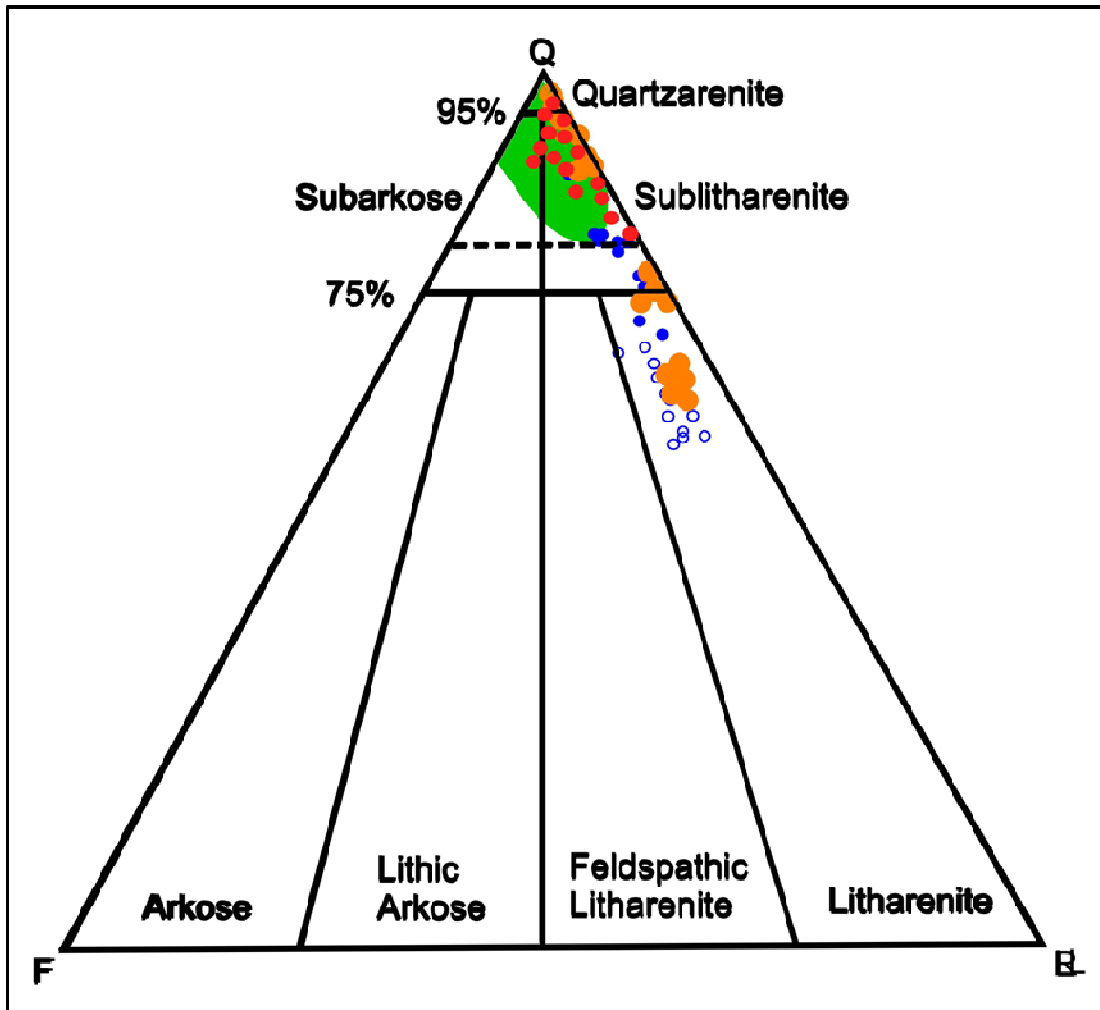


Figure 27: A comparison of the ternary diagrams listed in the text. The samples for this study are the red solid circles. Mack et al., (1981) are the orange solid and open circles. Graham et al., (1976) are the blue solid and open circles. Carlson, (1989) is the green shaded area. The red circles comparable to Mack and Carlson's results but fit neither close enough to be definitive. This study's results do not compare well with that of Graham et al., (1976).

CHAPTER 6

ROLE OF THE SUBDUCTION ZONE IN THE DEVELOPMENT OF ARCUATE
FOLD-THRUST BELTS

The most fundamental feature of any fold-thrust belt is the type of subduction

zone involved in its formation. The subduction zone type can affect every aspect of a

fold-thrust belt including: its duration, structural style, sedimentation, volcanism,

ophiolite obduction, and possibly the shape of the subducted plate (arcuate or straight).

Therefore, the type of subduction zone responsible for each of the orogenic belts has to

be established before comparisons can be conducted.

6.1 – **Chilean-Type vs. Mariana-Type**

A subduction zone is the zone of plate consumption along convergent plate

boundaries. A convergent plate boundary is where two or more plates collide. This

collision causes one plate to plunge under the other plate. Generally, the density

difference between the two plates determines which plate plunges under the other.

Uyeda, (1982) stated that:

"There are two end member types of subduction zones, and they are the Chilean-
type and the Mariana-type (Fig. 28). The fundamental differences between the two are
the stress regimes in the back arc region and the coupling strength of the plates involved
in the subduction. The Chilean-type has a compressive stress regime in the back arc basin
and the overriding plate is strongly coupled to the subducted plate; while, the Mariana-
type has a tensional stress regime in the back-arc region and the two plates are weakly
coupled.
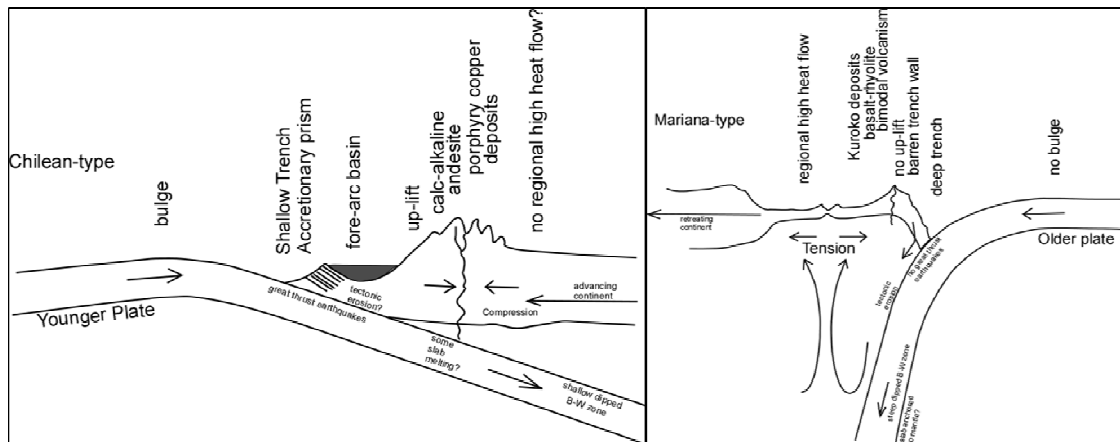
Figure 28: The two end member types of subduction zones along with their unique characteristics.(Modified from Uyeda, 1982)

The two different end members have several other subtle differences which allows for further distinctions between the two. The first is that the large earthquakes of magnitude greater than 8.0 only occur along Chilean-type subduction zones. Secondly, the trench associated with the Chilean-type subduction zone is notably shallower than that of the Mariana-type. The accretionary wedge of the Chilean-type is poorly developed; whereas, it is well developed along Mariana-type subduction zones. Thirdly, horst and graben structures of the subducted plate seem better developed on Mariana-type zones (Uyeda, 1982). The fourth notable difference is that there is no oceanic crust present is the fore arc of Mariana-type zones.  The fifth distinction is that calc-alkaline andesites are more prevalent along Chilean-type zones. Finally, porphyry copper mineralization is favored by compressive tectonic stress of the Chilean-type subduction zones whereas massive sulfide mineralization is favored by submarine hydrothermal activities in the rift-like situations of the back arc regions of the Mariana-type subduction zones (Uyeda, 1982)."

There are two questions that the theory proposed by Uyeda, (1982) does not answer completely. What accounts for the two distinct coupling strengths, and what provides the heat needed to make the back arc of the Mariana-type subduction zones extensional? Uyeda, (1982) has proposed several theories to answer these problems.

"The difference in coupling strength is due to one of the following or combination of the three: 1.) subduction zones have stages they start out Chilean-type and as they progress they move to a more Mariana-type (dip of the subducted plate increases as it moves down), 2.) The age of the subducted plate (the older and denser the plate faster it subducts), 3.) the direction of plate movement (if the subducted plate moves toward the subduction zone then it is Chilean, whereas if it moves away then it is Mariana). The second question that was left unanswered by Uyeda, was what provides the heat? He

offered two possible explanations from various thermal-mechanical models: 1.) frictional heating along the subducted plate gives rise to enough magma to cause rifting in the back arc, 2.) the formation of a secondary convection cell in the mantle wedge."

6.2 - **East Directed Vs. West Directed Subduction Zones**

The outstanding questions of Uyeda, (1982) have been answered by Doglioni et

al., (1999). Doglioni et al., (1999) stated that:

"Subdduction Zones appear primarily controlled by the polarity of their direction, i.e., W-Directed or E- to NNE-directed, probably due to the westward drift of the lithosphere relative to the asthenosphere (Doglioni et al., 1999). The west directed subduction zones are equivalent to Uyeda's Mariana-type subduction zones, and the east to NNE-directed subduction zones are equivalent to the Chilean-type subduction zones. The main control of subduction is the density difference between the two colliding plates. Therefore, when a denser oceanic lithosphere is located west of a lighter one, the subduction will dip to the east, and vice versa (Doglioni et al., 1999).
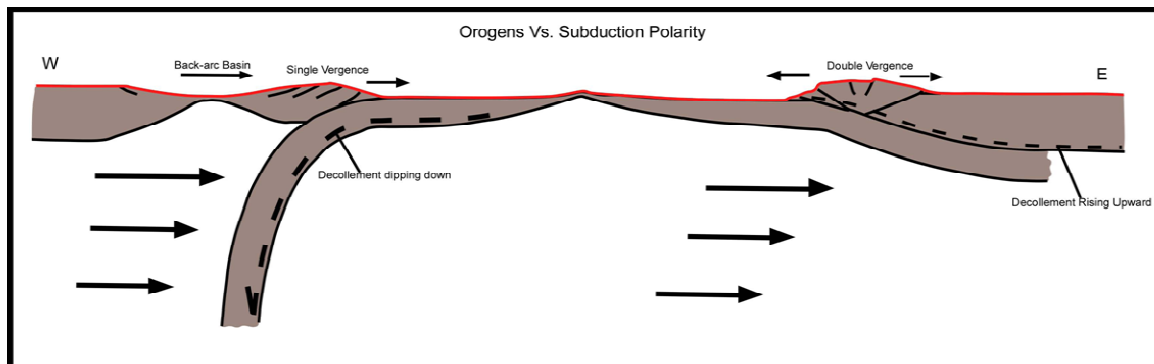


Figure 29: A diagram of a W-directed subduction zone and an E-NNE directed subduction zone (Modified from Doglioni et al., 1999)

West directed subduction zones are short lived (30-40 Ma) tectonic features. They are marked by an eastward propagating low relief structural wave. The subducting plate associated with a west directed subduction zone opposes the general flow of the upper mantle (Fig. 29). The majority of the plates flow to the west, thus the mantle has an eastward counter-flow. The subducted plate enters the upper mantle and is subsequently pushed eastward by the pre-mentioned mantle flow; therefore, steeping the dip of subducting plate. The west directed plate also generates a mantle plume under the

hanging wall because the asthenoshpere ride up the subducted plate like a ramp. The steeping of dip and the presence of a mantle plume answer both of the lingering questions about a Mariana-type subduction zone left by Uyeda. All W directed subduction zones generate a concave depression in the subducted plate, thus adding a little more proof that the subducted plate impedes the eastward mantle flow (Fig. 30).
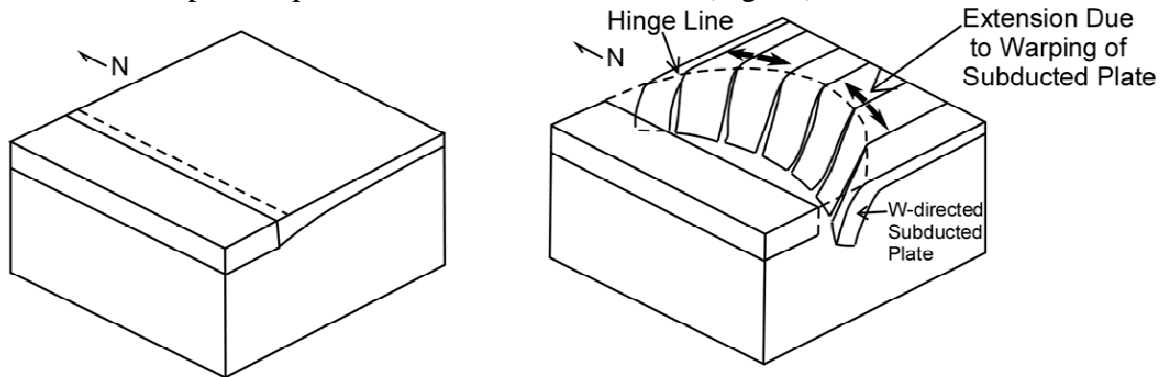
Figure 30: A diagram showing how a subducting plate may bow as it is being subducted. (Modified from Doglioni, 1999)

East directed subduction zones have a longer life span (100+ Ma) than that of the West directed subduction zones. This type of subduction zone is marked by topography and structure that is rapidly growing upward and outward. The dip of the subducting plate is synthetic to the mantle flow discussed earlier; therefore, when this plate is pushed eastward it is pushed up along the bottom of overriding plate. Thus answering the question about the coupling strength of the Chilean-type subduction zone  (Fig.29)."

CHAPTER 7

REVIEW OF LITERATURE ON THE ARCUATE FOLD THRUST BELTS

The review of literature is an important aspect of this study, because it allows for the examination of the five comparable criteria, listed in the statement of purpose. The major problem with this approach is that many studies are conducted in such a specific way that their results and interpretations become cumbersome outside the arc itself unless the same data set is available for all the arcuate bends being compared. This problem was alleviated by making the five comparable criteria broad in meaning, so that the data needed can be reconciled from existing literature. Each of these individual criterions is investigated further, as it pertains to the aforementioned arcuate bends, in the subsequent sections.

**7.1 The Ouachita Mountains**:

7.1.1 - Location:

The Ouachita Orogenic Belt stretches from central Mississippi to Northern Mexico (Fig. 1(A)).  Most of the orogenic belt is buried beneath a sedimentary cover, but it is exposed in two places, the Ouachita Mountains and the Marathon Uplift. The Ouachita Mountains extend from Central Arkansas into Southeastern Oklahoma (Fig.1 (B)).

7.1.2 - Timing:

The evolution of the Ouachita Orogenic Belt began with the breakup of the super-continent, Rodinia, in Latest Proterozoic. The breakup of the super continent Rodinia

created the Iapetus Ocean, and left a passive continental margin along the southern edge

of the North American Craton (Houseknecht, 1987). The exact type of passive margin is

the subject of much debate. Atlantic-type vs. Transform-type rift margin has a profound

effect on the geometry the southern coast line of the North American Craton. If the

margin was the

typical Atlantic-type

rift margin, then the

unique shape of the

Ouachita Orogenic

Belt was developed

during collision,

because the southern
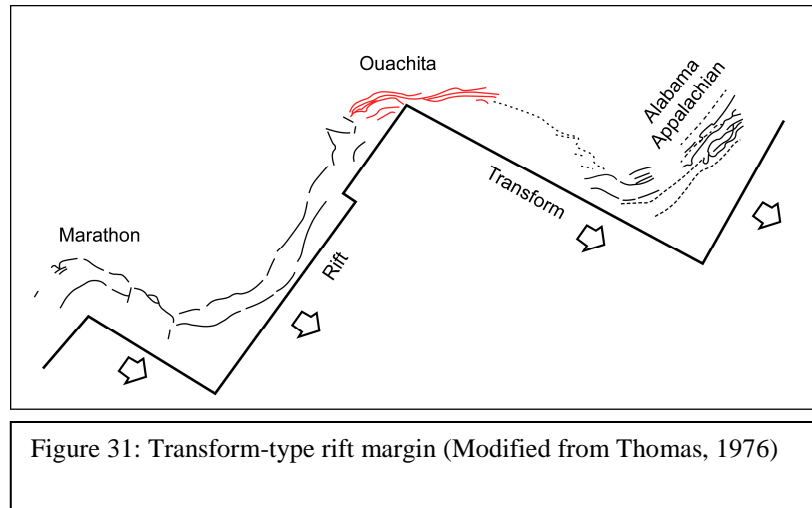


Figure 31: Transform-type rift margin (Modified from Thomas, 1976)

coast would have been relatively straight. If the passive margin was a Transform-type as

presented by Thomas, (1976 & 2005) then the initial rifting in the late Proterozoic is

responsible for the unique geometry of Ouachita Orogenic Belt (Fig. 31). Either way,

during most of the Paleozoic a rifted passive margin reigned over the southern coast of

the North American Craton (Fig.32 (A&B)).

According to Houseknecht, (1987):

"Beginning in the Late Paleozoic, the Iapetus ocean basin began to close (Fig.32 (C)). Although it is impossible to determine precisely when subduction began, it is clearly under way during the Mississippian, as suggested by detritus indicative of an orogenic provenance, locally abundant volcanic detritus in the Stanley Formation of the Ouachitas, and a significant increase in sediment accumulation rates in the deep Ouachita Basin (Houseknecht, 1987). The subduction zone consuming the ocean basin was a southward directed subduction zone pulling the oceanic crust of the Iapetus Ocean Basin beneath Llanoria. Llanoria is a generic name given to the land mass that collided with the southern margin of North America, because it is unclear whether this landmass was a fragment (micro-continent) or the South American Plate. The subduction continued
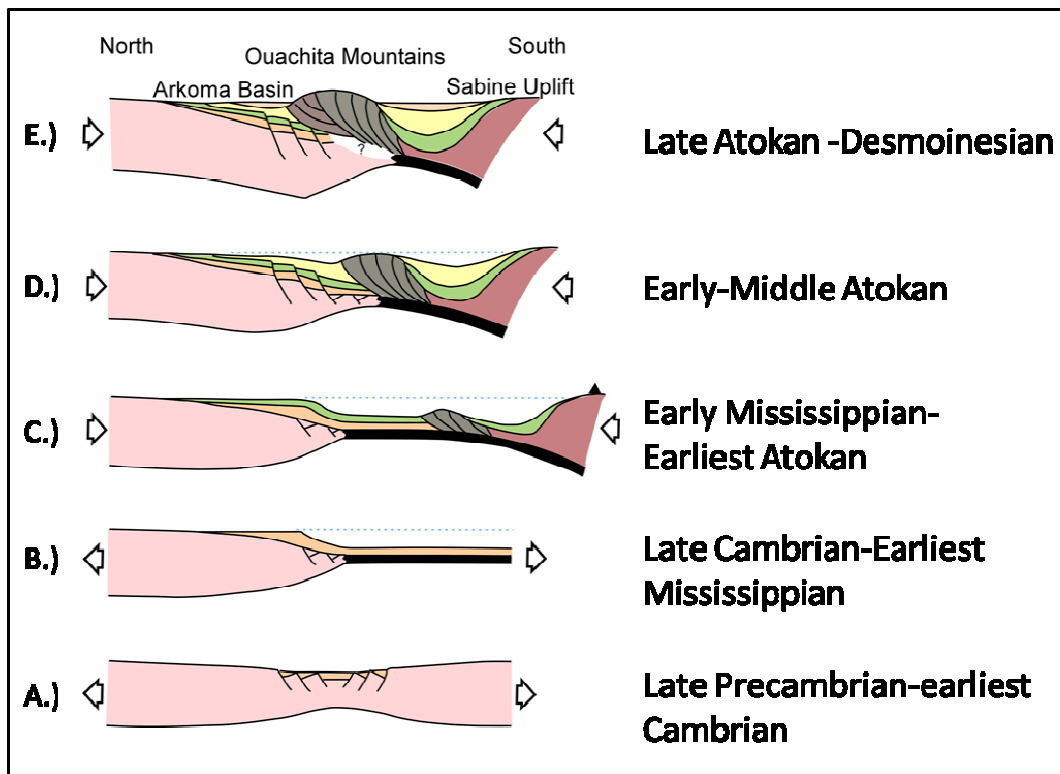
Figure 32: Schematic cross sections depicting the history of the Ouachita Mountains. (Modified from Houseknecht, 1987)

throughout the Mississippian and into the earliest Pennsylvanian (Fig. 32 (C)). During this time, 5 km of sediment was deposited in the trench and ocean basin in front of the advancing subduction zone. The Stanley, Jackfork, and the Johns Valley formations record the history of this time period.

The Iapetus Ocean basin was totally consumed by the early Atokan, and the subduction complex was being obducted onto the passive North American margin (Fig. 32 (D)). The downward pulling of the continental crust into the subduction zone and the vertical loading of obducted material caused the continental crust along the southern margin of North American Craton to be subjected to flexural bending. As a result of this down warping many along strike normal faults developed. These faults affected the entire crustal thickness up to the Atoka. Once, these normal faults broke the sediment accumulation and subsidence rates increased markedly (Houseknecht, 1987) (Fig. 37). The sedimentation at this time was predominantly along the axis of the Ouachita Orogenic Belt, from east to west.

The passive margin tectonics ended by the Late Atokan, when foreland-style thrusting was initiated. The continued uplift of accreted material caused the formation of a peripheral foreland basin. The down to the south normal faulting no longer dominated the subsidence; rather, it returned to a more flexural subsidence induced by thrust fault loading. The foreland basin continued to fill through the rest of the Atokan time and into the Desmoinesian time. At that time, the gross structural configuration of the Arkoma –

Ouachita system was essentially the same as at present (Houseknecht, 1987) (Fig. 32 (E)).”

7.1.3 Palinspastic Maps

The palinspastic maps that will be used in the comparisons are from Northern Arizona University's web site (http://jan.ucc.nau.edu/~rcb7/340Nat.jpg) (Fig. 33). These palinspastic maps are drawn in such way that the angle of the North American Plate in relation to the equator is easily discerned. This angle is important in determining which type of subduction zone was present during the Ouachita Orogeny.

Figure 33: Palinspastic maps depicting the Ouachita Orogeny. The angle of the North American Plate (NAM) relative to the South American Plate (SAM) is clearly visible in these maps, along with their relative latitudinal location. (Modified from Ron Blakely's tectonic evolution of North America maps, Northern Arizona University)

7.1.4 – Balanced Structural Cross Sections:

The balanced structural cross used in this study are limited in area covered and size. Most of the cross sections developed by the Structural Group of the Boone Pickens' School of Geology, Oklahoma State University, focus mainly around the Wilburton Gas Field, Pittsburg Co., Oklahoma; therefore, their application to a large regional study such as this is limited. The correctness of the geometries established within these cross sections, have been backed up by the high resolution 3D seismic used in Parker, (2007) and Sadeqi, (2007), thus the use of an older less correct cross section would not be prudent.

The balanced structural cross sections that will be used in this study are presented, along with location maps and proper citation, in Figure 34. They generally only cover the
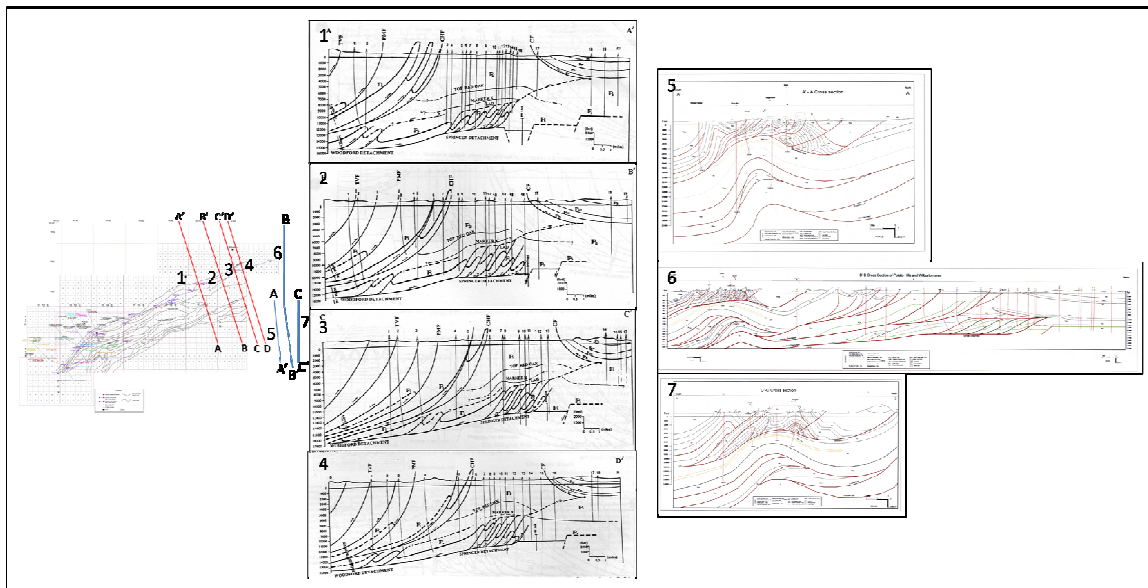


Figure 34: Seven balanced structural cross sections from the literature and close to the study area. Their locations are plotted on my location to minimize confusion. Cross sections 1-4 are from Cemen et al., 2001. Cross sections 5-7 are from Kaya, 2004.

frontal belt of the Ouachita Mountains; therefore, a simplified regional structural cross section will also be used in this study (Fig. 35).
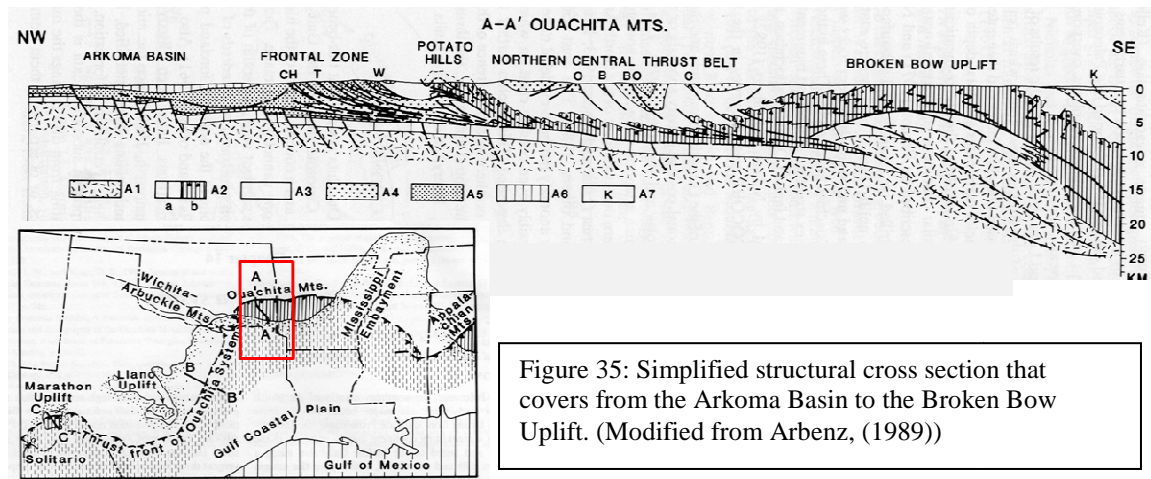


Figure 35: Simplified structural cross section that covers from the Arkoma Basin to the Broken Bow Uplift. (Modified from Arbenz, (1989))

### 7.1.5 - Arc Type:

The arc type has not been established in the literature for the Ouachita Mountain Arcuate Belt.

### 7.1.6 - Sedimentation:

According to Houseknecht, (1987):

"Sedimentation was continuous along the southern passive rift margin of the North American Plate up to the culmination of the Ouachita Orogenic Belt. The Precambrian to Cambrian sediment is only locally present in rift basins associated with the rifting that generated the passive margin. The typical sedimentation along a passive margin is dominant throughout the majority of the Paleozoic. The sedimentation habits only change once subduction is induced during the Mississippian. The deposition changes from an open ocean basin setting to a more restricted remnant ocean basin to finally a shallow marine setting towards the end of the subduction."

The Stanley, Jackfork, Johns Valley (Wapanucka locally), and the Atoka, are the formations that mark this transformation (Fig. 14). They are also the formations that make up the bulk of the central Ouachita Mountains. The Early Pennsylvanian formations

are the dominant formations in the study area; therefore, they are the units that I am going

to focus on, the Wapanucka Limestone (Upper Morrowan) and the Atoka Formation

(Atokan).
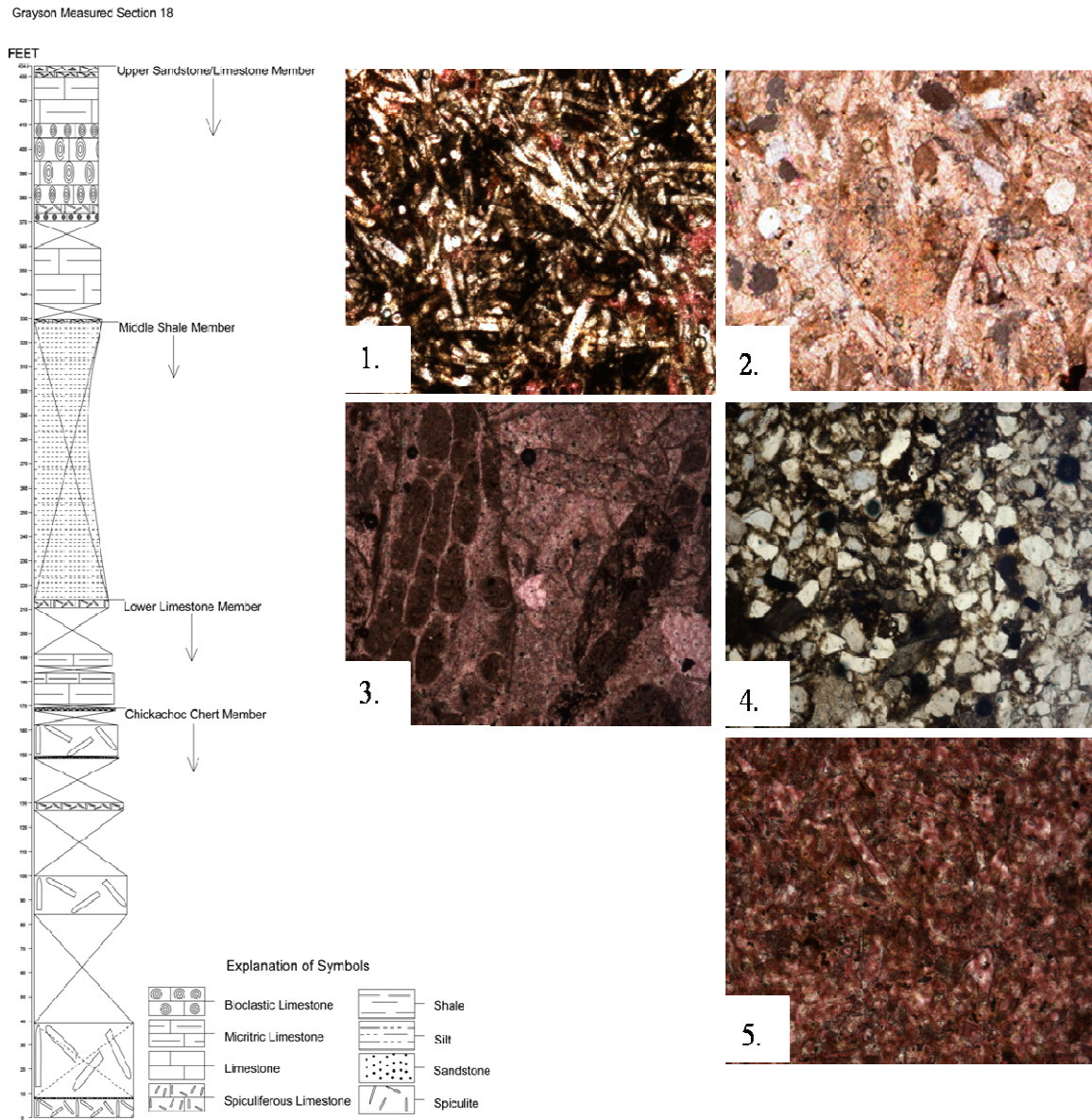


Figure 36: The Wapanucka Limestone at Grayson's measured section #18. This outcrop has all four units: the Upper Sandstone/Limestone Member, the Middle Shale Member, the Lower Limestone Member, and the Chickachoc Chert. Photomicrographs: 1) Spiculite under 10X magnification and PPL, 2) Spiculiferous Limestone under 10X magnification and CPL, 3) Bioclastic Limestone under 10X magnification and PPL, 4) Sandstone under 10X magnification and CPL, 5) Siltstone under 10X magnification and CPL.

Grayson, (1980) described the Wapanucka Limestone as follows:

"The Wapanucka Limestone is a thick (up to 500 ft) limestone unit consisting of four members and they are (from bottom to top): the Chickachoc Chert Member, the Lower Limestone Member, the Middle Shale Member, and the Upper Sandstone/Limestone Member (Fig. 36 and plate 10). The Chickachoc Chert member is the lowest member in the Wapanucka Limestone and it consists mainly of Spiculite. Spiculite is a dense blue/gray chert that is made up sponge spicule detritus (Fig. 36 (1) and plate 8). The Lower Limestone Member is mainly made up of a combination Spiculiferous Limestone and Bioclastic Limestone. The main difference between these two members is the constituents that make up the rock. Spiculiferous Limestone has a majority of spicule debris; while, the Bioclastic Limestone is made up of carbonate shell fragments (Fig 36 (2&3) and plate 8). The Middle Shale Member is generally covered in outcrop and has never been described in the literature.
The Upper Sandstone/Limestone Member is made up of the same beds as the Lower Limestone member with a few layers of inter-bedded sandstone (Fig. 36 (4) and plate 8).The sandstone beds are generally fine grained carbonate cemented quartz arenites with layers of bioclastic debris interbedded locally. For a more detailed description of the Wapanucka Limestone refer to Grayson, (1980)."
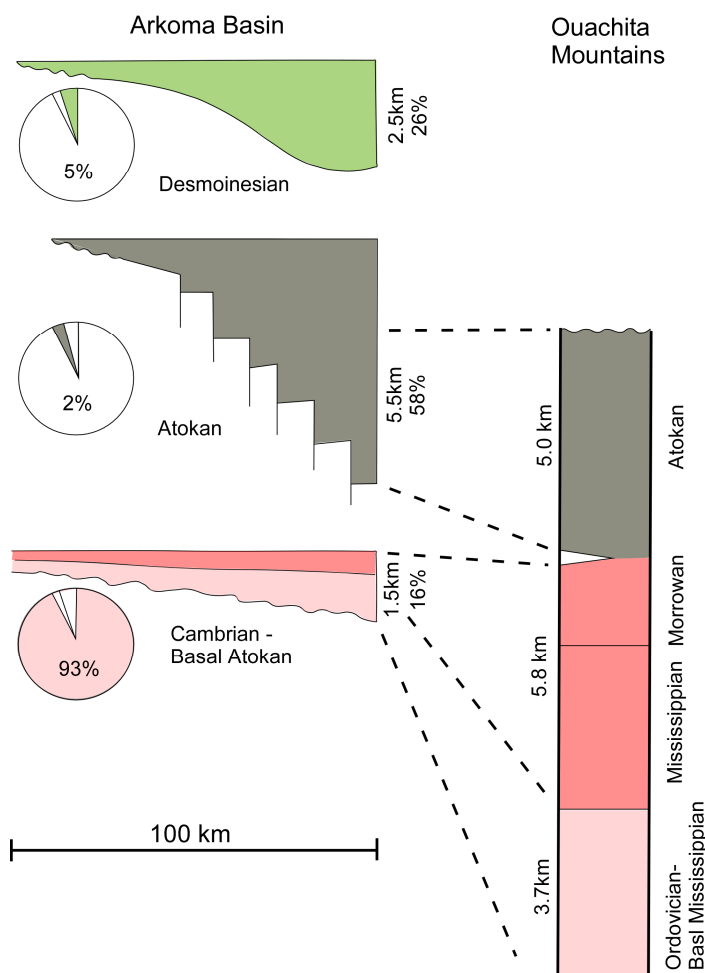


The most important and wide spread formation along the Ouachita frontal belt is the Atoka Formation.

Figure 37: This diagram demonstrates the amount of deposition that occurred during the Ouachita Orogeny. The pie charts show the amount of time each depositional episode was responsible for during the orogeny. (Modified from Houseknecht, 1987)

Houseknecht, (1987) stated that:

"This formation was deposited during the normal fault controlled subsidence; therefore, the sedimentation rates and formation thickness are the greatest of any formation within in the stratigraphic column. Across the Arkoma basin the Atoka thickens from 3,900 ft. to more than 18,000 feet, with syndepositional normal faults accounting for most of the increase (Houseknecht, 1987). These normal faults allowed for an extreme increase in accommodation. The sedimentation rates for the Atoka was on the order of 1000 (Ouachitas) to 1100 (Arkoma) m/my. By comparison, the Spiro (basal unit of the Atoka) had a sedimentation rate of only 7 m/my in the Arkoma Basin and the Jackfork had a sedimentation rate of 420 m/my within the Ouachita Orogenic Belt(Fig.37)."

The basal unit of the Atoka Formation is the Spiro Sandstone. This sandstone unit represents a shoreline deposit that has been reworked into a sheet-sand that inter-fingers with the Wapanucka Limestone to the west. This inter-fingering has lead to many doubt whether or not the Spiro is true the basal unit of the Atoka Formation, or rather a facies change of the Morrowan Wapanucka Limestone. No type locality has ever been described for the Atoka Formation. However, it is generally accepted that the Spiro Sandstone is the basal unit of the Atoka Formation. There are several aspects of the Atoka that are well established. These include: 1) it is sourced from the Black Warrior basin to the east and 2) the majority of the Atoka Formation is made up of turbidite deposits with periodic deltaic deposits.

7.1.7 - Associated Faults:

There are two main types of faults associated with the Ouachita fold-thrust belt, in the Ouachita Mountains, other than the south dipping imbricate fans that make up the hanging wall of the Choctaw fault zone (Fig. 34). The first one is the down to the south normal in the footwall of the Chaoctaw fault zone. The other one is the north dipping

back-thrust (Carbon Fault) located just north of the leading edge thrust, the Choctaw
Fault.

7.1.8 - Basin Type:

The Arkoma Basin is recognized as the foreland basin for the Ouachita Mountain
portion of the Ouachita Orogenic Belt, but there is neither a back-arc basin nor a fore-arc
basin recognized for the Ouachita Orogenic Belt.

7.2- **Jura Arc**

7.2.1 - Location

The Jura Arc or Jura Mountains of Central Europe (Fig. 2 (1)) is the youngest
fold-thrust belt of the Alps. It is located in the northwestern portion of the Western Alps'
foreland basin, the Molasse Basin. The Jura Mountain chain is oriented roughly northeast
to southwest, but it exhibits a $90^o$ rotation along strike. Meaning, that its eastern limb
strikes E-W; while, its western limb strikes N-S.

7.2.2 - Timing

 The Jura arc was formed during the last Alpine compressional event, Middle to
Late Miocene (~12 to 3 Mya). However, Homberg et al., (2002) state that:

"The Jura Arc had under gone three prior structural deformation episodes during
the Cenozoic. The Eocene is marked by N-S strike-slip regime. This stress regime
generated NNE-SSW strike slip faults in the external central Jura region along with a few
E-W reverse faults in the eastern Jura near the frontal thrust (Homberg et al., 2002).
During the Oligocene, an extensional stress regime reigned, and it generated numerous
normal faults. They were orient N-S and NE-SW along the external portion of the arc but
moved to a more WNW-ESE trend along what will be the frontal thrust area. The third
deformation episode occurred during the Miocene and it is marked by the return of a

compressional stress regime. It started with strike-slip faulting but culminated with thrusting. The strike-slip regime prevailed throughout the whole belt, with a fan shaped distribution of compression directions (Homberg et al., 2002). The fan shaped displacement generated tear faulting, thus around these fault the stress regime moved from being compressional toshear in areas already weakened by tectonism. The final deformation phase began with increasing stress from the Alpine region pushing northward ultimately creating a reverse thrust stress regime in the central Jura Belt. Homberg et al., 2002, shows that the strike and dip of the Miocene reverse faults identically match that of the Oligocene normal faults."

Palinspastic maps of the belt show the influences of the three tectonic phases (Fig. 38).



Figure 38: This schematic shows the orientation of Sigma 1 and 3 during the development of the Jura Arc, and it also the shows the location and types of faults that dominated each deformation phase. (Modified from Homberg et al., 2002)
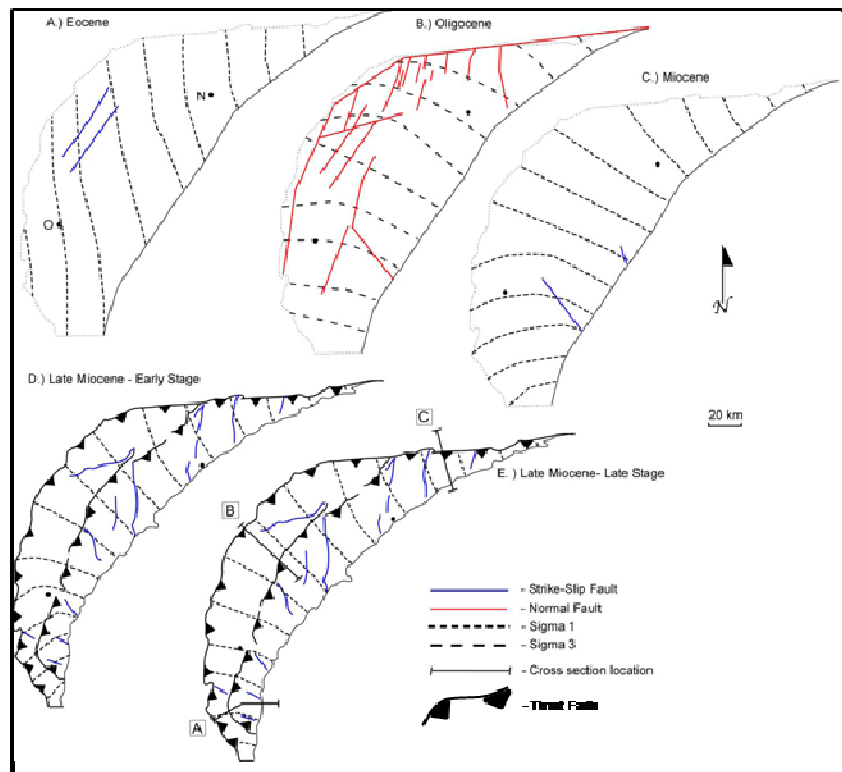
## 7.2.3 - Balanced Structural Cross Sections

The cross sections throughout this belt show the influence of all three tectonic episodes upon the final fault geometry (Fig. 39).

Figure 39: These three cross sections show the differences along the length of the Jura Arc. (Modified from Homberg et al., 2002)
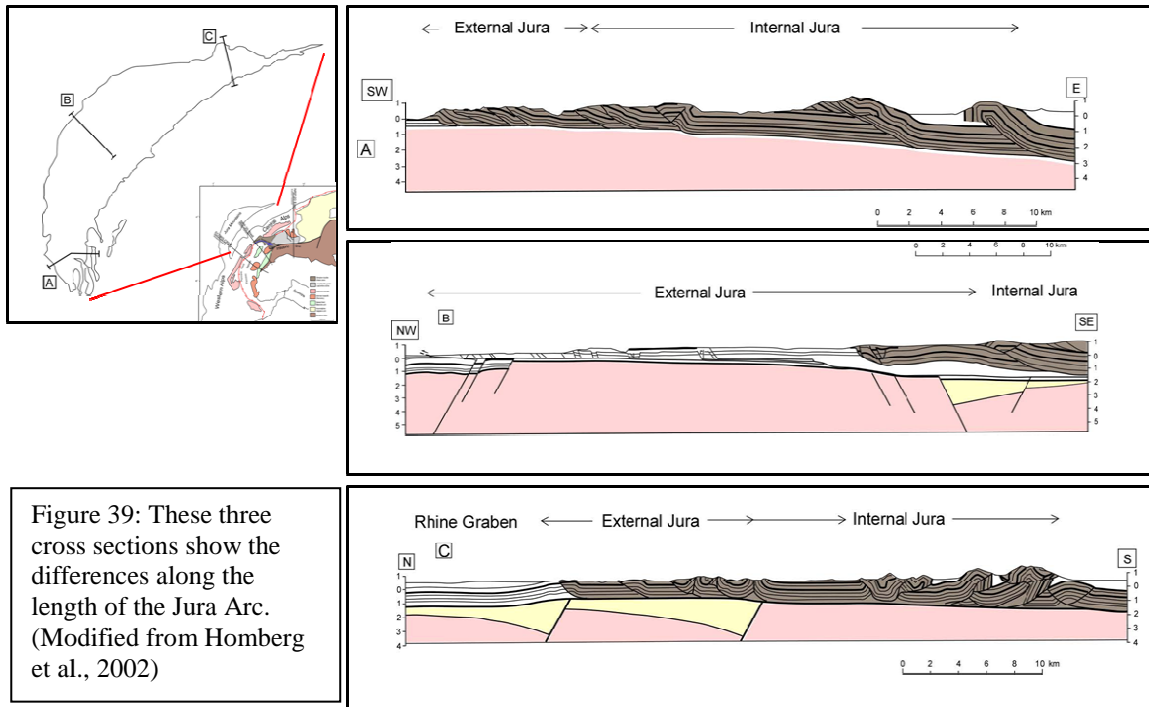
7.2.4 - Arc type

According to Hindle and Burkhard, (1999):

"The arcuate shape of this fold-thrust belt does not owe its shape to the fore mentioned tectonics but rather to the paleogeography of the area. The external border of the Jura arc coincides with the salt/gypsum pinchout and the arc mimics directly the original shape of the Triassic basin border (Hindle and Burkhard, 1999)."

There have been several attempts to model the formation of the Jura arc, but none have been completely successful. The thick-skinned models postulate sinistral strike-slip faults in the basement and en-echelon folds in the sediments above (Gehring et al., 1991). These models call for a counter clockwise rotation of more than $15^{o}$; while, the thin-skinned models suggest a clockwise rotation of less than $10^{o}$. The lack of high temperatures during the formation of the arc preserved the original magnetic orientation of the rocks. The paleomagnetic data of the region shows that the arc did not significantly

rotate during formation, thus the thin-skinned model is the most accurate, along with

proving that the arc formed as a primary arc.


7.2.5 - Sedimentation

See the sedimentation sub-section of the Western Alps section.


7.3 – **Southern Portion of the Western Alps**:


7.3.1 - Location:

Siddans, (1979) stated that:

"There are five distinct fold-thrust limbs that make up the arcuate bend within the southern portion of the Western Alps (Fig.2 (2)). The five limbs are easily recognizable on geologic maps and are oriented and located as follows: 1.) the first of these limbs strikes NNE-SSW and located between the towns of Grenoble and Die, 2.) the second limb strikes E-W between Die and Sisteron, 3.) the third limb strikes NNW-SSE and is situated around the town of Digne, 4.) the fourth strikes E-W and is located around the town of Castellane, 5.) finally, the fifth limb strikes N-S and dies out around the town of Nice (Siddans, 1979) (Fig. 40)."
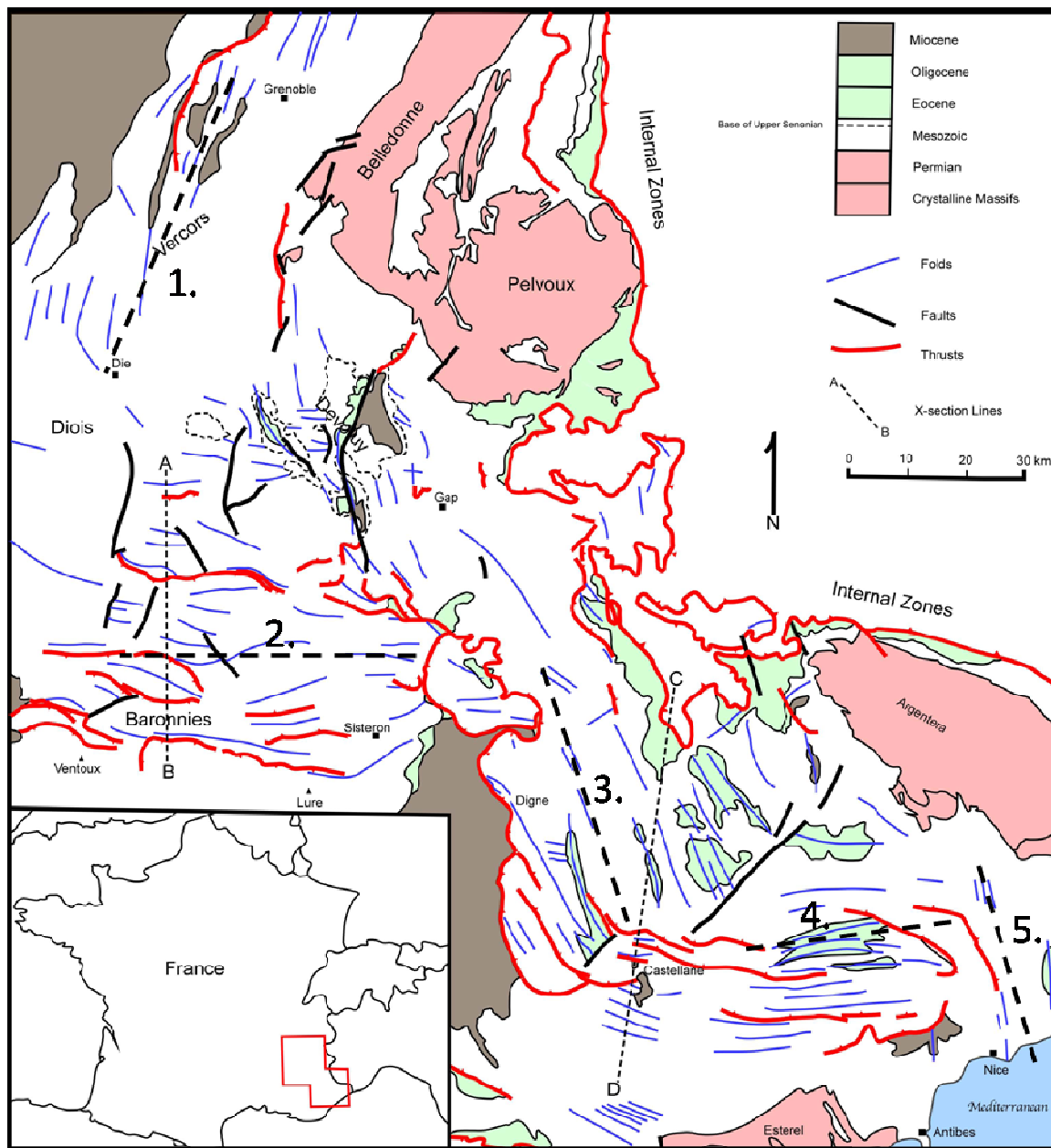
Figure 40: Simplified geologic map of the southern portion of the Western Alps. 1-5 – mark the five distinct fold belts and their orientations. (Modified from Siddans, 1979)

7.3.2 - Timing:

Siddans, (1979) stated that:

"The timing of the deformation represented by these limbs is a combination of several tectonic events (Fig. 41). The timing was established by the stratigraphy involved and orientation the folds along each limb. The first limb's deformation is associated with the main Alpine phase of deformation and was transported from the east to the west. The second limb is associated to two different deformation periods. The E-W folds belong to the Pyrenean-Provencal phase and later rejuvenated in the main Alpine Phase; while, the NNW-SSE folds around Devoluy are Pre-Senonian (90-80 Ma) in age. The third limb consists of two distinct fold belts. The first one southeast of Digne striking WNW-ESE are Pyrenean-Provencal in age. The second belt striking NNW-SSE crosses the first and is main Alpine in age. The fourth limb is thought be of the main Alpine phase but could possibly be of Pyrenean-Provencal age. The uncertainty is due to the fact that these folds cannot be traced laterally into the adjacent limbs; while the thrusts can be traced from both of the surrounding limbs. The fifth and final limb is of the main Alpine phase."
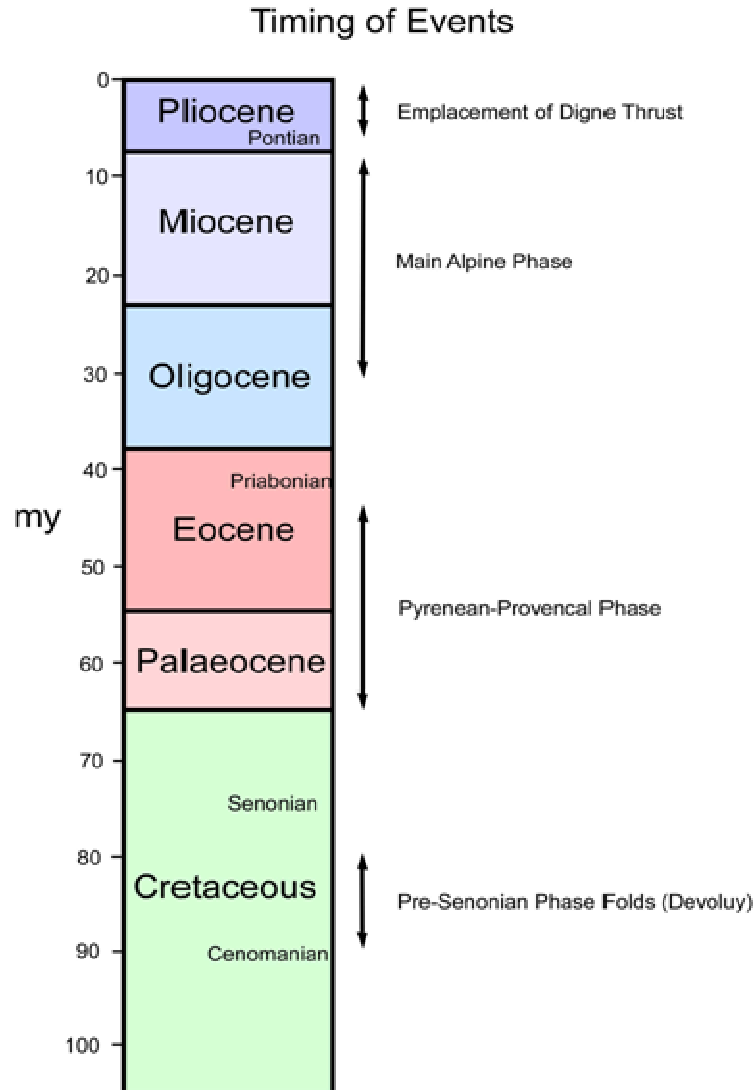


Figure 41: Simplified stratigraphic column highlighting specific tectonic events. (Modified from Siddans, 1979)

The orientations of the two main deformation phases described above are depicted in

Figure 42.



Figure 42: Geologic schematic map depicting the two main deformation phases that effected the development of the southern portion of the Western Alps. (Modified from Siddans, 1979)
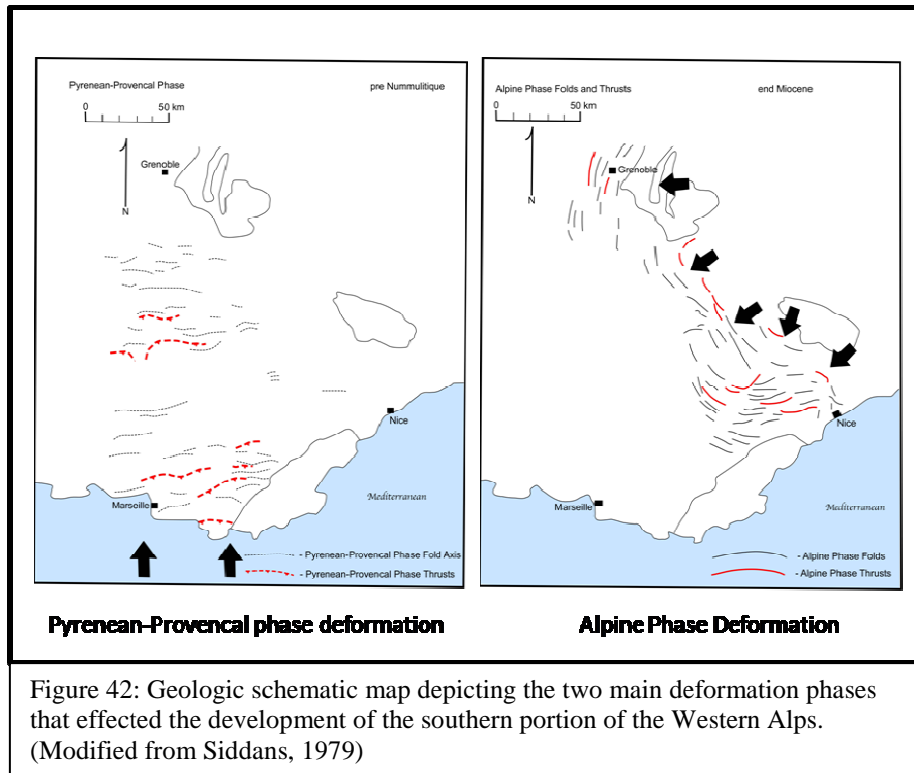
7.3.3 – Balanced Structural Cross Sections:

There are two simplified structural cross sections, indicated by the dashed lines on the geologic map provided (Fig. 40), positioned in a manner to capture the main deformation stages discussed in the prior section, the Pyrenean-Provencal to the main Alpine phase. Cross section A-B is oriented N-S and cuts through the heart of the second limb



Figure 43: The two simplified structural cross section for the southern portion of the Western Alps. a) cross section through the 2nd limb (Pyr-Pro deformation), b) cross section through the 3rd limb (Alpine deformation). (Modified from Siddans, 1979)

60
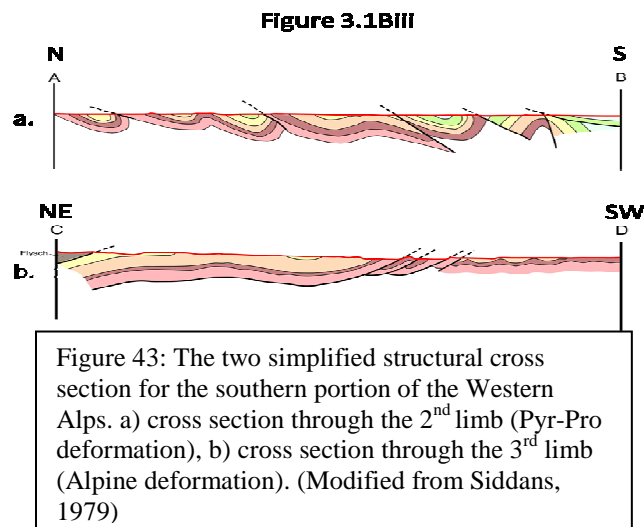
(Fig. 43 (a)). This cross section shows that the main transport direction is from the south

to the north almost 180$^{o}$ off from the transport direction depicted in the cross section C-D

(Fig. 43 (b)).

### 7.3.4 – Arc Type

There is no specific arc type mentioned in the literature for the southern portion of

the Western Alps.

### 7.3.5 – Sedimentation

See the sedimentation sub-section of the Western Alps section.

### 7.4 - **Western Alps**:

### 7.4.1 - Location:

The Western Alps are

commonly defined as being

the portion of the Alpine

Mountains south of the

Rhone-Simplon line (Fig. 44).



Figure 44: Simplified geologic map of the Western Alps. The dotted red line is the border between the Central Alps and the Western Alps. (Modified from Schmid and Kissling, 2000)
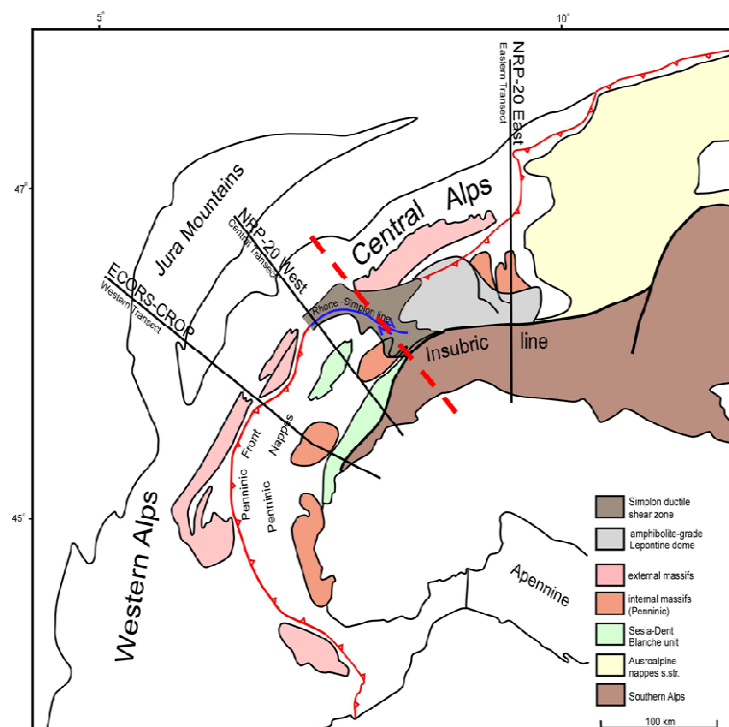
7.4.2 – Timing/Evolution:

The formation of the Alps started with the fragmentation of Pangaea, but for the

purpose of this study the time table has been condensed to the main tectonic episodes that

most greatly affected the
formation of the western
Alps. Frisch, (1979) stated
that:

"The orogenic
events began with the
closing of the Piedmont
Ocean during the beginning
of the Late Cretaceous (~80
Ma) (Fig. 45 and plate 9).
The Piedmont Ocean was
not completely closed when
the focus of the
compression moved north to
the next oceanic basin, the
Valais Ocean (Fig.45 and
plate 8). The timing of the
subduction in the Valais
ocean basin is not well
constrained, but is ended
when the northern Helvetic
zone started to be subducted
(Fig. 45 and plate 8)."

Schmid and

Kissling, (2000) state that:

"This collision
marks the beginning of the
modern Alpine Mountains.
The first tectonic episode in
the Alpine orogenic process,
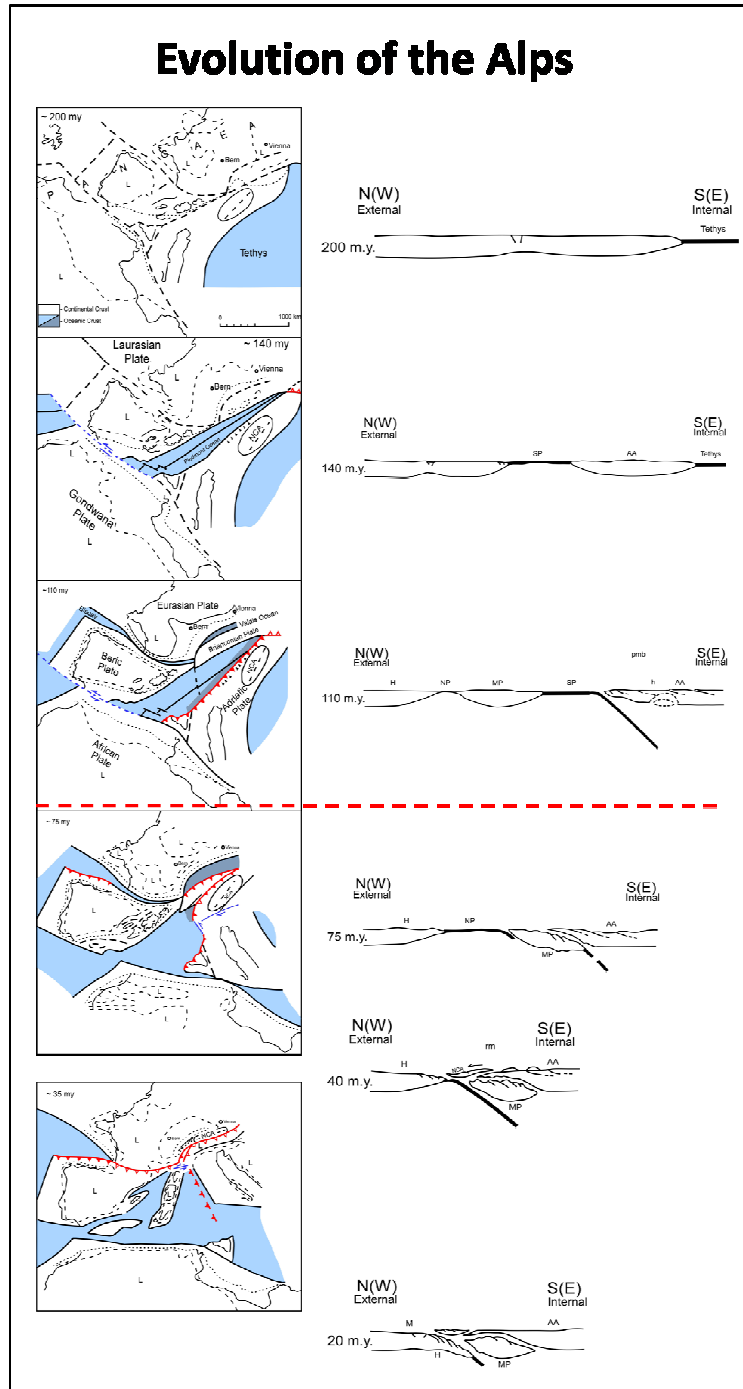


Figure 45: This figure shows the evolution of the Alps from Pangaea to the formation of the Alps. The red dashed line denotes the beginning of the formation of the Alps with the closing of the Piedmont Ocean and the start of the closing of the Valais Ocean. (Modified from Frisch, 1979)

35-30 Ma, began when the Brianconnias basement was back-thrusted over the Gran Paradiso units (Schmid and Kissling, 2000). Then in the early Miocene, the main Alpine tectonic phase started. Then finally around 11Ma, the external portions, namely the Jura Mountains underwent shortening.

The main Alpine orogenic event started with the convergence of the Eurasian Plate with the Adriatic Plate. The convergence was initially north to form the Central and Eastern Alps. The Western Alps at this time were dominated by sinistral lateral faults rather than thrusts (Fig. 46 (A)).

The west directed component of the thrusting in the Western Alps was kinematically linked with the west directed component of movement of the Adriatic microplate (Schmid and Kissling, 2000). At some point after 35 Ma the Adriatic microplate started to shift westward and rotate $15^o$ in an anticlockwise direction (Fig. 46 (B)). The Tonale-Simplon shear zone accommodated ~100 km dextral movement, thus decoupling the western Alps from the central and eastern Alps. The orogenic parallel extension generated by the rotation of the Adriatic microplate is the sole reason for its arcuate shape."
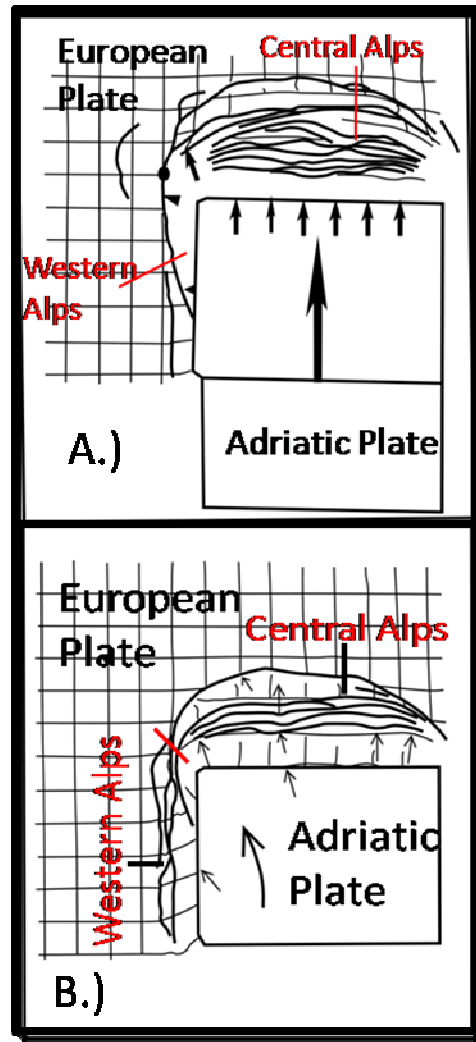


Figure 46: Lickorish et al. (2002), performed numerous sandbox experiments showing how fold-thrust belt evolve depending on the orientation of the indentor. These two diagrams show how the Alpine orogeny evolved. A.) orthogonal , B.) rotation ~ 15degrees

7.4.3 – Balanced Structural Cross Sections:

Unlike the previous section, there are many structural cross sections throughout the western Alps. I will only focus on two of them in this sub-section. The first is a large regional cross section drawn by Schmid and Kissling, 2000 (Fig. 47). This cross section is drawn using the ECORS-CROP deep seismic profile. This seismic profile gives an unprecedented glance at the deep structures and strata, but, the shallow geometries were

taken from others. The second cross section is from Butler, (1983). This cross section is drawn along the ECORS-CROP line west of the Penninic front, and it gives a more detailed interpretation of the shallow features (Fig. 48).
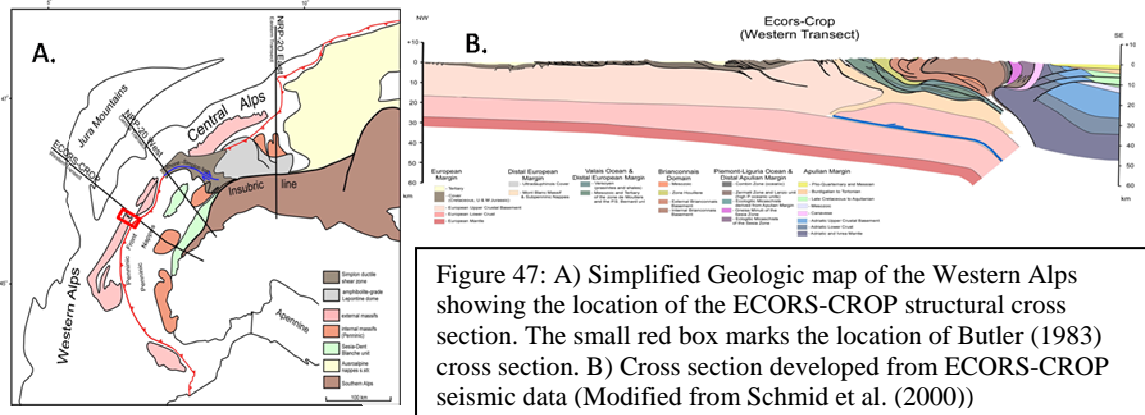


Figure 47: A) Simplified Geologic map of the Western Alps showing the location of the ECORS-CROP structural cross section. The small red box marks the location of Butler (1983) cross section. B) Cross section developed from ECORS-CROP seismic data (Modified from Schmid et al. (2000))
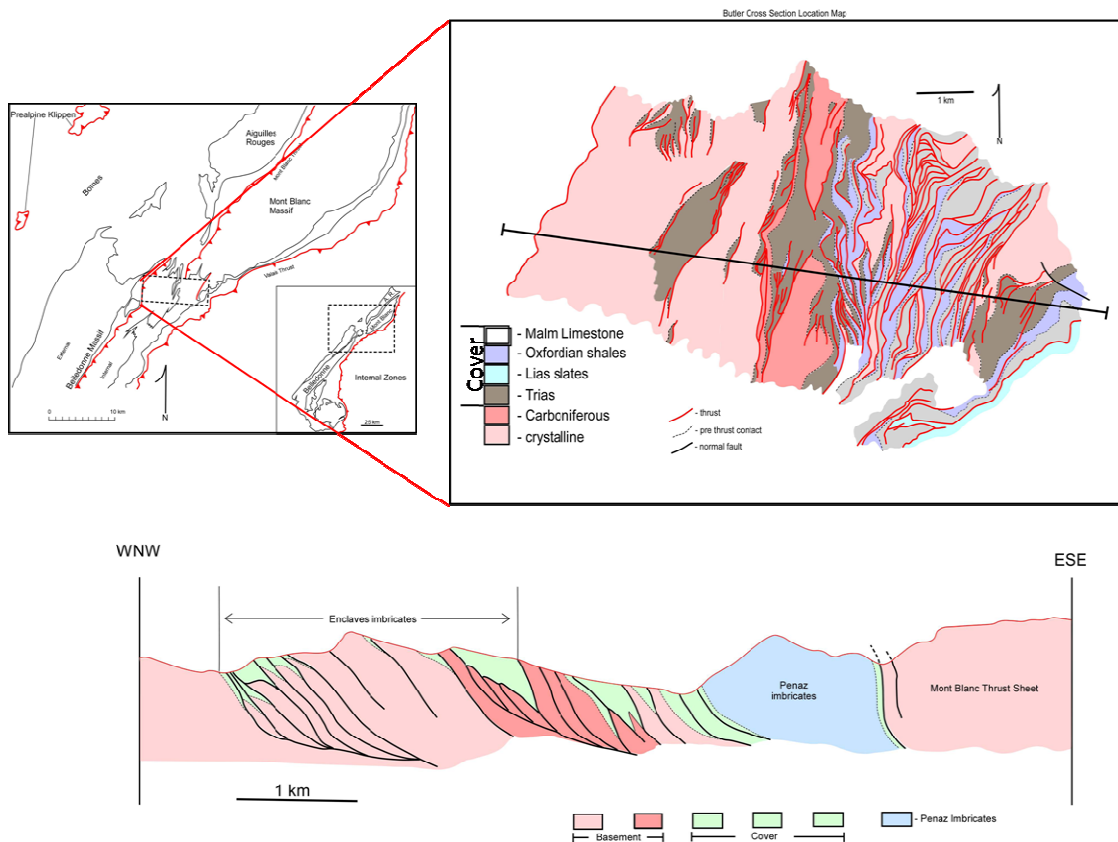


Figure 48: Butler (1983) geologic map and balanced cross section shows the complexity the thrusting involved in the Subalpine Chain in the Western Alps.

7.4.4 – Arc Type

There is no specific arc type given for the Western Alps in the literature.

7.4.5- Sedimentation:

The foreland basin of the western Alps is a combination of several basins. The main two basins that comprise the majority the foreland basin are the North Alpine Foreland Basin (Molasse Basin) and the West Alpine Foreland Basin. The West Alpine Foreland Basin represents an overall deep-water West Alpine Foredeep, which was transformed into a shallow-water West Alpine Molasse Basin at the end of the Eocene (Sissingh, 2001). The basin was asymmetric and moved westward matching the advance of the mountain chain and the down-warping of the subducted European plate until it was ultimately overridden by the advancing mountain belt. The depositional history within the Western Alpine Foreland Basin ended in the Oligocene, it was overridden. A schematic representation of the West Alpine Foreland Basin's complex history is given in appendixB. The North Alpine Foreland Basin is better known as the Molasse Basin. This basin is not directly discussed in the literature other than when discussing the the entire Alpine foreland basin system; therefore, the sedimentation of the West Alpine Foreland Basin will be implied to the North Alpine Foreland Basin.

Sissingh, (2001) describes the sedimentation of the Western Alpine Basin as follows:

"The sedimentation within the West Alpine Foreland Basin began during the middle Eocene, Lutetian, with the deposition of the Nummulitic Limestone (100 m). This deposit reflects rapid transgression. This transgression continued with the deposit of the 400 m of Marls of Priabonian age. The next bed is the Annot and Chamsaur sandstones that are classified as turbidite deposits. This bed is correllateable to other units in the area such as the Aiguilles d' Arves and the Tavayannaz turbidtes. These beds range in thickness from 500-800 meters in the Annot and Chamsaur to 2000 meters in the Aiguilles d'Arves to 300-600 meters in the Tavayannaz. The clastic sediments that make

up these respective formations were derived from the approaching mountain belt and continental region to the south.  The transition from Eocene aged deposition to Oligocene is marked by the Clumanc and Saint-Antonin Conglomerates. The lower two layers of these formations are Priabonian; while, the upper most layer is Rupelian. The lower Eocene layers in the Clumanc Formation consist of marine sediments and volcanic sediments respectively. The upper Oligocene layer consists of shallow marine limestones in the Clumanc Formation and a sandy marl conglomerate in the saint-Antonin. By the middle Oligocene, the West Alpine Foreland Basin is filled and completely cutoff from from marine influence (due to uplifting), thus transforming it to the West Alpine Molasse Basin. A few isolated deposits mark this transformation (Molasse Rouge, Molasse Grise, and Green Sands). The Molasse Rouge consists of red and greenish marls, siltstones, sandstones, breccias and conglomerates, as well as freshwater limestones (Sissingh, 2001). This formation marks the rapid continentalization of the North Alpine Molasse Basin. The Molasse Grise conformably overlies the Molasse Rouge and consists of calcareous mudstones in low lying depocenters along with conglomerates and breccias derived from local paleohighs (Sissingh, 2001). The Green Sands unconformably overlies the Molasse Grise in France. This unit is a serpentine bearing fluvial sandstone that got its unique mineral assemblage from the ophiolite bearing nappes that bordered region to the east. This bed marks the end of deposition in the West Alpine Molasse Basin."

7.4.6 - Associated Faulting:

The Western Alpine balanced structural cross sections show the complexity of the thrusting, but, the geologic maps associated with the structural cross sections shows that there are also several strike-slip and normal faults active within the Western Alps. Their contribution to the tectonic events and the deformation of the Western Alps has been discussed in prior sections.

7.4.7 - Gravity Profile:

The gravity profile for the Western Alps is provided by Doglioni et al., (1999) (Fig. 49 (A)).
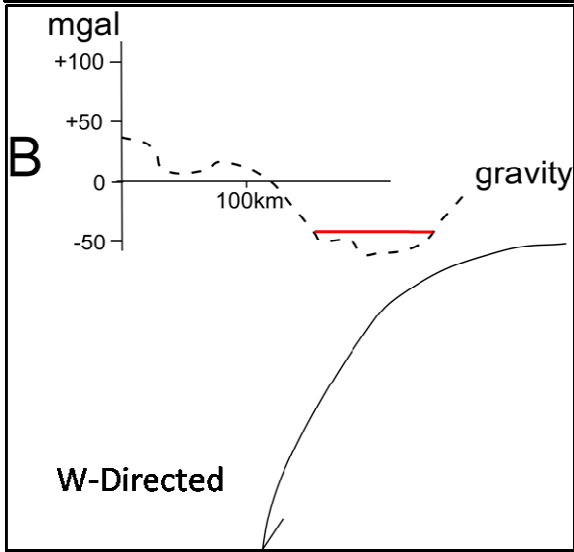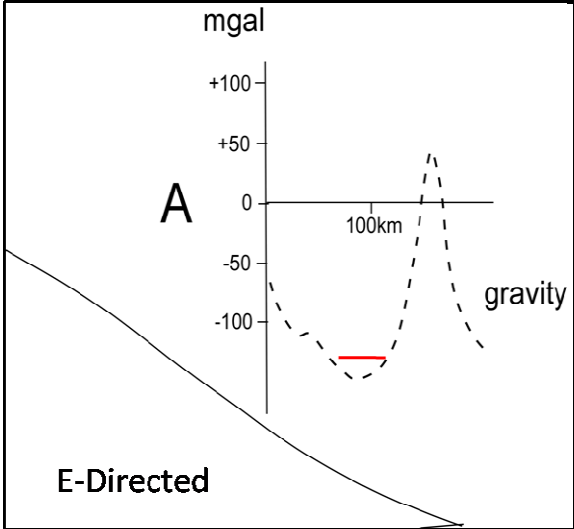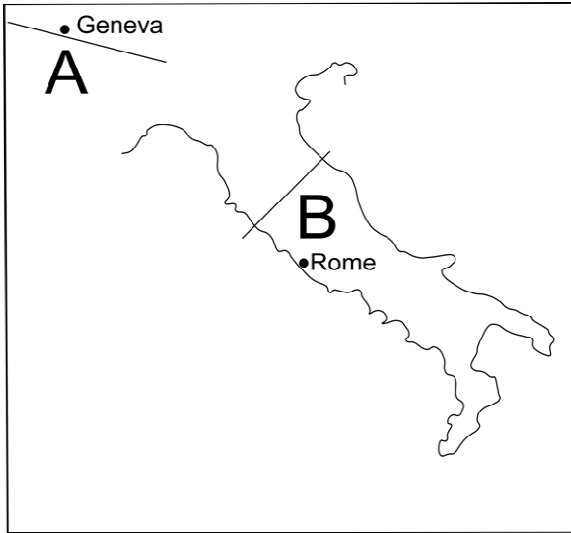
Figure 49: Example gravity profiles from Doglioni et al., 1999. A.) is taken cross the Western Alps (E-directed), B.) taken across the Apennines (W-directed)
(Modified from Doglioni et al., 1999)

7.5 - **The Carpathians**:

7.5.1 - Location:

The Carpathian Mountains are located on the eastern end of the Eastern Alps (Fig 50). They are a semi-circular mountain belt that stretches from the Czech Republic through Slovakia and the Ukraine ending in Romania. The Carpathians are sub-divided into three sections: the Western Carpathians, the Eastern Carpathians, and the Southern Carpathians (Fig. 50). The Western Carpathians are located just east of the Eastern Alps
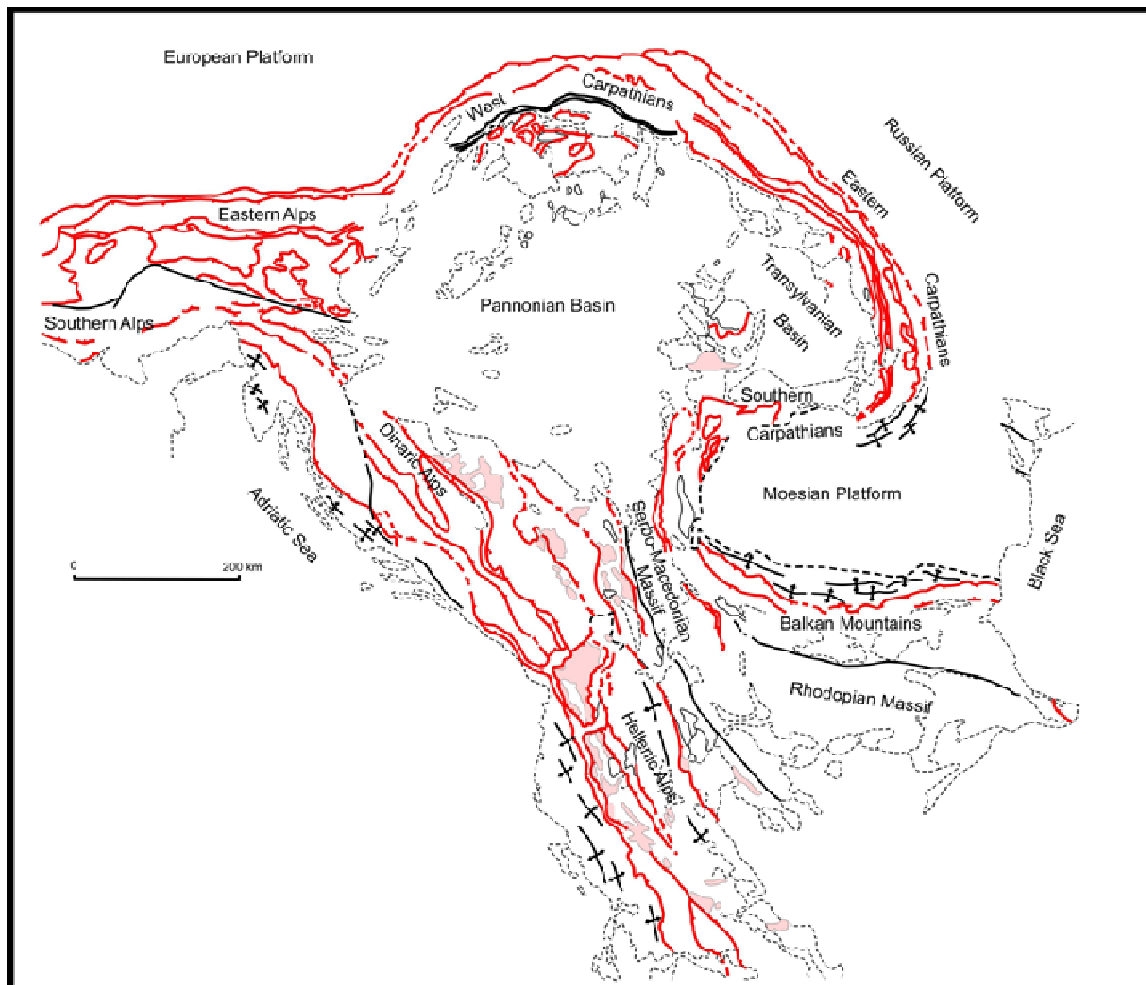


Figure 50: Simplified geologic map of the Carpathian Mountains. The map gives the location of the Carpathian Mountains relative to the Eastern Alps and other prominent tectonic features. (Modified from Burchfiel and Royden, 1982)

and trend SW to NE. The Eastern Carpathians are located east of the Western

Carpathians as the mountain belt turns to the SE. The Southern Carpathians run EW and

are located at the southern end of the Eastern Carpathians as the belt

turns west.


7.5.2 - Timing:

       Burchfiel, (1980) stated that:

       "The Carpathian Mountains were formed as the result of the convergence of
several fragments with the European and Russian plates. The three main fragments that
had the most significant role in the formation of the Carpathian Mountains are the
Apulian fragment, the Rhodopian fragment, and the Moesian fragment (Fig. 51).  The
deformation that formed the Carpathian Mountains started during the late Jurassic and
continues to the present.
       The first significant compressional event occurred during the late Jurassic and
continued uninterrupted until the Albian (Latest Early Cretaceous). This deformation
started with the subduction of the oceanic crust between the Apulian and the Rhodopian
fragments. It is marked by the placement of ophiolites placed upon the Auplian fragment
and a small volcanic island arc southwest of the Rhodophian plate (Fig. 51 (A)). The total
shortening during this episode is on the order of ~300 km. The polarity of the subduction
involved is not certain, but the eastward dipping thrust, the emplacement of the
ophiolites, and the plutonic and high temperature metamorphism along the southeastern
part of the Rhodopian fragment indicates an east-dipping subduction zone.
       The first continent to continent collision occurred during Albian time, and is best
documented in the Southern Carpathians where the Rhodopian and Moesian fragments
collided along a west-dipping subduction zone (Burchfiel, 1980) (Fig. 51 (B)). The
Rhodopian fragment was narrowed during this subduction by as much as 60-100 km.
This narrowed region of the northern Rhodopian fragment is now the inner crystalline
zone of the Eastern Carpathians. The crustal thickness below this region is anomalously
thin at 25-47 km. This episode of deformation involved no subducted oceanic crust.
       The Albian subduction along the Rhodopian and Moesian fragments ended by the
Cenomanian; when the deformation shifted to the northern margin of the Auplian
fragment. A south-dipping subduction zone accommodated the nearly 150 km of
shortening (Fig. 51 (C)).
       After the Cenomanian, an eastward directed convergence took over from the
Coniacian to the Paleocene. The southern half of the Rhodopian fragment was more and
more consumed by an east-dipping subduction zone; while, the northern half was rotated
clockwise around the Moesian fragment along a west-dipping subduction zone by the
advancing Apulian fragment. The two opposing subduction zones along the Rhodopian
fragment were compensated by a transform fault zone indicated in Figure 51 (D).

The major tectonic event that occurred during the Eocene-Oligocene was the return to northward convergence along the northwestern portion of the Apulian fragment and the southern edge of the European Plate. Both the Apulian fragment and the European plate were narrowed by at least 50-100 km and the upper part of the Apulian continental crust overrode the European plate by more than 100 km (Burchfiel, 1980).

The Miocene deformation is marked by thrusting only in the external flysch zones. This thrusting event is unique because it appears to have occurred contemporaneously all the way around the fold-thrust belt. The final stage of deformation (Pliocene) within the Carpathian Mountains occurred within the Southern Carpathians as the Apulian-Rhodopian fragments moved east to complete the convex-east Carpathian loop of the orocline (Burchfiel, 1980) (Fig. 51 (E))."



Figure 51: Palinspastic maps (A-F) showing the location of the different micro-continents during the different stages of formation of the Carpathian Mountains. There are several plate and fragments denoted in the figure and they are: A. is the Auplian fragment, R. represents either the Russian Plate or the Rhodopean fragment, ND is the North Dobrogea, M is the Moesian fragment, and finally the E is the European Plate. The red lines are the thrust faults, the blue lines are the strike-slip faults and the black triangles are the associated volcanoes (Modified from Burchfiel, 1980)

7.5.3– Balanced Structural Cross Sections:

　　　　The Western and Eastern Carpathian Mountains are almost completely covered by balanced structural cross section. The complicated tectonic history of the Carpathian Mountains makes balancing most of these cross sections speculative at best, but the balanced structural cross sections that use the greatest amount of subsurface data were chosen. These cross sections also provide complete coverage of the Carpathian Mountains. Their locations are indicated in Figure 52.

　　　　The first area of focus is the Western Carpathians and it is covered by two cross sections from Picha, (1996). The first cross section is a large regional cross section that runs from the foreland basin into the back-arc basin (Fig. 53(A) and plate 10). The second, more detailed, cross section focuses on the outer flysch belt of the Western Carpathians (Fig. 53(B) and plate 10).
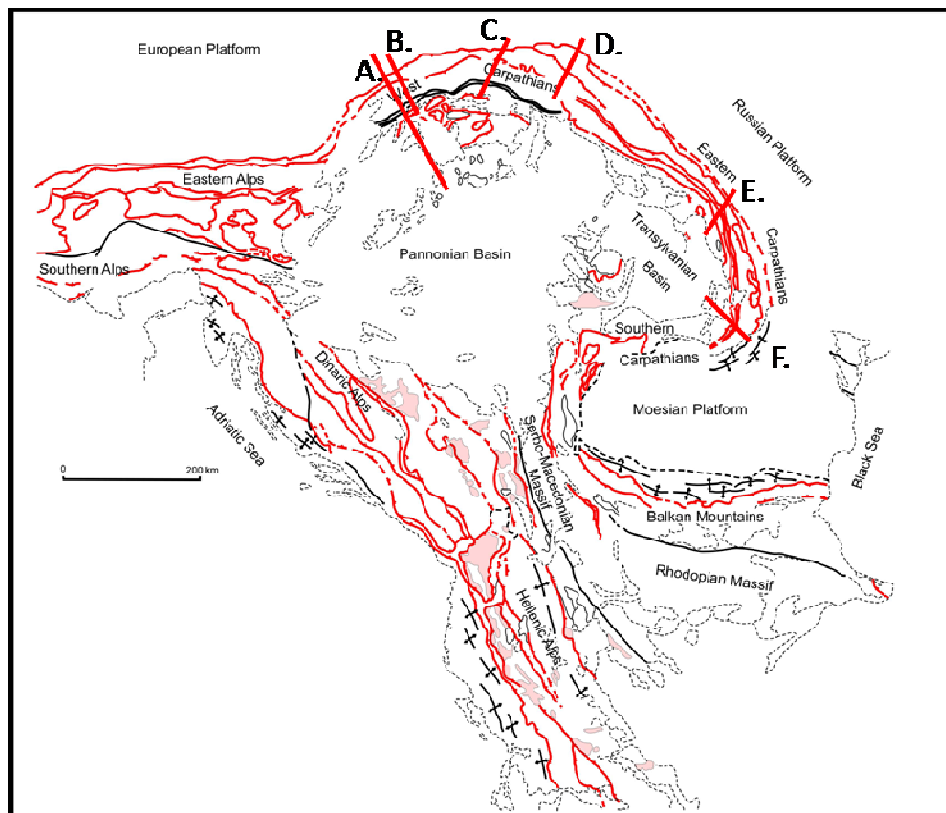


Figure 52: Location map of the selected cross sections. (Modified from Burchfiel and Royden, 1982)

71
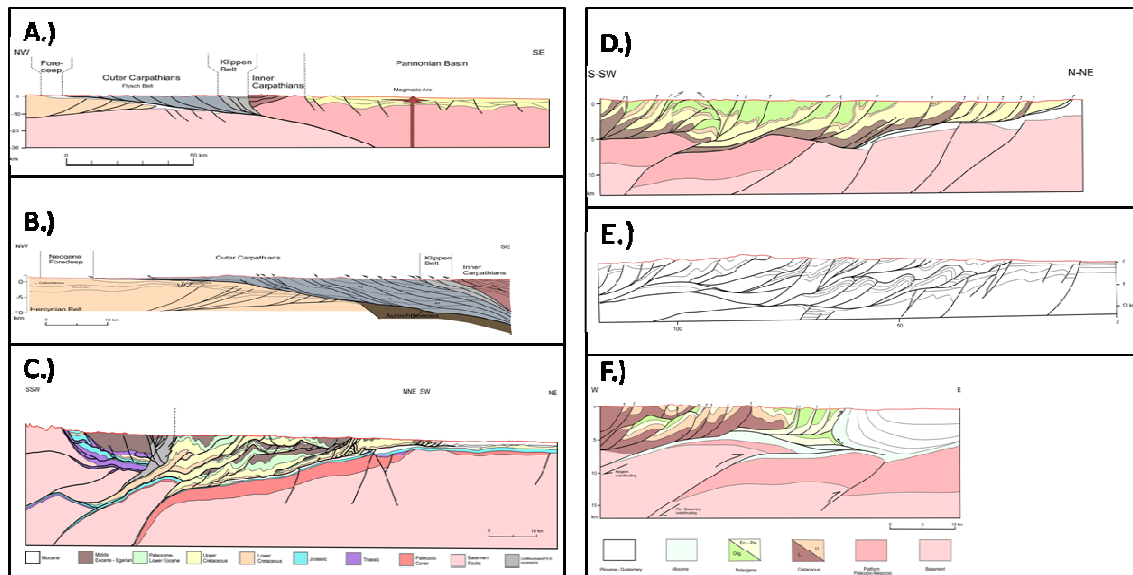
Figure 53: Several balanced cross sections gathered from the literature. These cross sections were selected because they effectively show the complex thrust geometries around the perimeter of the Carpathian fold-thrust belt. They also allow the examination of how the geometry changes from cross section to cross section. A) modified from Picha, 1996, B) modified from Picha, 1996, C) modified from Roca et al., 1995, D-F) modified from Roure et al., 1993

The second area of concentration is the transition zone between the Western Carpathians and the Eastern Carpathians. The far western balanced cross section is redrawn from Roca et al., (1995) (Fig. 53 (C) and plate 10). This cross section transects both the Outer and Inner Carpathian Belts.  The next cross section, cross section "D", is from Roure et al., (1993) and is located to the right of the transition zone. It only covers the outer flysch belt, but it does; however, give greater insight into the structures located within the Outer Flysch Belt (Fig. 53 (D) and plate 10).

The next region is located in the southern half of the Eastern Carpathians. The first cross section, "E", is redrawn from Roure et al., (1993) and it covers the breadth of the Eastern Carpathians (Fig. 53 (E) and plate 10). The last cross section, "F", is from Roure et al., (1993), and it is located within the transition zone between the Eastern Carpathians and the Southern Carpathians. This balanced cross section shows the results

of the last compressional episode recorded within the Carpathian Mountain Belt (Fig. 53 (F) and plate 10). There are no cross sections that dissect the Southern Carpathians.

7.5.4 - Arc Type:

The Carpathian Mountains have classically been described as an orocline.

7.5.5 - Sedimentation:

The sedimentation for the Carpathians is as complicated due to its structural evolution and its location (crossing more than one International Border). There is no one definitive stratigraphic column for the entire Carpathian Mountain Belt, because the type and age of the sediments within the mountain belt depends on tectonic history of that specific region within the mountain belt. The general sediment types involved in the Carpathian Mountains are: shallow marine carbonates deposited along passive margins, turbiditic flysch deposits deposited in deep basins in front of approaching thrust belt, and continental-shallow marine molasse deposits deposited as the sea-level fell due to basin fill or uplift.

7.5.6 - Associated Faulting:

Extensional normal faults are the only other fault type associated with the Carpathians themselves, but there are hundreds of lateral faults located within the back arc basin (Fig. 51 (E)).

7.5.7 - Basin Types:

The Carpathian Mountains have both a foreland basin and two back-arc basins. The foreland basin associated with the Carpathians is relatively narrow, because it has been overridden by subsequent compressional episodes. The back arc basins (Pannonian and Transylvanian Basins) of the Carpathians; however, are well developed and show tremendous extensional properties.

CHAPTER 8

DISCUSSION

8.1 **Subduction Zone Type**

8.1.1: Palinspastic Map Comparisons

Examination of the palinspastic maps reveals that there are similarities between the orientation of the Ouachita Mountains and that of the Eastern Carpathian Mountains; while, the Ouachita Mountains are almost orthogonal to the Western Alpine Mountains (Fig. 54 and plate 11). The Ouachita Mountains and the Eastern Carpathian Mountains had a bearing of nearly $130^o$ during their conception; however, the bearing for the Western Alpine Mountains is approximately $30^o$, almost orthogonal to the Ouachita Mountains.

The bearings listed above allow for the direction of their subduction to be discerned (Fig. 55). The Ouachitas and the Eastern Carpathians had a subduction zone bearing approximately $220^o$, which is roughly southwest; while, the Western Alpine Mountains had a subduction zone bearing nearly $120^o$, southeast. These results show that the Ouachitas and the Eastern Carpathians are more than likely the product of a W-directed/ Mariana-type subduction zone, while the Western Alpine Mountains are likely the product of an E-NNE-directed/ Chilean-type subduction zone.

**Ouachita Orogeny**

Panthalassa Ocean

Upper Pennsylvanian (~300 Ma)

Equator (0°)

NAM

~130°

MEX

Ouachita Orogeny

Appalachian Orogeny

Paleotethys Ocean

Yucatan

Florida

30° S

AFR

SAM

GONDWANA

~5000km at Equator

3.)

N

~130°

W

E

S

**Alpine Orogeny**

~ 35 my

0   1000 km

Vienna

L

~30°

NCA

L

L

L

L

- Continental Crust

- Oceanic Crust

2.)

N

~30°

W

E

S

**Carpathian Orogeny**

N

~130°

W

E

0   200 km

Miocene

1.)

N

~130°

W

E

S
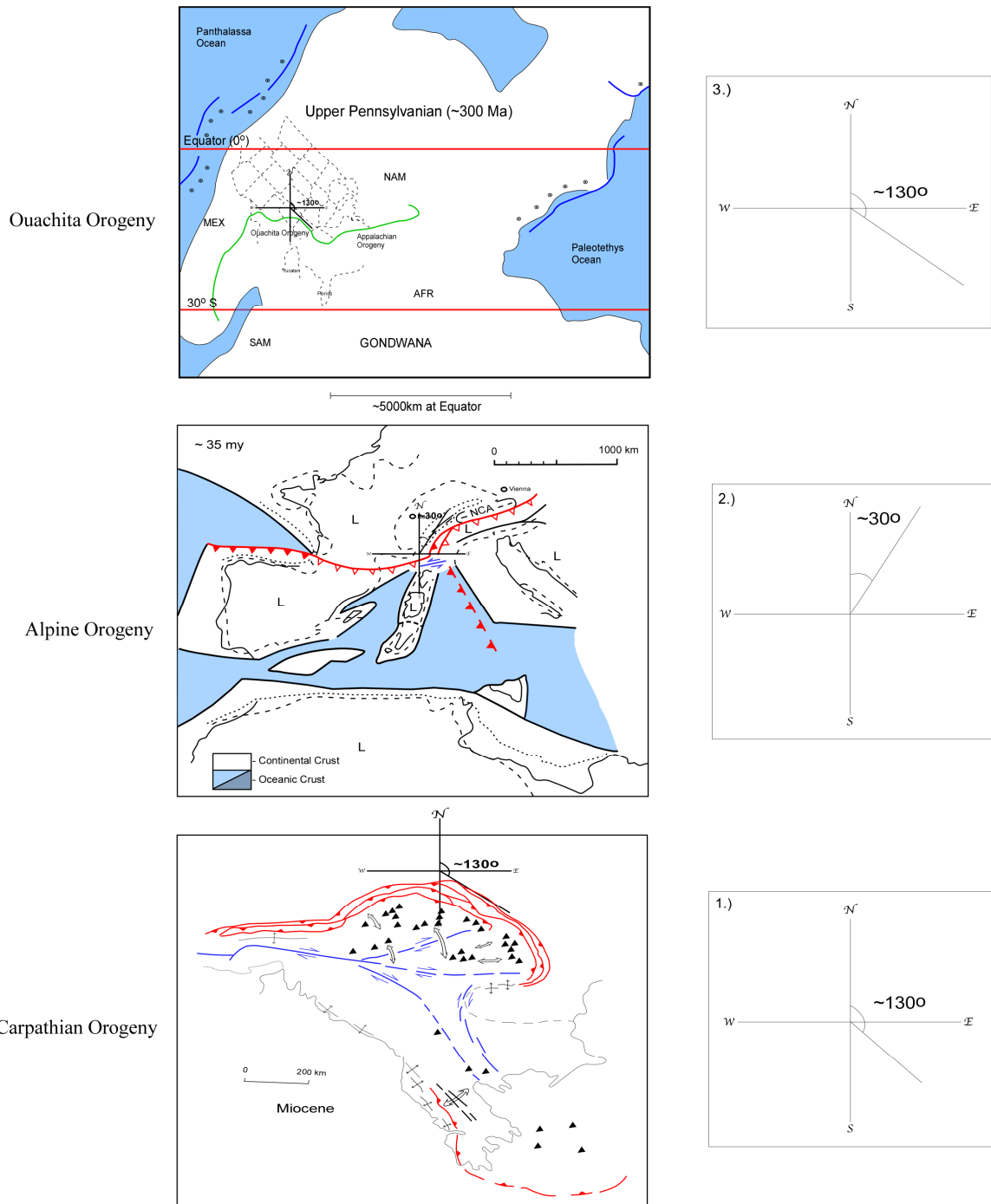
Figure 54: A comparison of the palinspastic maps of the three orogenies. The bearing of each orogeny is taken from the maps. The Ouachita and Carpathian bearings match to within a few degrees and are approximately 100 degrees off of the bearing of the Western Alpine Mountains. (Palinspastic maps modified from Blakely, 2006,  Frisch, 1979, and Burchfiel, 1980, respectively)

Figure 55: Diagram showing the bearing in which the subduction occurred (red arrows). The Ouachita and Carpathian subduction bearing was at approximately 220 degrees (SW), while, the Western Alpine subduction was at approximately 120 degrees (SE). 1, 2, and3 are taken from figure 53.
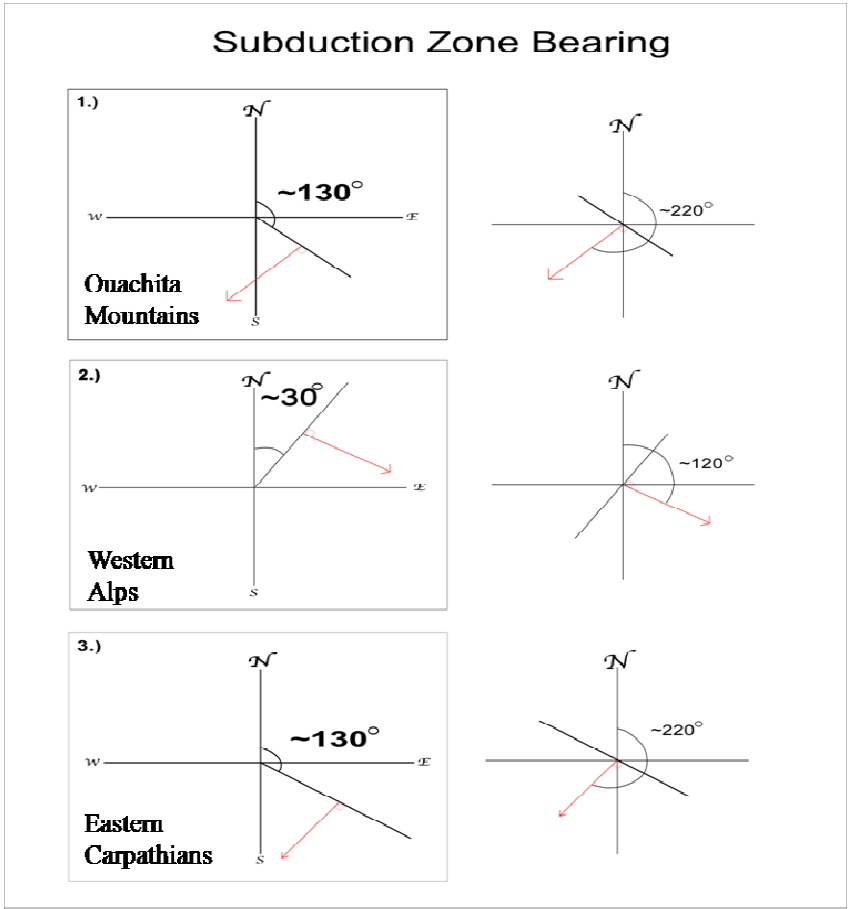
### 8.1.3 Structural Feature Comparison

The differences between the two end members have been established in sub-sections 6.1& 6.2 (Fig. 56). The subduction zone responsible for the Western Alps (this includes the southern portion and the Jura Arc) is a Chilean/ E-directed subduction zone. The majority of the reasons, other than the aforementioned palinspastic map evaluations,

for the Western Alps being a Chilean-type are evident in Figure 57, and they are as

follows: 1) the bulge in the subducted plate located under the
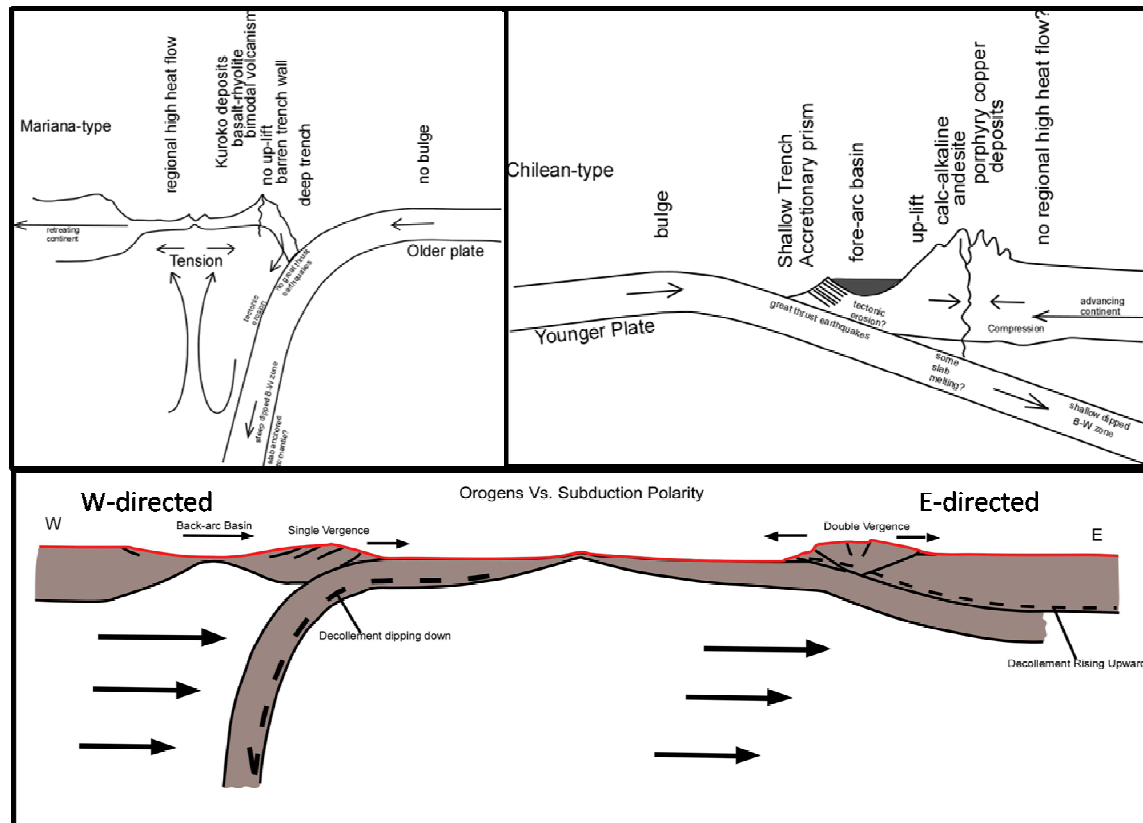
Figure 56: Diagram showing the unique features of each type of subduction zone. Top Row: Uyeda, (1982) Mariana and Chilean- type subduction zones; Bottom: Doglioni et al., (1999) W- and E-NNE-directed subduction zones

Jura Arc, 2) the relatively thin sedimentary cover indicating a shallow trench, 3) the

emplacement of ophiolites and oceanic crust, 4) the thick-skinned nature of the thrusting,

and 5) the double vergence of the thrust faults. Other reasons why the Western Alps are

classified as an E-directed/Chilean-type subduction zone are not evident in the regional

cross section, and they are: the topographic relief of the Western Alps is high and the

back arc basin is compressional.
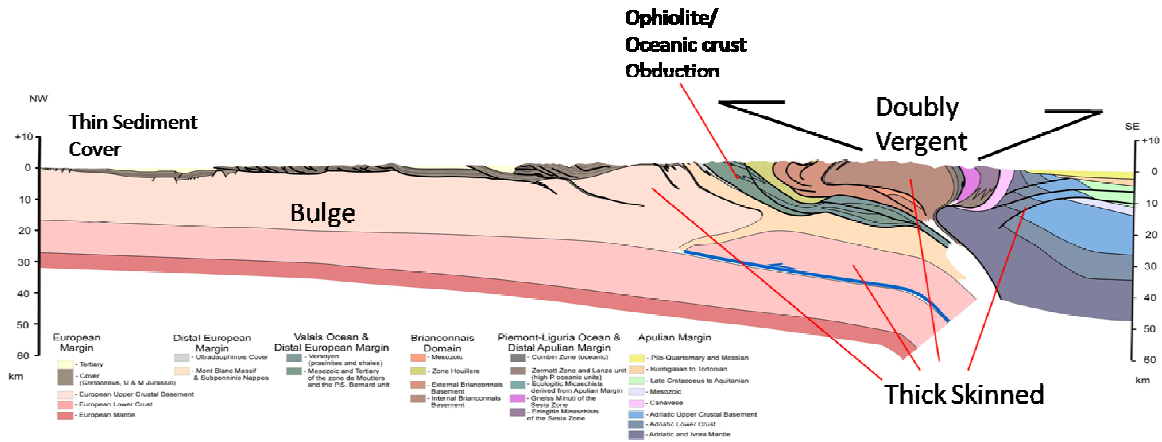
Figure 57: This figure shows the characteristics that make the Western Alps a Chilean-type/ E-directed subduction zone. (Modified from Schmid and Kissling, 2000)

The Carpathians are classified as a Mariana-type/W-directed subduction zone, based on the palinspastic map evaluations described in the previous section, but cross sectional examinations add significant substantial data to bolster this claim. The cross sectional reasons for this classification are evident in Figure 58, and they are as follows: 1) the back arc basin is extensional, 2) the thrusts are thin skinned, 3) the lack of obducted ophiolites or oceanic crust, 4) the relatively thick sedimentary cover, 5) the lack
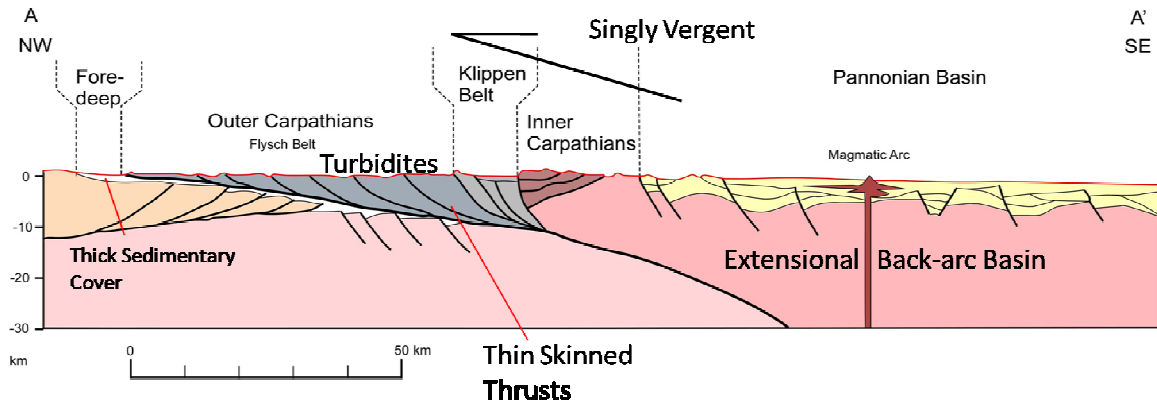


Figure 58: Cross section showing the subduction zone type characteristics for the Carpathian Mountains. (Modified from Picha, 1996)

of a bulge in the subducted plate, 6) the thick turbidite beds (Flysch Belt), 7) the single

vergent thrust faults, and 8) the low topographic relief.

The type of subduction zone responsible for the Ouachita orogeny has never been

clearly defined in the literature, but, due to the palinspastic map evaluation in the

previous section, the Ouachita orogeny was the product of a W-directed/Mariana-type

subduction zone. Several lines of evidence from the literature and the examination of the

Arbenz, (1989) simplified structural cross section (Fig. 59) can be used to bolster this

claim. The lines of evidence are as follows: 1) there is no recording of a bulge in the

Arkoma Basin, 2) the thickness of the sedimentary cover, 3) the thrusts within the

Ouachita Mountains are singly vergent thrusts, 4) the thrusts are thin skinned, 5) no

obducted ophiolites or oceanic crust, and 6) the topographic relief of the Ouachita

Mountains is low. The back arc basin for the Ouachita Mounatins has not been identified

in the literature, but with the rifting involved in the formation of the Gulf of Mexico and

the thinness of the crust hinterlandward from the orogeny it is not unreasonable to assume

that the Ouachita back arc basin was extensional in nature.
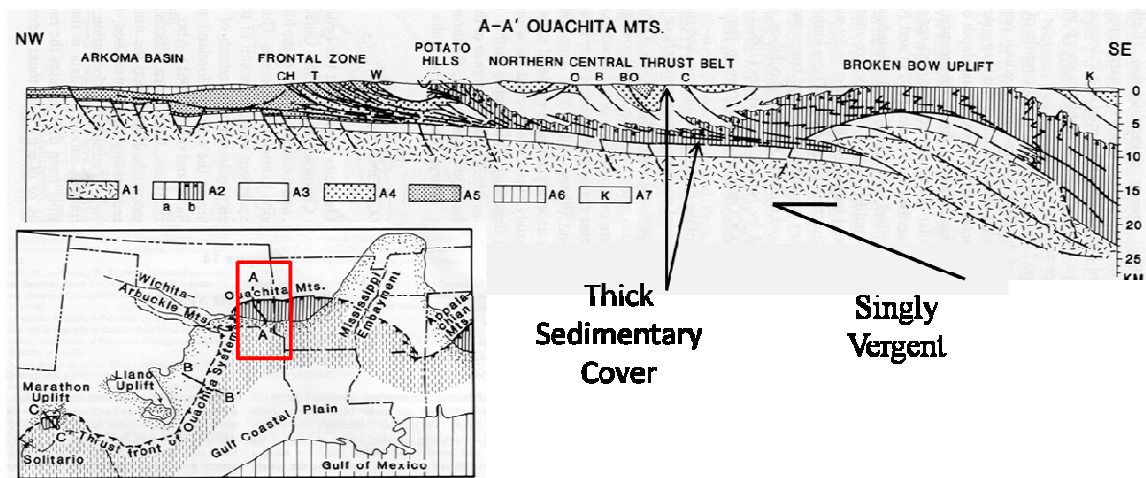


Figure 59: Simplified structural cross section through the width of Ouachita Mountains. This cross section shows that the Ouachita Mountains are singly vergent, have a thick sedimentary cover (~10km), and are topographically low. The observations can go no further due to the simplified nature of this cross section. (Modified from Arbenz, (1989))

## 8.2 **Arc Types**

The Jura arc has been described as both a primary arc and an orocline (Hindle et al. (1999) and Gehring et al. (1991), resprectively). The argument for it being an orocline stated that the rotation of the Adriatic plate in the formation of the Western Alps was transferred to the Jura arc, but, the timing of this event and the lack of large lateral faults parallel to the arc axis left this argument lacking. The evidence for the arc being a primary arc is based on the pinch outs of key beds.

The other two arcs of the Western Alps have not had their arc type defined, but from the available data it can be assumed that the southern portion of the Western Alps is an orocline, because it was formed as the Western Alps wrapped around the Pyrenean-Provencal deformation and the Western Alps can be classified as an orocline due to the ~15$^{o}$ rotation of the Adriatic Plate.

The southern portion of the Carpathian Mountain Chain is an orocline because of the rotation of Rhodopian fragment as it bent around the Moesian fragment; therefore, the entire belt has been classified as an orocline. Doglioni et al., (1999) has shown that the W-directed subduction zones can form an arcuate belt through the action of subduction. Aside from the area influenced by the aforementioned rotation it is possible that the Carpathians are an arc form other than an orocline

The arc type for the Ouachita Mountains has not been definitively defined, and the majority of thisresearch went into answering this one question. In an oroclinal arc there is always some measure of along strike extension, and most of this research was aimed at looking for lateral movement. The correlation of the Wapanucka Limestone along with thin section analysis failed to produce a usable result, but the work of Lickorish, (1999) provides another way to decipher what type of arc the Ouachita Mountains represent (Fig. 60). Lickorish's resultant fault geometries from each of his sandbox experiments were compared to the fault geometries in the Ouachita Mountains. Of these experiments, the best match was the experiment where the indentor came in at a
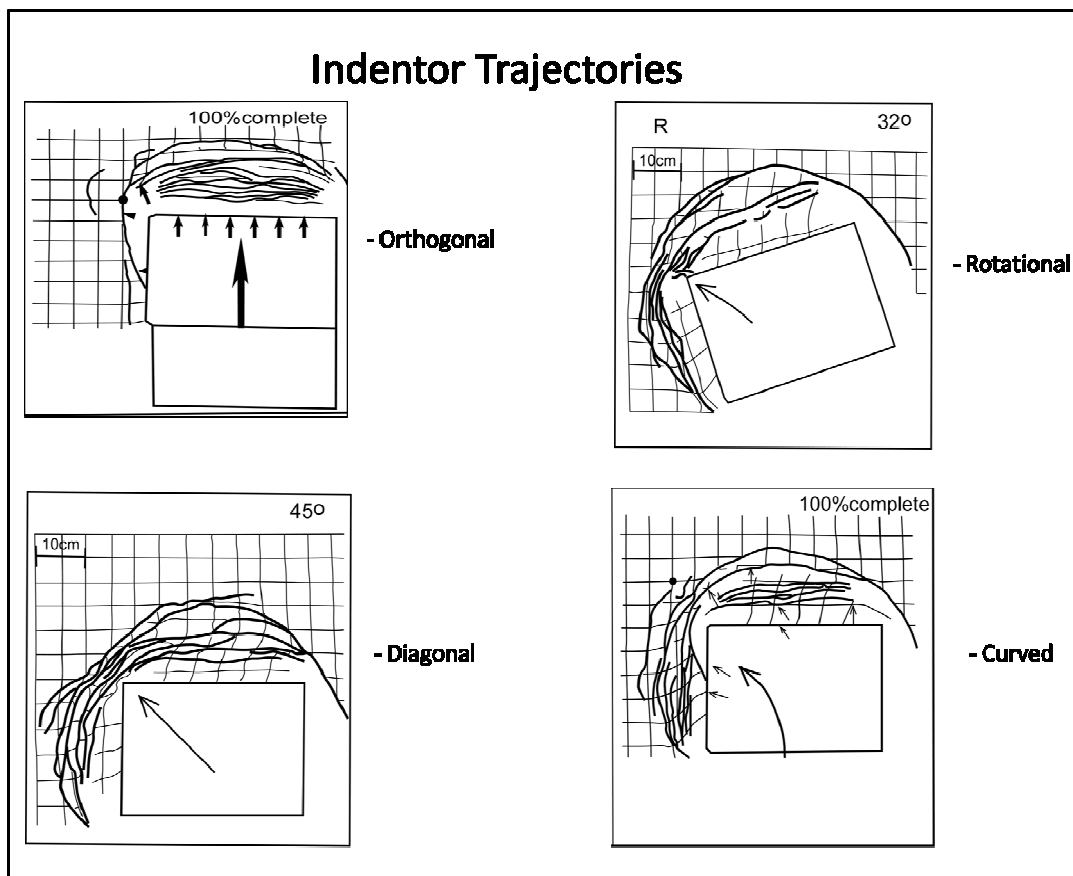


Figure 60: Example results from the Lickorish, 1999, sandbox experiments. (Modified from Lickorish, 1999)

$45^{\circ}$ angle to the indented margin. The concentration of thrusts at the bend and the relaxation of thrusts away from the bend are similar in both the experimental model and the Ouachita Mountains. This also is a line of evidence for the irregular margin by Thomas (1976).

The correct scale to make the previous comparison was unattainable but enough side-by-side comparisons were made to feel confident in the results. This comparison indicates that the likely candidate for producing the recognized fault geometries within the Ouachita Mountains was an indentor with a trajectory that was not curved or rotational. Therefore, the traditional ways to form an orocline were not active in the Ouachita Mountains.

A displacement trajectory map was developed for the Ouachita Mountains, southeastern Oklahoma (Fig. 61). The displacement trajectory map shows that the displacement in the Ouachita Orogeny was radial suggesting a diagonal arc type. However, without knowing the amount displacement this information is only suggestive of the type of arc.
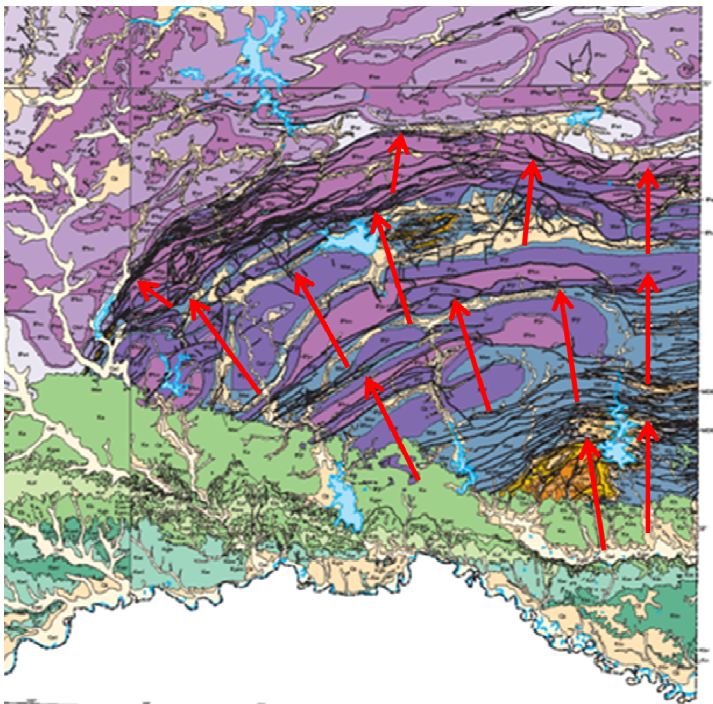


Figure 61: A displacement map of the Ouachita Mountains. Note the radial shape of displacement.

Several theories have been postulated that could allow for assumptions to be drawn about the type of arc represented by the Ouachita Mountains. Thomas, (1976) stated that the Ouachita arcuate belt formed in the location and shape that it is presently situated because of an embayment that was generated along this transform margin (Fig. 62), thus the Ouachita arcuate belt would be a primary arc or piedmont glacier, but Carlson, (1989) noted that the Hunton Anticline was uplifting contemporaneously with the Ouachita Orogeny. This uplift could act as a buttress to the propagation of the orogenic belt, thus generating an orocline. The only problem with this assumption, based off of Carlson, (1989), is that the displacement trajectories where the impedance could have occurred should be reversed, and that reversal is not visible in any maps.

The evidence is not concise enough to prove what type of arc is present in the Ouachita Mountains, but it does show that the possibility of the arc being an orocline is rather unlikely. The arcuate belt is probably a primary arc as it is implied by experimental studies and displacement field map. Further studies need to be performed in order to answer this question.

Concise comparisons of the arcuate belts based on their arc types are unattainable with the data presented above, but, with a little

Figure 62: Transform rift margin explanation of the shape and size of the Ouachita Mountains. 1) Carbonate bank, 2) Deep basin black shale, 3) Shallow shelf and deltas, 4) Flysch, 5) Margin, 6) Active thrusts, 7) Active growth faults, 8) Volcanoes, 9) plate motion (Modified from Thomas, 1976)

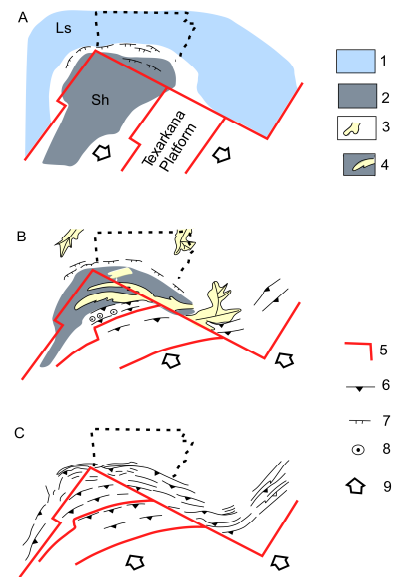interpolation, similarities can be drawn. The Western Alpine Mountains are arcuate due to a fifteen degree rotation of the Adriatic Plate; therefore, due to this rotation they are most similar to the Southern Carpathians. The southern portion of the Western Alps is arcuate due to the belt bending around the previous deformation; therefore, it is similar to the Ouachitas if the Hunton Anticline was already formed before the Ouachita Orogeny. The Ouachitas and the Eastern Carpathians are similar because they are both the product of W-directed subduction zones. Thomas', (1976) embayment theory for the formation of the Ouachita arcuate belt implies that the Ouachitas are similar to the Jura arc.

## 8.3 **Fault Geometries**

8.3.1 - Fault Geometries in Map View

The geologic maps available in the literature did not provide the resolution needed to make good comparisons, but they did provide enough evidence to exclude at least one arc. The geologic map provided for the Carpathians shows that the fault geometries are reasonably close to that exhibited in the Ouachitas. The map of the Jura Arc, however, provides no insight on fault geometries, whereas, the scale of the map for the southern portion of the Western Alps is too large to be useful. The Butler (1983) map of the Western Alps is useful and shows a large amount of thrusting over a relatively small area (~ 4km wide) (Fig. 48). This pattern is not expressed anywhere within the Ouachita Mountains; therefore, the Western Alps map view fault geometries are different from that of the Ouachitas.

8.3.2 - Cross Sectional Fault Geometries

The uniqueness of the Jura arc fault geometries have already been discussed in
section 8.1.2, but, in this section, they are broken down to a more workable scale for
comparisons. The three different cross sections analyzed for the Jura arc show striking
differences.  Cross section "A" crosses the southern tip of the arc and shows only east
dipping thrusts exhibiting ramp style geometries (Fig. 63(A) and plate 12).  Cross section
"B", located in the middle of the arc, shows only a few east dipping thrusts to the
southeast. The majority of this cross section shows a tremendous amount of normal
faulting in the sediment cover and basement (Fig. 63 (B) and plate 12). Cross section "C"
crosses the eastern tip of the Jura Arc and is more complicated than the two prior cross



Figure 63: The Jura Arc
cross sections. A.)
Southern most cross
section , B.) Cross section
across the middle of the
arc, C.) cross section on the
NE edge of the arc
(Modified from Homberg
et al., 2002)
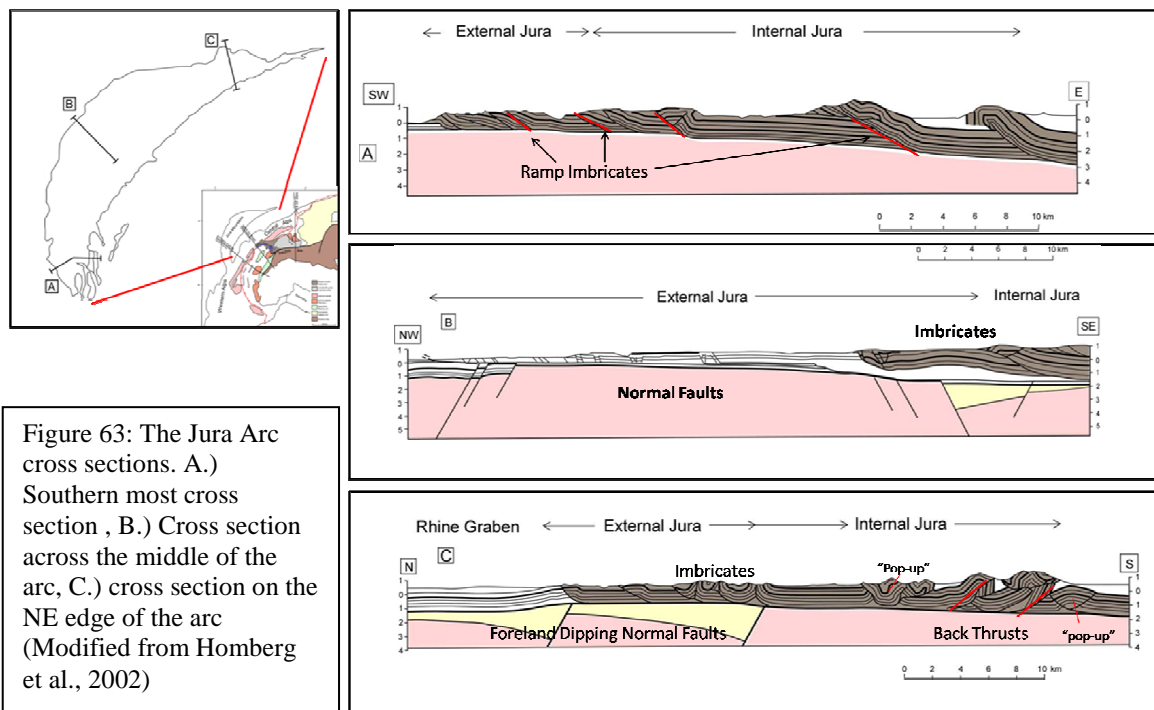
sections (Fig. 63 (C) and plate 12).The thrusts in this cross section are both south dipping

and north dipping. There are several back thrusts and "pop-up" features located on the

southern end of this cross section. The normal faults in this cross section are both down

to the north.

The two available cross sections within the Western Alps provide minimal data to describe fault geometries. The larger scale Ecors-Crop cross section shows that the thrust belt is doubly vergent, and thick skinned in nature (Fig. 64(A) and plate 12). The smaller scaled cross section by Butler (1983) shows that this thick skinned thrust belt is highly imbricated with one possible duplex (Fig. 64(B) and plate 12), but, over large portions of this cross section the imbricates are grouped together; therefore, this cross section is too simplified to be useful.
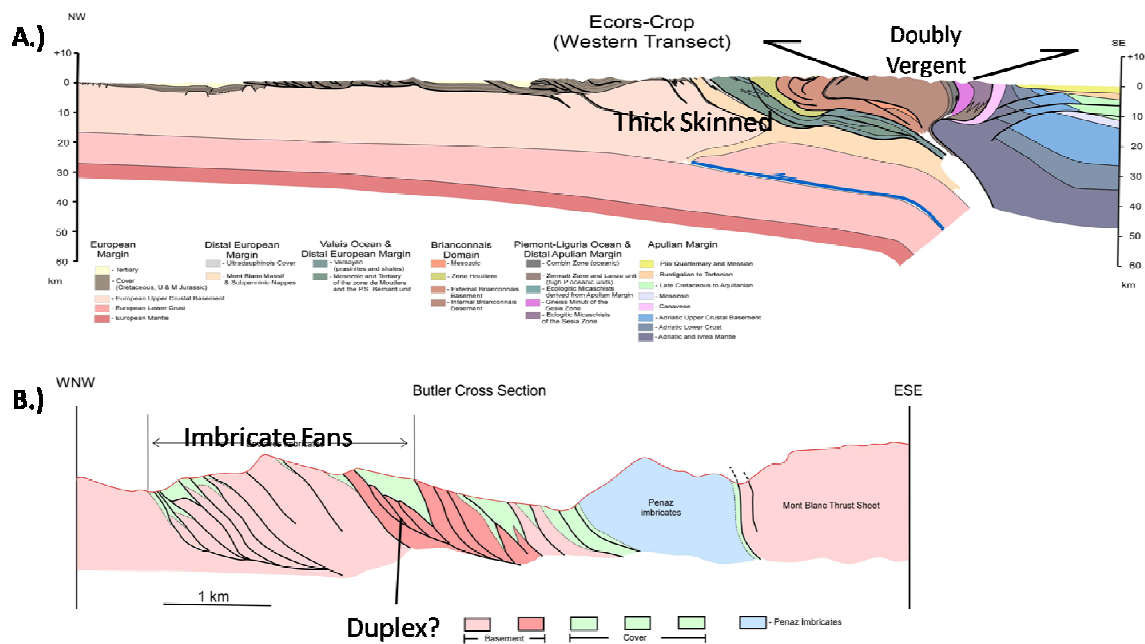


Figure 64: Cross sections for the Western Alps. A) Schmid and Kissling, 2000, B) Butler, 1983

There are several cross sections provided for the Carpathians (Picha (1996), Roca et al. (1995), and Roure et al. (1993)), covering the breadth of the mountain belt (Fig. 65). Each cross section show minor changes in the thrust fault geometries along the axis of the fold and thrust belt. Cross section "A" has a scale too large to be useful in describing fault geometries (Fig. 66 (A) and plate 13). Cross section "B" shows that the Outer

Carpathians are highly imbricated with south dipping imbricates and that the Inner

Carpathins are less imbricated (Fig. 66 (B) and plate 13). Both cross section "A" and "B"

show that the Hercynian thrust belt is highly imbricated with north dipping imbricates,

and that there is a horst and graben complex in the basement below the thrust belt.

Cross section "C" is the most complicated cross section provided (Roca et al.

(1995)) for the Carpathians (Fig. 67 and plate 13) and shows evidence for thick skinned

thrusting. More importantly, this cross section shows that there are hinterland dipping

duplexes, an antiformal stack, a possible blind imbricate complex, and the outer flysch

belt lacks imbricate fans. This cross section also shows down to the southwest normal

faults located in the basement below the thrust belt.
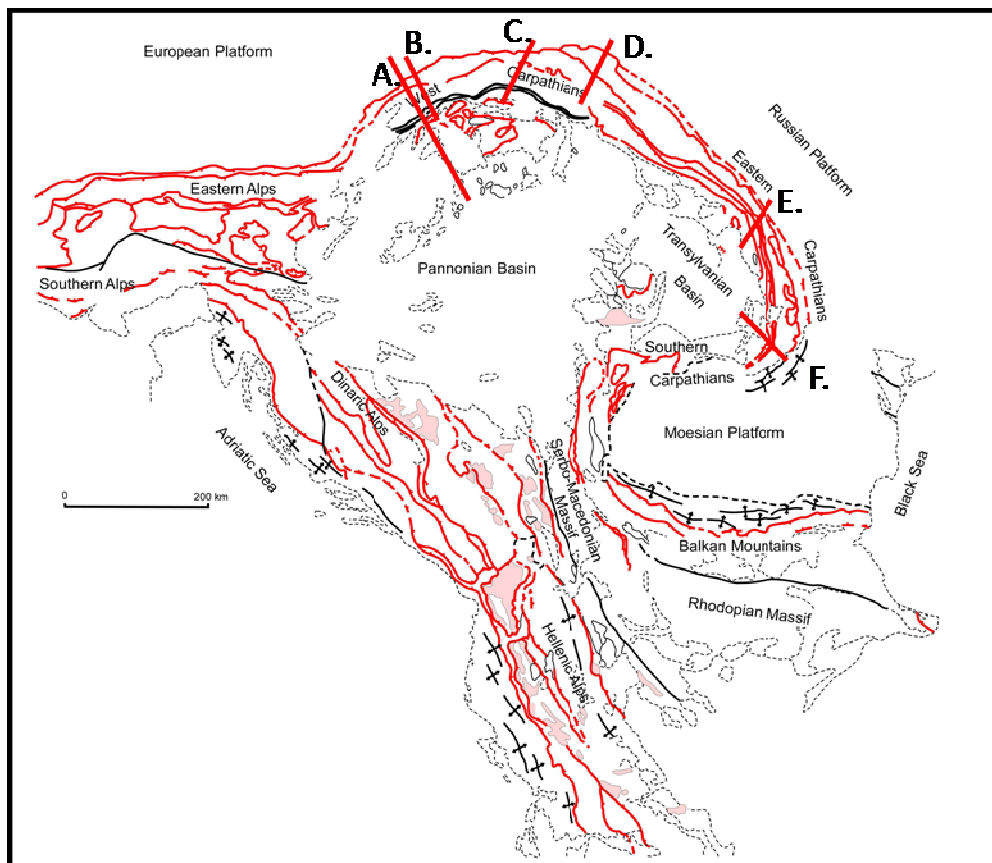


Figure 65: Location map of the Carpathian structural cross sections. (Modified from Burchfiel et al. (1982))
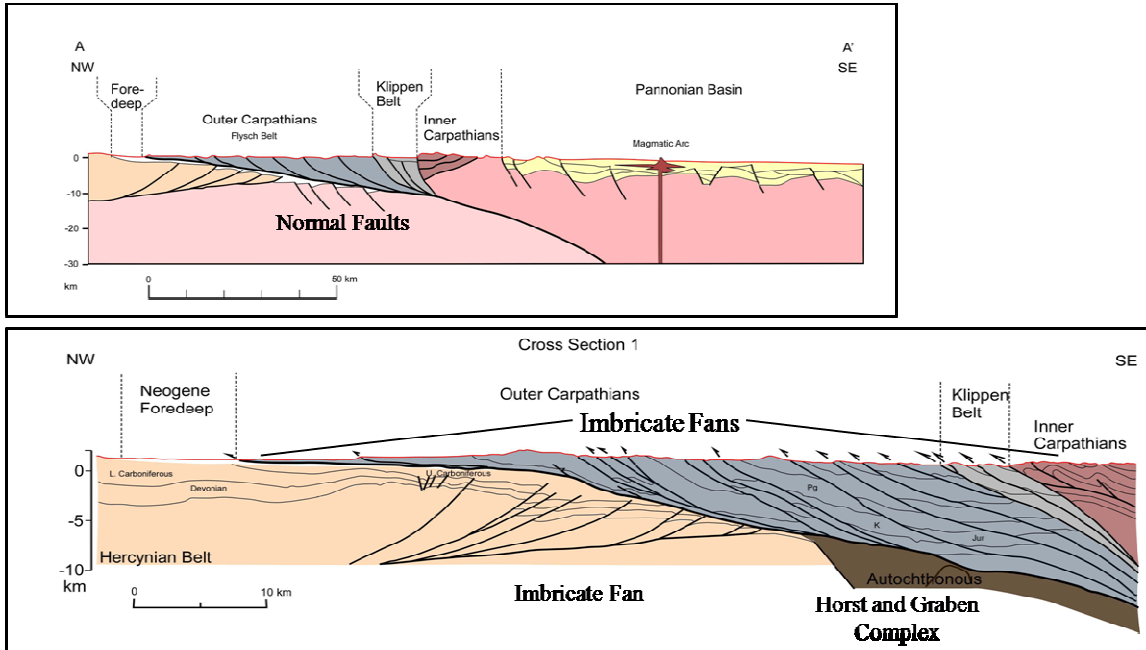
Figure 66: Cross Sections "A" & "B". (Modified from Picha, (1996))
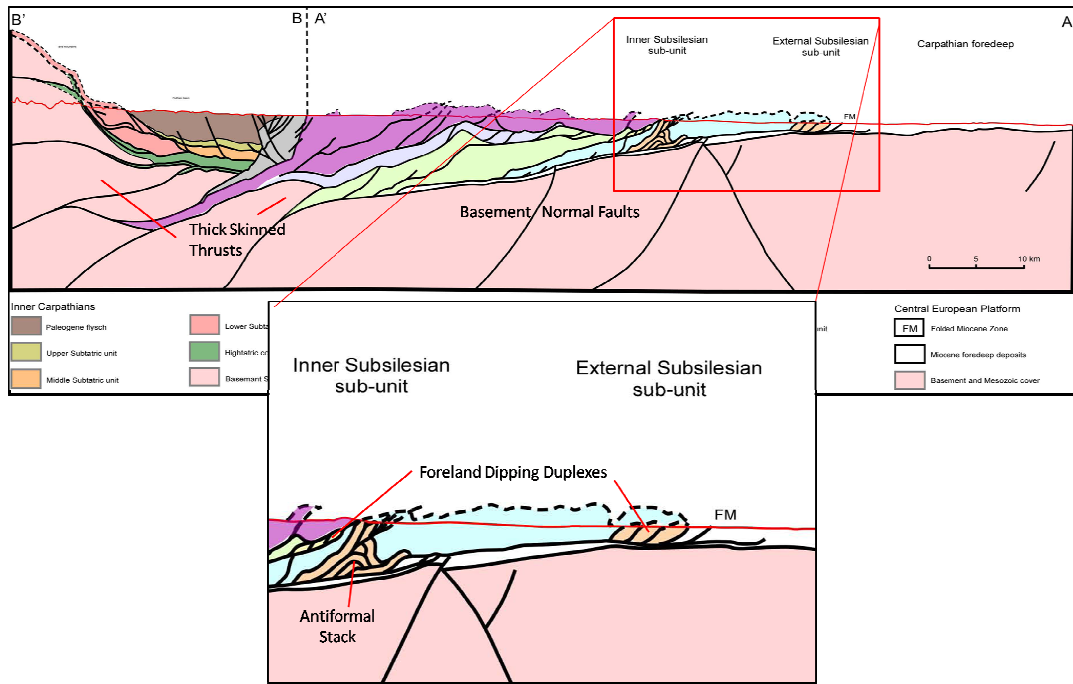


Figure 67: Cross section "C" (Modified from Roca et al., 1995)

Cross section "D" (Roure et al. (1993)) shows the same basic fault geometries as cross section "C" minus the duplexes. The most notable geometry in this cross section is a back thrust generating a blind imbricate complex (Fig. 68 (A) and plate 13).  Cross section "E" (Roure et al. (1993)) exhibits a duplex and down to the southwest normal faults in the basement (Fig. 68 (B) and plate 13); while, cross section "F" (Roure et al. (1993)) has a duplex, a triangle zone, and thick skinned thrusting (Fig. 68 (C) and plate 13).
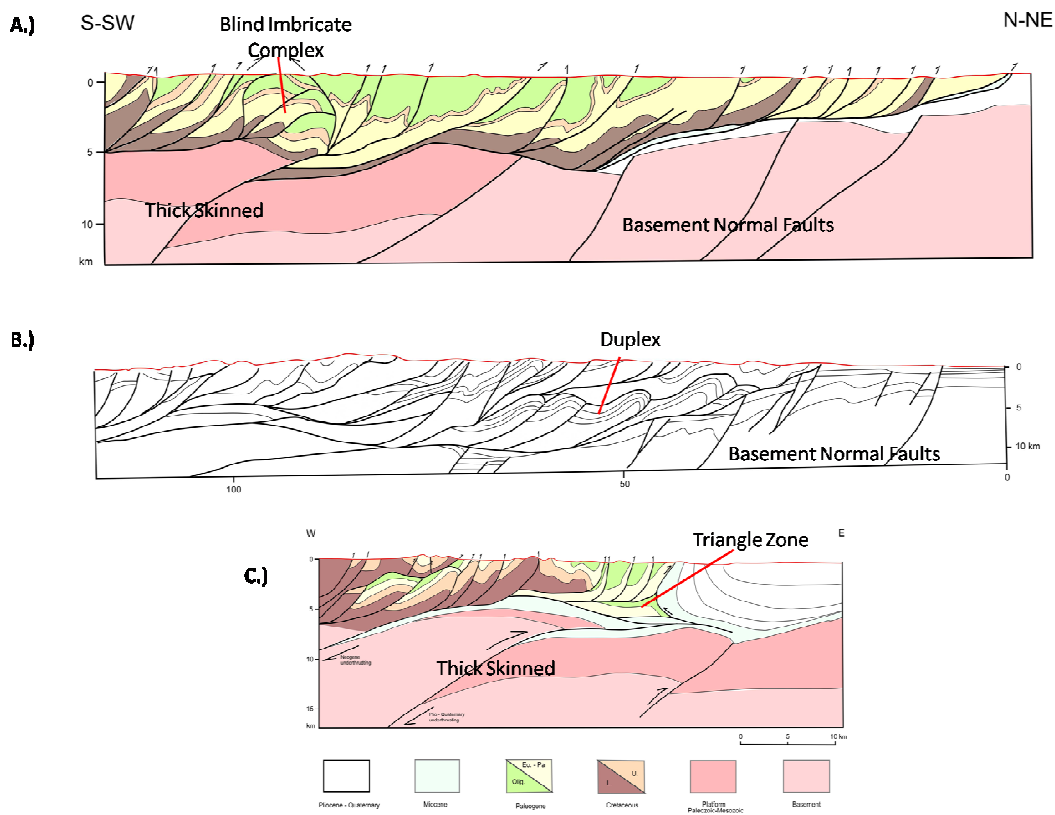


Figure 68: Cross sections "D", "E", and "F".  (Modified from Roure et al., 1993)

The cross sections for Ouachita Mountains only cover the frontal belt except for the simplified structural cross section from Arbenz, (1989). The Arbenz, (1989)

simplified structural cross section covers from the Broken Bow Uplift into the Arkoma

Basin. This cross section shows that hinterland from the frontal belt the thrusts become
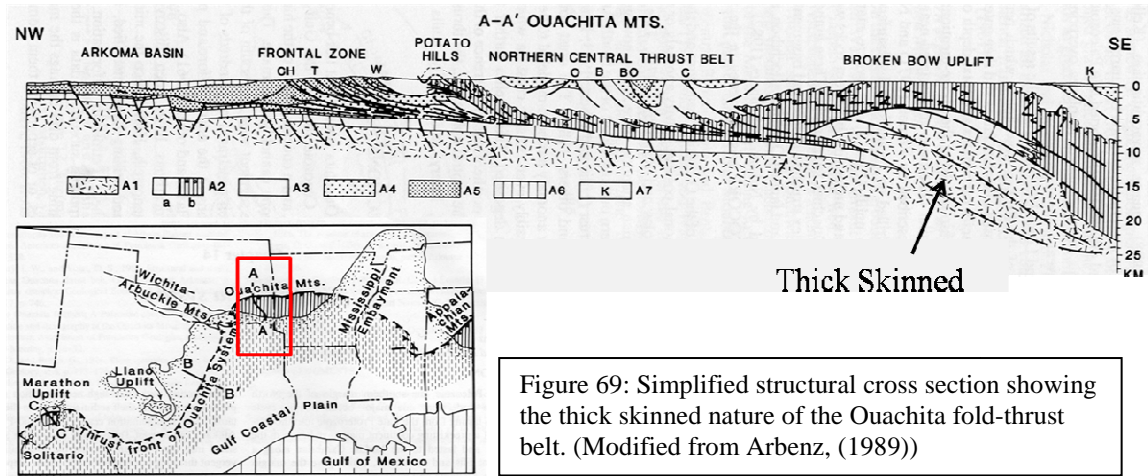


Figure 69: Simplified structural cross section showing the thick skinned nature of the Ouachita fold-thrust belt. (Modified from Arbenz, (1989))

thick skinned in nature (Fig. 69 and plate 14).

The Cemen et al., (2001) published several cross sections showing the exact same

fault geometries, hinterland dipping imbricate fans, a hinterland dipping duplex, and a

triangle zone in the footwall of the leading edge imbricate. There are also down to the

south normal faults in the footwall (Fig. 70and plate 14).

The Kaya, (2004) constructed cross sections more hinterlandward than the Cemen

et al., (2001) cross sections (Fig. 71 and plate 14). Cross section "6"covers from the

Potato Hills area to the Red Oak area of the Arkoma Basin and exhibits the duplex, the

triangle zone, and the basement normal faults like in the Cemen et al., (2001) cross

sections. Cross section "6"shows an antiformal stack under the Potato Hills region

 (Fig. 71 (A)).
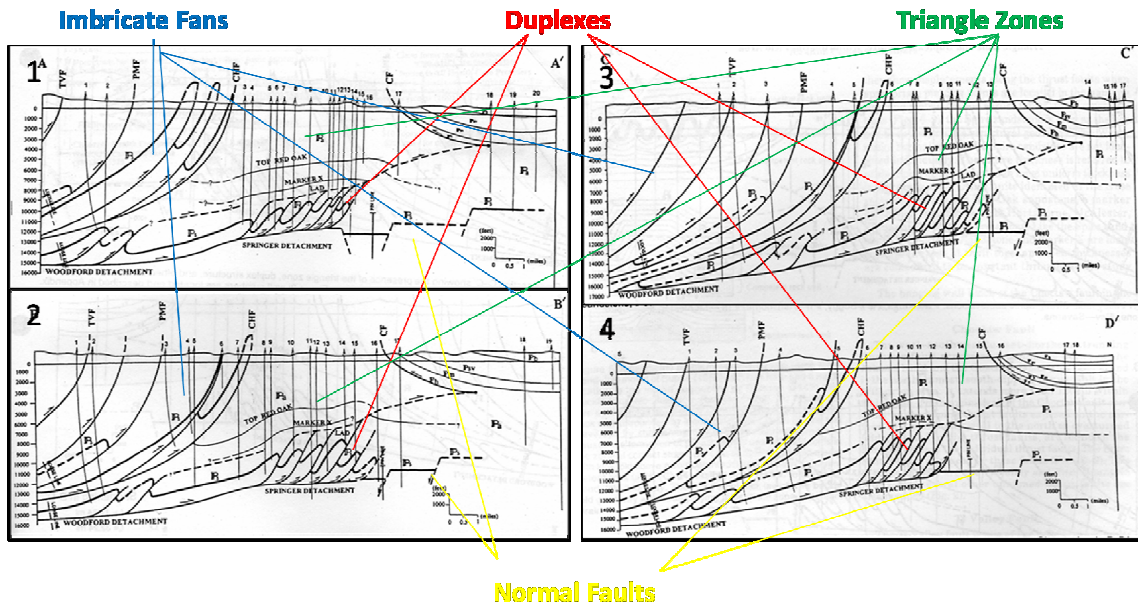
Figure 70: Cross sections adapted from Cemen et al., 2001. The numbers correspond to the location map.
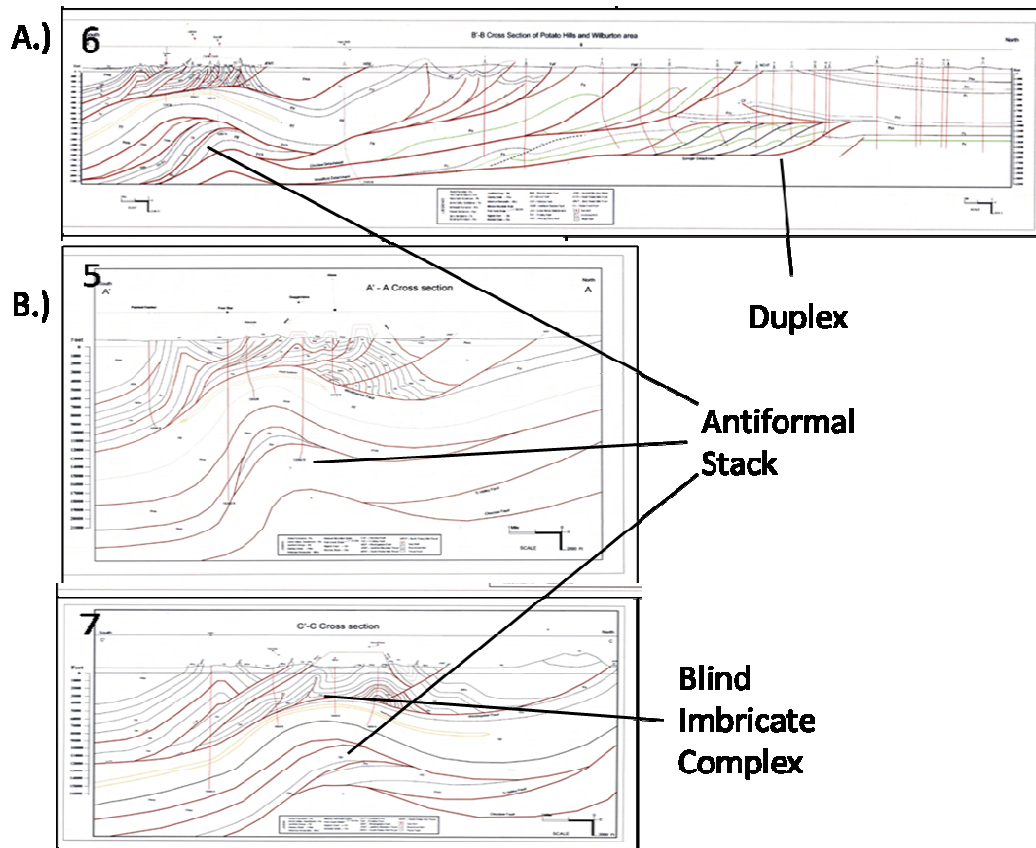


Figure 71: Cross sections adapted from Kaya, 2004. The numbers correspond to the number on thelocation map.

8.4 **Sedimentation**

The lack of comprehensive data on the pre-orogenic sedimentation in these areas will not allow for comparative analysis, but Garzanti et al., (2007) has shown that QFL ternary plots can be used to identify what part of and ultimately what type of orogenic belt produced the sediment collected (Fig. 72). Therefore, the point counts for the 14 siliciclastic samples collected for this study have been plotted along with point count data from Graham et al., (1976), Mack et al., (1981), and Carlson, (1989) (Fig. 73). The combined ternary plots compared closest to Garzanti et al.'s, (2007) "clastic wedge provenance" and the "recycled" portion of the "continental block provenance". These results fit given the locations of the collection sites, which were all within the frontal belt and the foreland basin of the eastern half of the
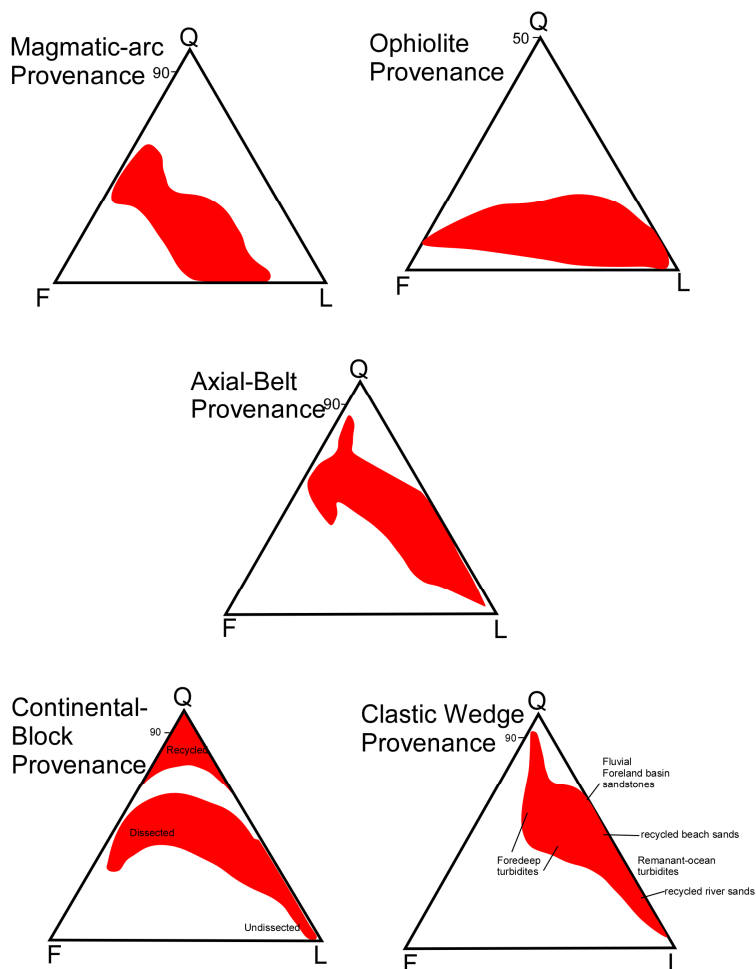


Figure 72: QFL Plots showing different provenances around orogenic belts. (Modified from Garzanti et al., 2007)

Ouachita Orogeny. If samples had been collected throughout the width of the orogenic belt, the results provided more insight.

Figure 73: A combined ternary diagram of the samples collected for this study and Mack et al., (1981), Graham et al., (1976), and Carlson, (1989). The samples for this study are the red solid circles. Mack et al., (1981) are the orange solid and open circles. Graham et al., (1976) are the blue solid and open circles. Carlson, (1989) is the green shaded area. The red circles comparable to Mack and Carlson's results but fit neither close enough to be definitive. This study's results do not compare well with that of Graham et al., (1976). Note: The location where these combined samples plot is not a perfect match to any of Garzanti's ternary diagrams.

## 8.5 **Gravity Profiles**

According to Doglioni et al., (1999) each subduction zone type has a unique gravity signature. The main differences in the gravity profiles of the two types of subduction zones is the width of the trough, the location of the trough compared to the hinge line of thesubduction zone, and the negativity of the anomaly. When comparing the trough of the E-directed and the W-directed subduction zones, it is apparent that the E-directed subduction zone has a very narrow trough; while the W-directed subduction zone's trough is much wider. Example of an E-directed and W-directed subduction zone gravity profiles are given in Figure 74. The width of the E-directed trough is approximately 50km, the negativity of the anomaly is less than -150mgals, and the

anomaly is not centered above the subduction zone's hinge-line. Compared to the W-

directed trough that has a width of approximately 120km, a negativity of approximately -

50mgals, and the anomaly is centered above the hinge-line.

A gravity profile for the Ouachita Mountains is provided in Figure 75, and shows

data provided by the USGS, that was collected with 10km spacing but has been reduced

down to 1km spacing by the USGS. The resultant profile (Fig. 75) shows a wide trough

approximately 100km wide with a negativity of ~ -112 mgals, but, the location of the



Figure 74: Example gravity profiles from Doglioni et al., 1999. A.) is taken cross the Western Alps (E-directed), B.) taken across the Apennines (W-directed)
(Modified from Doglioni et al., 1999)
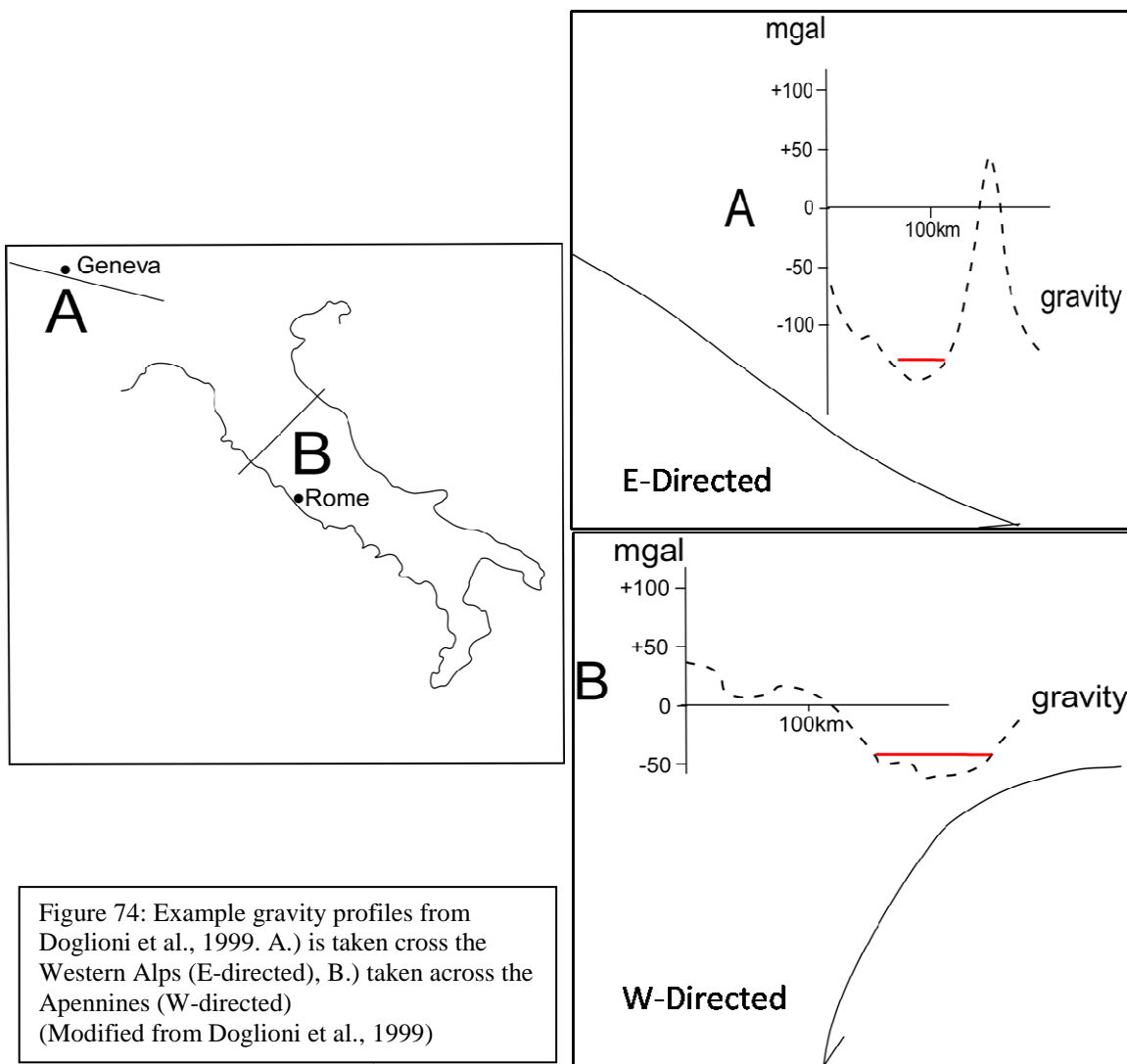
Ouachita hinge-line is unknown. These results are not very conclusive because they fall between the example profiles, but the lack of an immediate positive anomaly after the negative trough suggests that the Ouachita subduction zone is not E-directed.
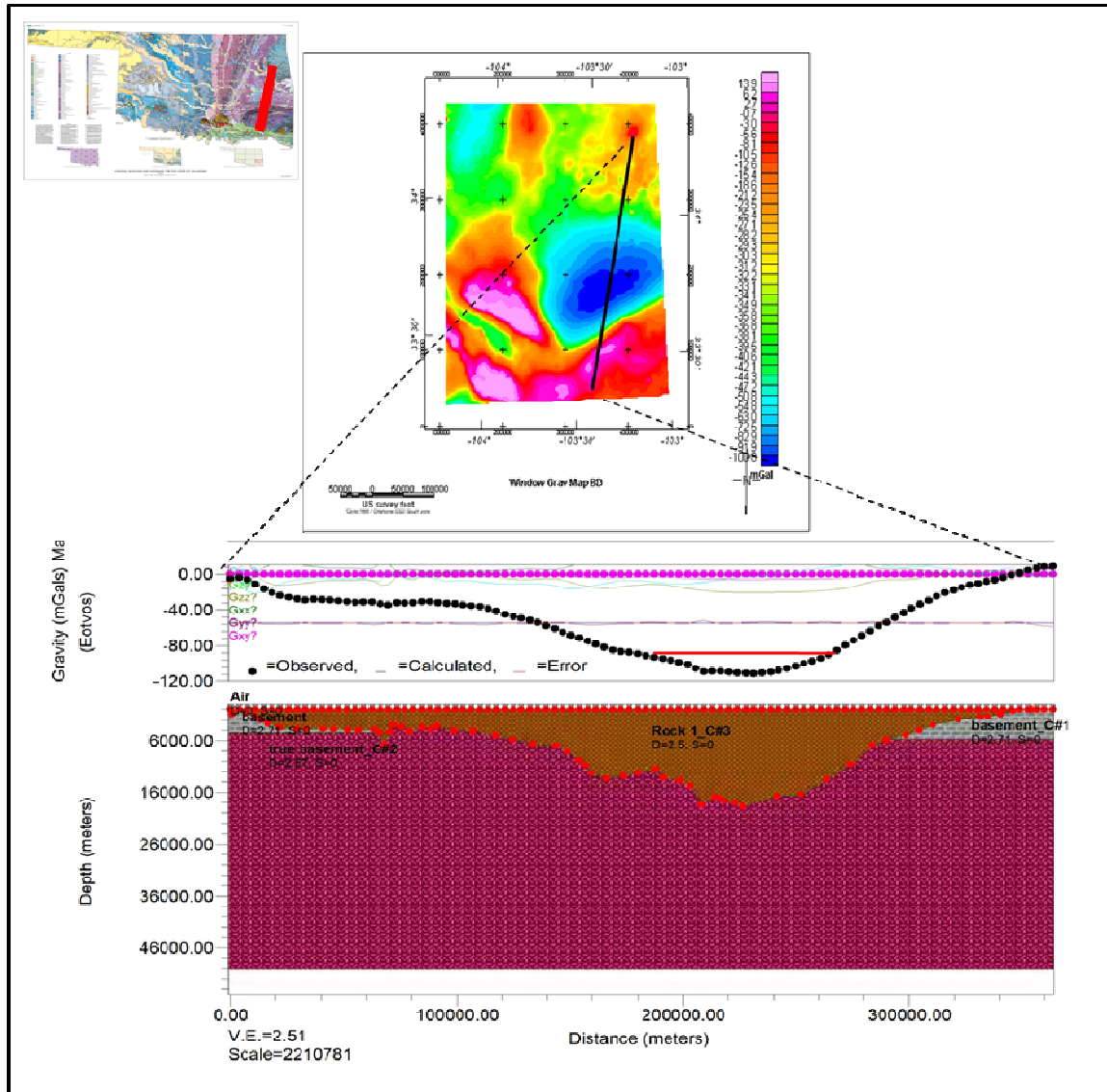


Figure 75: A gravity profile across the Ouachita Mountains. The line extends from the Ozark Uplift through the Ouachita Mountains.

CHAPTER 9

CONCLUSIONS

The main objective of this study was to comprehensively compare the Ouachita Mountains to four other acruate bends. Three of these arcuate bends were in the Western Alps; while, the forth consisted of the Carpathian Mountains. The comparison was to be based on the following five criteria: 1) orogenic evolution (subduction zone type), 2) arc type, 3) fault geometries, 4) sedimentology, and 5) gravity profiles.

1.) The Ouachita Mountains compared closest to the Carpathians when just comparing their orogenic evolution (subduction zone type), because they both exhibit more Mariana-type characteristics than they do Chilean-type characteristics.

2.) Further work is needed to decisively define the arc type for the Ouachita Mountains; therefore, no comparison could be made using this criterion.

3.) The Carpathians again proved to be closest when comparing map expressions of the fault geometries, but the geologic maps provided were of such poor quality that no definitive comparisons could be made.

4.) The Ouachita Mountains match the Carpathians the best in cross section fault geometries. They both exhibit hinterland dipping duplexes, antiformal stacks, blind imbricate complexes, triangle zones, hinterland dipping normal faults, and some measure of thick skinned thrusting toward the hinterland. To make

a definitive match between these two thrust systems, the Ouachita cross sections need to cover the breadth of the Ouachita Mountains and be drawn down to the MOHO.

5.) No comparison can be made on the sedimentation, because a more comprehensive sample collection effort needs to be made. All of the samples collected and plotted were taken from the foreland side of the orogenic belt. If samples were collected throughout the width of the orogeny then a comparison could possibly be made.

6.) The gravity profile across the Ouachita Mountains is ambiguous and lies in the gray area between both averaged end member profiles, but, does lack the immediate positive anomaly associated with the E-directed subduction zone. No definite comparisons can be drawn from this data at this time.

The Ouachita Mountains compare closest to the Carpathian Mountains in two out of the five criteria listed above. The other three criteria could not be used in comparisons due to poor quality or missing data. Further work needs to be done on collecting the missing data and improving the available data.

CHAPTER 10


REFERENCES


10.1 Literature

Arbenz, J. K., 1989, The Ouachita system, *in* Bally, A. W., and Palmer, A. R., eds., The Geology of North America-An overview: Boulder, Colorado, Geological Society of America, The Geology of North America, v. A, p. 371-396.

Archinal, B. E., 1979, Atoka Formation (Pennsylvanian) Deposition and Contemporaneous Structural Movement, Southwestern Arkoma Basin, Oklahoma, *in* TGS's: Pennsylvanian Sandstones of the Mid-Continent, p. 259-267.

Bergerat, F., 1989, From pull-apart to the rifting process: the formation of the Pannonian Basin: Tectonophysics, v. 157, p. 271-28.

Boyer, S., E., and Elliot, D., 1982, Thrust Systems: AAPG Bulletin, v. 66, n. 9, p. 1196-1230.

Briggs, G., and Cline, L., M., 1967, Paleocurrents and Source Areas of Late Paleozoic Sediments of the Ouachita Mountains, Southeastern Oklahoma: Journal of Sedimentary Geology, v. 37, n. 4, p. 985-1000.

Burchfiel, B., C., 1980, Eastern European Alpine System and the Carpathian Orocline as an Example of Collision Tectonics: Tectonophysics, v. 63, p. 31-61.

Burchfiel, B., C., and Royden, L., 1982, Carpathian Foreland Fold and thrust belt and Its Relation to Pannonian and Other Basins: AAPG Bulletin, v. 66, n. 9, p. 1179-1195.

Burrett, C. F., 1972, Plate Tectonics and the Hercynian Orogeny: Nature, v. 239, p.155-156.

Butler, R., W., H., 1983, Balanced cross-sections and their implications for the deep structure of the northwest Alps: Journal of Structural Geology, v. 5, n. 2, p. 125-137.

Butler, R., W., H., 1987, Thrust sequences: Journal of the Geologic Society, London, v. 144, p. 619-634.

Carlson, M., C., 1985-1989, A Petrographic Analysis of Surface and Subsurface Atoka Formation (Lower Pennsylvanian) Sandstone, Western Margin of the Arkoma Basin, Oklahoma: The Shale Shaker Digest XII, vol. XXXVI-XXXIX, 1985-1989,   pp. 256-272.

Çemen, I., Sagnak, A., and Aktar, S., 2001, Geometry of the Triangle Zone and Duplex Structure in the Wilburton Gas Field Area of the Arkoma Basin, Southeastern Oklahoma: Oklahoma Geological Survey Circular, v. 104, p. 87-97.

Clark, C., J., Bouma, A., H., Constantine, D., A., 1999, Turbidites from the Lower Atoka Formation Jacksonville, Arkansas: Gulf Coast Association of Geological Societies Transactions, v. 49, p. 172-183.

Corredor, F., Shaw, J., H., and Bilotti, F., 2005, Structural styles in the deep-water fold and thrust belts of the Niger Delta: AAPG Bulletin, v. 89, n. 6, p. 753-780.

Doglioni, C., 1995, Geological remarks on the relationship between extension and convergent geodynamic settings: Tectonophysics, v. 252, p. 253-267.

Doglioni, C., Harabaglia, P., Merlini, S., Mongelli, F., Peccerillo, A., and Piromallo, C., 1999, Orogen  and slabs vs. their direction of subduction: Earth-Science Reviews, v. 45, p. 167-208.

Frisch, W., 1979, Tectonic Progradation and Plate Tectonic Evolution of the Alps: Tectonophysics, v. 60, p. 121-139.

Garzanti, E., Doglioni, C., Vezzoli, G., and Andò, S., 2007, Orogenic Belts and Orogenic Sediment Provenance: The Journal of Geology, v. 115, p. 315-334.

Gehring, A., U., Keller, P., and Heller, F., 1991, Paleomagnetism and tectonics of the Jura arcuate mountain belt in France and Switzerland: Tectonophysics, v. 186, p. 269-278.

Golonka, J., Ślączka, A., and Picha, F., J., 2006, The Western Carpathians and Ouachitas: A Comparative Study of Geodynamic Evolution, *in* J. Golonka and F. J. picha, eds, the Carpathians and their foreland; geology and hydrocarbon resources: AAPG Memoirs 84, p. 787-810.

Graham, S., A., Ingersoll, R., V., and Dickinson, W., R., 1976, Common Provenance for Lithic Grains in Carboniferous sandstones from Ouachita Mountains and Black Warrior Basin: Journal of sedimentary Petrology, v. 46, n. 3, p. 60-632.

Grayson, R., C., Jr., 1980, The Stratigraphy of the Wapanucka Formation (Lower Pennsylvanian) along the Frontal Margin of the Ouachita Mountains, Oklahoma: PH.D. Thesis: The University of Oklahoma.

Hindle, D., Besson, O., and Burkhard, M., 2000, A model of displacement and strain for arc shaped mountain belts applied to the Jura arc: Journal of Structural Geology, v. 22, p. 1285-1296.

Hindle, D., Burkhard, M., 1999, Strain, displacement and rotation assoiciated with the formation of the curvature in the fold belts; the example of the Jura arc: Journal of Structural Geology, v. 21, p. 1089-1101.

Homberg, C., Bergerat, F., Philippe, Y., Lacombe, O., and Angelier, J., 2002, Structural inheritance and Cenozoic stress fields in the Jura fold-and-thrust belt (France): Tectonophysics, v. 357,  p. 137-158.

Houseknecht, D., W., 1987, The Atoka Formation of the Arkoma Basin: Tectonics, Sedimentology, Thermal maturity, Sandstone Petrology, Tulsa Geological Society Short Course Notes.

Houseknecht, D. W., 1992, Thin Section Analysis: AAPG Methods in Exploration 10: Development Geology Reference Manual, p. 233-236.

Houseknecht, D., W., Kuhn, M., A., Matteo, A., P., Jr., Steyaert, D., J., Zaengle, J., F., and Iannacchione, A., T., 1984, High-Constructive, Tidally-Influenced Deltaic Sedimentation in the Arkoma Basin: The Desmoinesian Hartshorne Sndstone, *in* Technical Proceedings of the 1981 AAPG Mid-Continent Regional Meeting, p. 26-41.

Hubbard, M., and Mancktelow, N., S., 1992, Lateral displacement during Neogene convergence in the western and central Alps: Geology, v. 20, p. 943-946.

Ingersoll, R., V., 1988, Tectonics of sedimentary basins: GSA Bulletin, v. 100, p. 1704-1719.

Kaya, G., 2004, Structural Geometry of Thrust Faulting in the Potato Hills Area of the Ouachita Mountains, Southeastern Oklahoma, Master's Thesis Oklahoma State University.

Keller, G., R., and Hatcher, R., D., Jr., 1999, Some comparisons of the structure and evolution of the southern Appalachian-Ouachita orogen and portions of the Trans-European Suture Zone region: Tectonophysics, v. 314, p. 43-68.

Knechtel, M., M., 1937, Geology and Fuel resources of the Southern Part of the Oklahoma Coal Field; Part 2: The Lehigh District Coal, Atoka, and Pittsburg Counties: USGS Bulletin 874-B, p. 91-147.

Lickorish, W., H., Bürgisser, J., and Cobbold, P., R., 2002, Arcuate thrust systems in sandbox experiments: A comparison to the external arcs of the Western Alps: GSA Bulletin, v. 114, n. 9, p. 1089-1107.

Lumsden, D., N., Pittman, E., D., and Buchanan, R., S., 1971, Sedimentation and Petrology of Spiro and Foster Sands (Pennsylvanian), McAlester Basin, Oklahoma: AAPG Bulletin, v.55, n. 2, p. 254-266.

Mack, G., H., James, W., C., and Thomas, W., A., 1981, Orogenic Provenance of Mississippian Sandstones Associated with Southern Appalachian-Ouachita Orogen: AAPG Bulletin, v. 65, n. 8, p. 1444-1456.

Mack, G., H., Thomas, W., A., and Horsey, C., A., 1983, Composition of Carboniferous Sandstones and Tectonic Framework of Southern Appalachian-Ouachita Orogen: Journal of Sedimentary Petrology, v. 53, n. 3, p. 931-946.

Marshak, S., 1988, Kinematics of Orocline and Arc Formation in Thin-Skinned Orogens: Tectonics, v. 7, n. 1, p. 73-86.

Marshak, S., and Woodward, N., 1988, Introduction to Cross-Section Balancing, *in* Marshak, S., and Mitra, G., (eds.) Basic Methods of structural geology: Prentice-Hall, Engle Cliffs, New Jersey, p. 303-326.

Mount, V., S., Suppe, J., and Hook, S., C., 1990, A Forward Modeling Strategy for Balancing Cross Sections: AAPG Bulletin, v. 74, n. 5, p. 521-531.

Nally, D., V., 1996, A Stratigraphic and Sedimentologic Analysis of a Lower Atoka Sandstone, Frontal Ouachita Thrustbelt, Western Arkansas: Transactions of the 1995 AAPG Mid-Continent Section Meeting, p. 74-83.

Nicolas, A., 1972, Was the Hercynian Orogenic Belt of Europe of the Andean Type?: Nature, v. 236, p. 221-223.

Picha, F., J., 1996, Exploring for Hydrocarbons Under Thrust Belts – A Challenging New Frontier in the Carpathians and Elsewhere: AAPG Bulletin, v. 80, n. 10, p. 1547-1564.

Picha, F., J., Stráník, Z., Krejčí, O., 2006, Geology and Hydrocarbon Resources of the Outer Western Carpathians and Their Foreland, Czech Republic, *in* J. Golonka and F. J Picha, eds, the Carpathians and their foreland: Geology and hydrocarbon resources: AAPG Memoir 84, p. 49-175.

Roca, E., Bessereau, G., Jawor, E., Kotarba, M., and Roure, F., 1995, Pre-Neogene evolution of the Western Carpathians: Contraints from the Bochnia-Tatra Mountains section (Polish Western Carpathians): Tectonics, v. 14, n. 4, p. 855-873.

Roure, F., Roca, E., and Sassi, W., 1993, The Neogene evolution of the outer Carpathian flysch units (Poland, Ukraine, and Romania): kinematics of a foreland/fold-and-thrust belt system: Sedimentary Geology, v. 86, p. 177-201.

Schmid, S., M., and Kissling, E., 2000, The arc of the western Alps in the light of geophysical data on deep crustal structure: Tectonics, v. 19, n. 1, p. 62-85.

Seward, D., and Manchtelow, N., S., 1994, Neogene kinematics of the central and western Alps: Evidence from fission-track dating: Geology, v. 22, p. 803-806.

Siddans, A., W., B., 1979, Arcuate fold and thrust patterns in the Subalpine Chains of Southeastern France: Journal of Structural Geology, v. 1, n. 2, p. 117-126.

Sissingh, W., 2001, Tectonostratigraphy of the Western Alpine Foreland: Correlation of Ternary sedimentary sequences, changes in eustatic sea-level and stress regimes: Tectonophysics, v. 333, p. 361-400.

Stark, P., H., 1966, Stratigraphy and Evironment of deposition of the Atoka Formation in the Central Ouachita Mountains, Oklahoma, *in* (KGS) Flysch Facies and Structure of the Ouachita Mountains: Guidebook, 29th Field Conference, p. 164-176.

Suppe, J., 1985, The Geometry of Map-Scale Structures, *in* Principles of Structural Geology, Prentice Hall, Englewood Cliffs, New Jersey, p. 36-75.

Thomas, W., A., 1976, Evolution of Ouachita-Appalachian Continental Margin: Journal of Geology, v. 84, p. 323-342.

Uyeda, S., 1982, Subduction Zones: An Introduction to Comparative Subductology: Tectonophysics, v. 81, p. 133-159.

10.2 Maps:

Haley, B., R., Glick, E., E., Bush, W., V., Clardy, B., F., Stone., C., G., Woodward, M., B., and Zachry, D., L., 1993, Geologic Map of Arkansas, USGS, 1:500,000 scale.

Knechtel, M., M., 1937, Geologic map and Structural Sections of the McAlester District, Oklahoma: USGS Bulletin 874-B, 1:63,360 scale.

Marcher, M., V., and Bergman, D. L., 1994, Reconnaissance of the Water Resources of the McAlester and Texarkana Quadrangles, Southeastern Oklahoma (Geologic Map HA-9), USGS, 1:250,000 scale.

USGS, Topographic map of the Adamson Quadrangle, Oklahoma, 1967 (revised 1978), 1:24000 scale.

USGS, Topographic map of the Colgate SE Quadrangle, Oklahoma, 1957 (revised 1979), 1:24000 scale.

USGS, Topographic map of the Damon Quadrangle, Latimer Co., Oklahoma, 1971, 1:24000 scale.

USGS, Topographic map of the Gowen Quadrangle, Latimer Co., Oklahoma, 1971, 1:24000 scale.

USGS, Topographic map of the Hartshorne Quadrangle, Oklahoma, 1967 (revised 1978), 1:24000 scale.

USGS, Topographic map of the Hartshorne SW Quadrangle, Pittsburg Co., Oklahoma, 1967, 1:24000 scale.

USGS, Topographic map of the Higgins Quadrangle, Latimer Co., Oklahoma, 1971, 1:24000 scale.

USGS, Topographic map of the Kiowa Quadrangle, Oklahoma, 1967 (revised 1978), 1:24000 scale.

USGS, Topographic map of the Limestone Gap Quadrangle, Oklahoma, 1957 (revised 1978),  1:24000 scale.

USGS, Topographic map of the Pittsburg Quadrangle, Pittsburg Co., Oklahoma, 1967 (revised 1978), 1:24000 scale.

USGS, Topographic map of the Ti Quadrangle, Pittsburg Co., Oklahoma, 1973, 1:24000 scale.

USGS, Topographic map of the Wilburton Quadrangle, Latimer Co., Oklahoma, 1971, 1:24000 scale.

CHAPTER 11


APPENDICES


11.1 Appendix A


The 58samples collected from the Wapanucka Limestone were processed in order
to collect the conodonts. The limestones were broken down using Formic Acid. The
procedure for the breaking down process is as follows: 1) attain 550 grams of the sample
broken into 1 inch fragments (for increased surface area), 2) place the sample in a plastic
five gallon bucket, 3) add 5 liters of $H_2O$, and finally 4) add 500mL of the Formic acid.
The calcite within the limestone should dissolve within a twenty-four hour period,
leaving only residual constituents, the conodonts. 5) The residue is then sieved using a
120 gauge sieve. 6) The collected remains must then be dried in a heating oven until
completely dry. Once, the sample is completely dry the conodonts can be collected by
using the following procedure: 1) place a small amount of the sample in a small specimen
tray, 2) use a teasing needle to sift through the sample under a Leica L2 binocular
microscope, 3) retrieve the conodonts using a wet 003 paint brush, and 4.) place the
retrieved conodont on an specimen slide and cover. The conodonts can then be identified
using the published literature on the local assemblages of conodonts.

The shale samples collect were processed using 35% $H_2O_2$. The procedure for this
method is simpler than the abovementioned Formic Acid method. The 550 grams of the

sample are placed in a 5 gallon bucket, and the 35% $H_2O_2$ is poured in until it complete

covers the sample. The reaction can be violent depending on the amount of organic

matter in the sample, so this procedure should be conducted inside a fume hood or if need

be outside. After the sample is broken down then follow the retrieval process described

above.

## 11.2 **Appendix B**
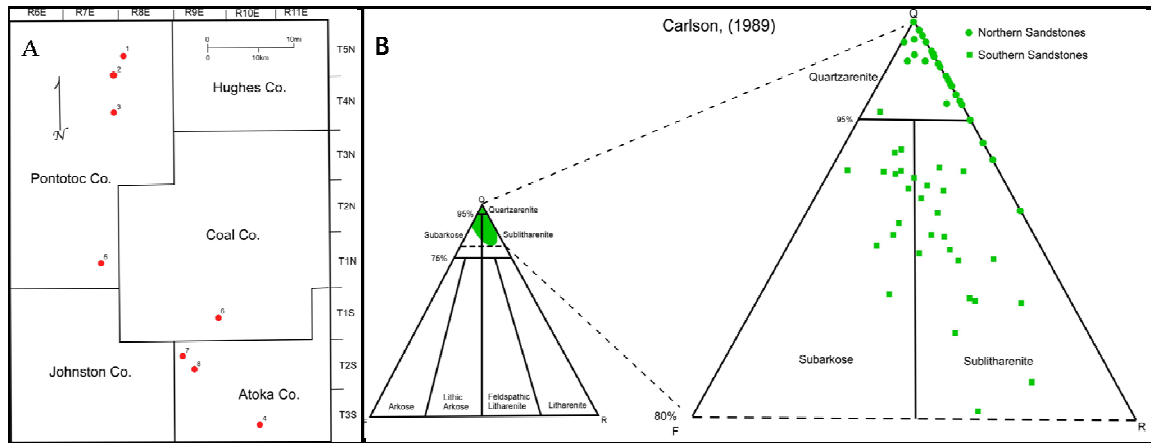


Carlson (1989): Ternary diagram (B) and collection site location map (A). There is a noticeable difference between the northern samples and the southern samples. These samples are collected closest to my thesis area, but were collected in mostly sub-surface sites.
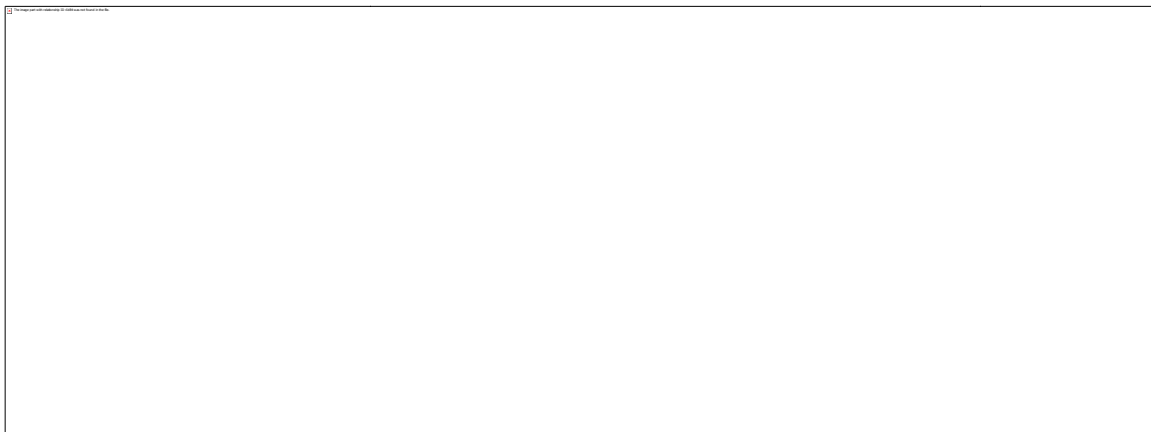


Graham et al. (1976): Ternary diagram (B) and collection site location map (A). Solid blue circles are the samples collected in the Ouachitas; while, the open circles are from the Black Warrior Basin.
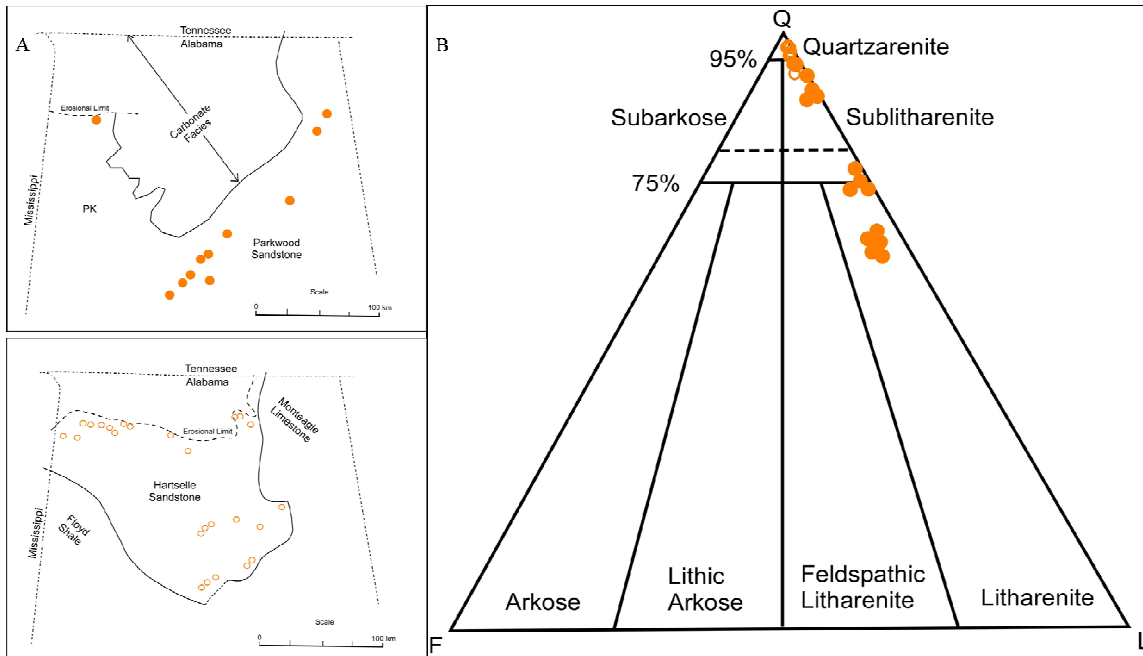
Mack et al. (1981): Ternary diagram (B) and collection site location maps (A). Open circles are the samples collected from the Hartselle Sandstone. Solid circles are samples collected from the Parkwood Sandstone. All samples collected from the Black Warrior Basin.